Kinetics and mechanisms of methanol to hydrocarbons conversion over zeolite catalysts

A THESIS
SUBMITTED TO THE FACULTY OF
UNIVERSITY OF MINNESOTA
BY

Ian Hill

IN PARTIAL FULFULLMENT OF THE
REQUIREMENTS FOR THE DEGREE OF
DOCTOR OF PHILOSOPHY

Adviser: Aditya Bhan

May, 2013

Acknowledgements

I would, first and foremost, like to thank my adviser, Aditya Bhan, for all of his insightful discussions and for helping me become the researcher I am today. The amount of time, energy, and patience that he has put forth throughout the past 5.5 years has not gone unnoticed. My fellow classmates, Hsu Chiang, Elizabeth Mallon, Samia Ilias, and Mark Mazar, for helping build Amundson 250 from the empty room that we inherited to the full lab that it is today, and making every work day enjoyable. My current and past lab mates: Michael Skinner, Yasser Al-Wahedi, Srinivas Rangaragan, Sam Blass, Jeremy Bedard, Dongxia Liu, Do-Young Hong, Jikku Thomas, Cha-Jung Chen, Minje Kang, Rachit Khare, Joseph DeWilde, and Mark Sullivan, who have all helped with my own education and with whom I was able to make so many friends and colleagues. The undergraduates with whom I have had the pleasure of working throughout my stay at the University of Minnesota: Nicole Delany (Ecolab), Bingxin Fan (Grad Student at Penn State), Joelle Fawaz (Grad Student at the Petroleum Institute), Yong-Sam Ng, and Nicholas Schlicker (current student). I wish you all the best in your future endeavors.

I would like to thank my family for being understanding throughout this process and keeping flexible about the fact that even though I was only a stone's throw away physically, that I needed the time and space to achieve this step in my life. I appreciate all your support and the occasional respite from my studies to grab a meal and catch up.

Lastly, and most certainly not least, I would like to acknowledge all of the time, patience, support, help, and understanding that my wife, Corine Hill, has given me throughout this whole process. After over 2 full years apart in a 4-year marriage to date, there is very little that has impressed me more than how strong we were able to stay despite being hundreds of miles apart in most every way. I look forward to joining you in Virginia with our wonderful cat, Grizzabella, and taking life as it comes.

Ты моя любовь

Abstract:

The methanol-to-hydrocarbons (MTH) process over zeolite catalysts is the final step in the synthesis of commodity chemicals and fuels from alternative carbon sources via synthesis gas intermediates. Emerging research has shown that olefins and aromatics are critical intermediates, acting as scaffolds for the addition of methyl groups from methanol or dimethyl ether (DME) in an indirect "hydrocarbon pool" mechanism. Outstanding questions in this research pertain to (i) the quantitation of reaction rates for C_1 homologation and (ii) the mechanism of activating methanol or DME for the formation of carbon-carbon bonds. This research reports rate constants and activation energies of olefin and aromatic methylation steps over zeolites of different pore sizes and geometries from steady-state methylation reactions, as well as isotopic and post-reaction titration studies to determine mechanistic details regarding the structure of the active zeolite surface species.

Specifically, isolated steady-state methylation of C_2 to C_4 olefins over zeolites at differential conditions have shown that reactions producing higher degrees of substitution of intermediate carbocations have rate constants that are an order of magnitude higher than less substituted intermediates. Benzene and toluene methylation reactions show similar kinetic behavior to propylene and linear butene, respectively, over H-ZSM-5. Pressure-dependent studies show a first-order rate dependence on olefin or aromatic pressures which is invariant of DME partial pressures, indicating a surface saturated in DME-derived species reacting with a gas phase co-reactant in the rate-limiting step. These surface species have been identified as methoxides, as observed using post-reaction titration and isotopic studies.

The methylation of *para*- and *ortho*-xylene with DME at low conversions showed linear dependence of the reaction rate at low pressures of xylene, but the reaction rate became zero-order at higher xylene pressures over H-ZSM-5. The reaction rate remained zero-order in DME pressure, and when taken in conjunction with results from isotopic studies and surface titrations, indicates that the surface methoxides become saturated in adsorbed xylene isomers. A reduction in the critical diffusion length by a factor of >150 did not increase the reaction rate, indicating that the effect is adsorption and not one of

transport limitations. Arguments based on derived rate equations modeling observed trends in kinetic, isotopic, and titration studies set a basis for building a microkinetic model for MTH reactions over H-ZSM-5, which can predict expected product distributions for a given set of reaction conditions.

Table of Contents

List of Tables

List of Figures

Chapter 1: Introduction

1.1 Catalysis

The field and study of catalysis has been the backbone of chemical conversion of petroleum to precursors for plastics and bulk quantity fine chemicals. A catalyst is a chemically active species present during a chemical reaction that is regenerated either through the chemical reaction itself or a side reaction with reactants or a spectator species. Catalysts can have acid, base, or metal functionality and can exist in the same phase as the reactants (homogeneous) or in a separate phase (heterogeneous). The role of a catalyst in a chemical reaction is to enhance the reaction rate by providing an alternative pathway from products to reactants (Figure 1). Specifically, catalysts lower the energy required to activate a reactant for reaction, and this is achieved through stabilizing chemical complexes in the transition state, or through breaking the reaction down in multiple lower-energy steps.

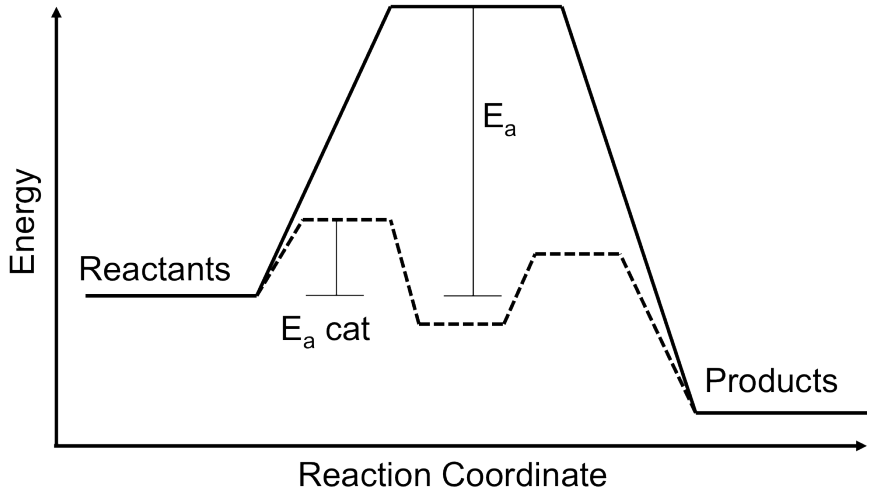

Figure 1. Reaction coordinate diagram for an example un-catalyzed reaction (solid line) and a possible catalyzed route that lowers the energy of activation (E_a).

1.2 Zeolites

Zeolites are a class of solid acid catalysts that contain networks of internal pores with openings on the order of molecules. The pore networks allow for these materials to

have low gravimetric densities and unusually high surface areas (hundreds of m^2g^{-1}). Individual zeolites are grouped by their pore size as small pore (<10 oxygen atoms in the pore ring), medium pore (10 oxygen atoms in the pore ring), and large pore (>10 oxygen atoms in the pore ring) frameworks, and are distinctly classified based on their pore tortuosity (Figure 2). [1]

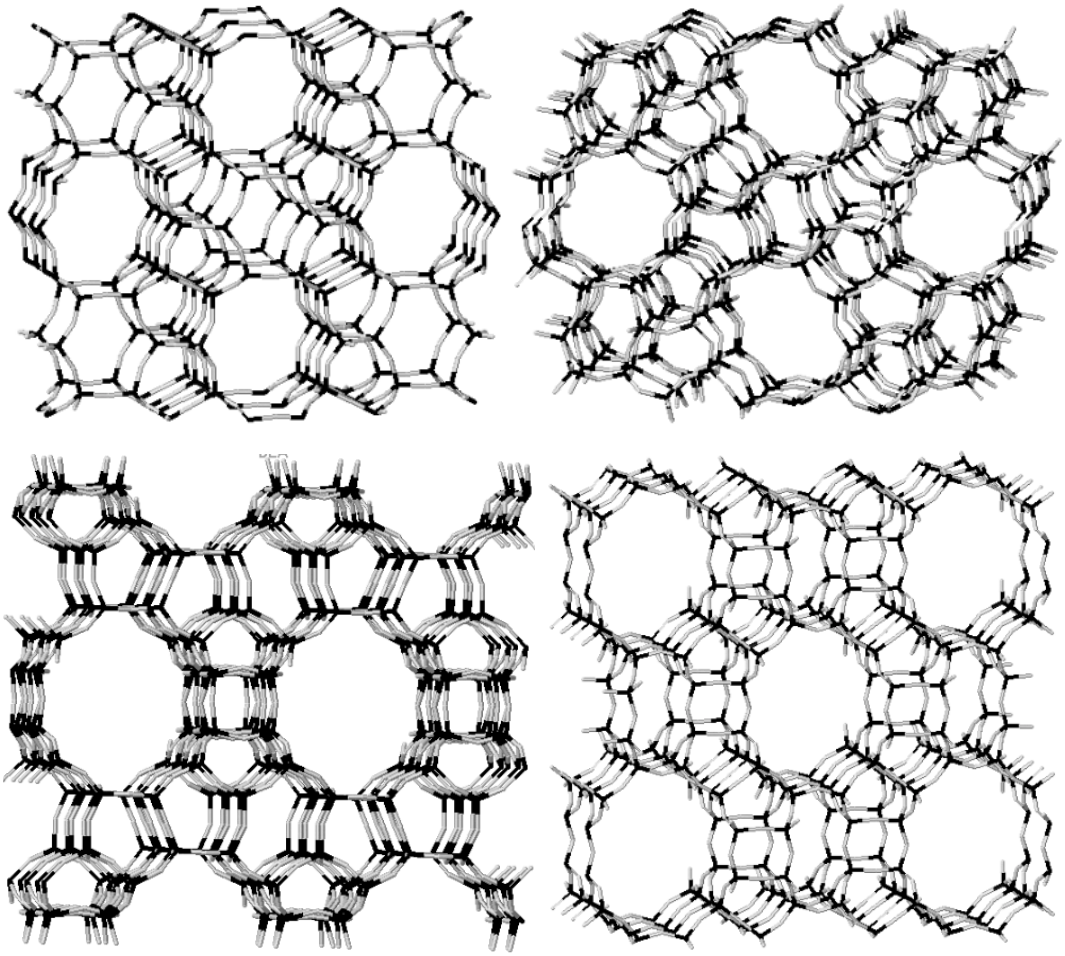

Figure 2. Zeolite structures used in this work. Upper left: 8 x 10 membered-ring (MR) FER. Upper right: 10 x 10 MR MFI. Lower left: 12 x 12 MR BEA. Lower Right: 8 x 12 MOR. Si atoms in black, O atoms in gray.

Zeolites are aluminosilicate materials and the acidity arises from aluminum substitutions in the silica framework, leading to a charge imbalance from displacing a four-valent silicon atom and replacing it with a three-valent aluminum atom. This charge imbalance is centered on a bridging oxygen atom between silicon and aluminum, which is compensated with a counter ion. When this counter ion is a proton, a Brønsted acid site

is formed, which is available for catalytic reactions (Figure 3). The chemical formula of a zeolite is: $Si_{x-n}O_{2x}Al_nH_n$ where x is the number of tetrahedral sites in a zeolite unit cell, dictated by the structural symmetry and n is the average aluminum content in a zeolite unit cell.

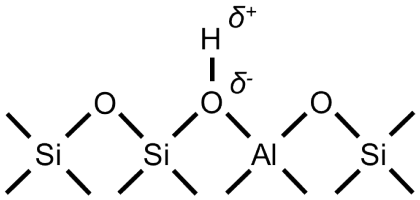

Figure 3. Structure of a Brønsted acid site on the surface of a zeolite.

1.2.1 Titration of Brønsted Acid sites with DME

In zeolite acid catalysis, it is not the Al atom that is responsible for chemical reaction steps, but rather the proton that is supported by the charge imbalance introduced by the Al atom. When normalizing reaction rates to active sites, therefore, it is important to normalize by surface protons rather than Al atoms. Cheung et al. [2] showed that each Brønsted acid site can adsorb 0.5 DME molecules because DME reacts with surface hydroxyl groups to form persistent methyl groups. Chemical titration of zeolite Brønsted acid sites using dimethyl ether (DME) over H-FER, H-MFI, H-MOR, and H-BEA materials was performed in a tubular packed-bed quartz reactor (10 mm inner diameter) under atmospheric pressure. A mixture of DME/Ar/He (0.17 cm^3 s^{-1}; 24.9% DME, 25.1% Ar and 50% He; Praxair) was introduced by He (0.67 cm^3 s^{-1}, ultrapure, Minneapolis oxygen) during each pulse with 90s intervals. The physisorbed DME and water formed were subsequently removed by He (1.67 cm^3 s^{-1}) for 1.5 to 2.5 hours.

The DME uptake ratio per Al site on the three zeolites is tabulated in Table 1. The concentration of Brønsted acid sites in the four zeolites used in this study is nearly identical to that inferred from the framework Aluminum content in these materials. The DME titration data reported herein has been reproduced from previous work by Chiang et al. [3,4] and indicates that the majority of Al in all of the zeolite frameworks tested resides on the pore surface and is accessible to DME.

1.2.2 Surface area and pore size determination via nitrogen adsorption

Measuring the uptake of nitrogen in the micropores of a zeolite allows for the determination of surface area and pore volume, based on a fixed size for nitrogen molecules, and the assumption that a monolayer of nitrogen atoms forms prior to additional pore filling. Nitrogen adsorption/desorption measurements were carried out at 77 K on an Autosorb-1 analyzer (Quantachrome Instruments). Prior to the measurement, samples were evacuated overnight at 573 K and 1 mm Hg. The specific surface area and the pore size distribution were calculated using the Brunauer–Emmett–Teller (BET) and BJH method, respectively. Conventional t-plot methods were used as an extra means for extracting micropore volume and external surface area from the nitrogen adsorption data over t ranges from 3 to 5 Å. The BET equation was used to calculate the BET specific surface area from the adsorption data obtained at P/P_0 between 0.1 and 0.3. Derived values from Liu et al. [5] are reproduced in Table 1.

Zeolyst zeolite sample (Si/Al)	**Si/Al (ICP-OES)[a]**	**DME/Al[b]**	**BET Surface Area (m^2g^{-1})[c]**	**BET micropore Volume (cc/g)[c]**
H-FER (10)	11.5	0.45	317	0.16
H-MFI (40)	42.6	0.49	406	0.13
H-MOR (10.5)	11.1	0.48	424	0.21
H-BEA (12)	12.0	0.42	579	0.19

Table 1. Characterization information for catalyst samples used in this study. a) ICP-OES elemental analysis as performed my Galbraith Laboratories. b) Adsorbed DME per Al atom on zeolites at 438 K. c) BET parameters fit to nitrogen adsorption data as taken from a Quantachrome Autosorb.

1.2.3 Zeolite structure and crystallinity via X-ray diffraction

Powder X-ray diffraction (XRD) measurements allow for the confirmation of crystallinity and identity of the catalyst samples employed. XRD patterns were collected on a Bruker AXS D5005 diffractometer using Cu- Kα radiation. Data were collected with a step size of 0.04° and a step time of 3 s. These experiments confirm that these commercial samples are their indicated structures (Figures 4 – 7).

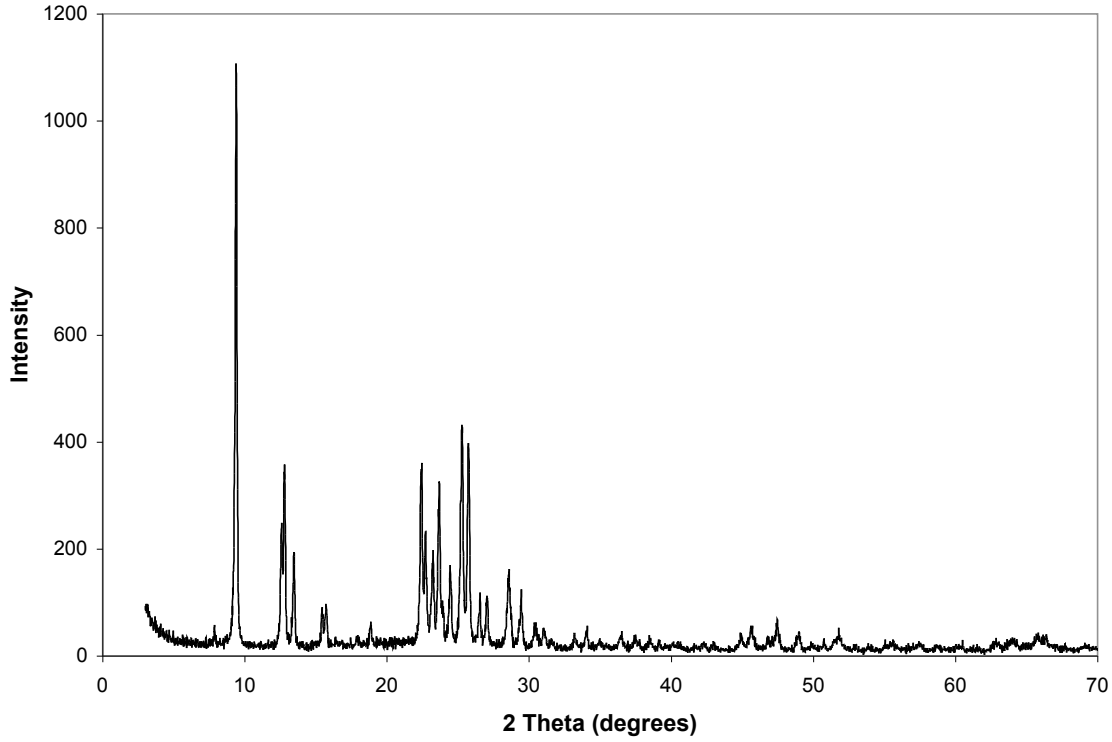

Figure 4. XRD pattern for H-FER (Si/Al = 11.5).

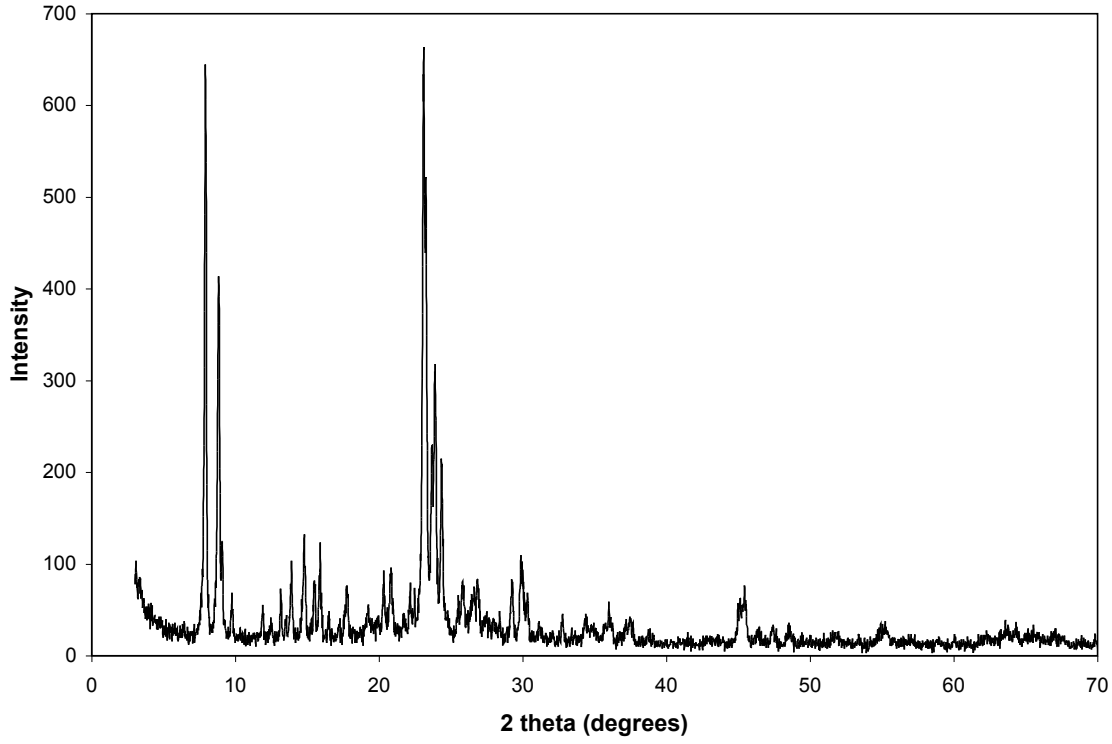

Figure 5. XRD pattern for H-MFI (Si/Al = 42.6).

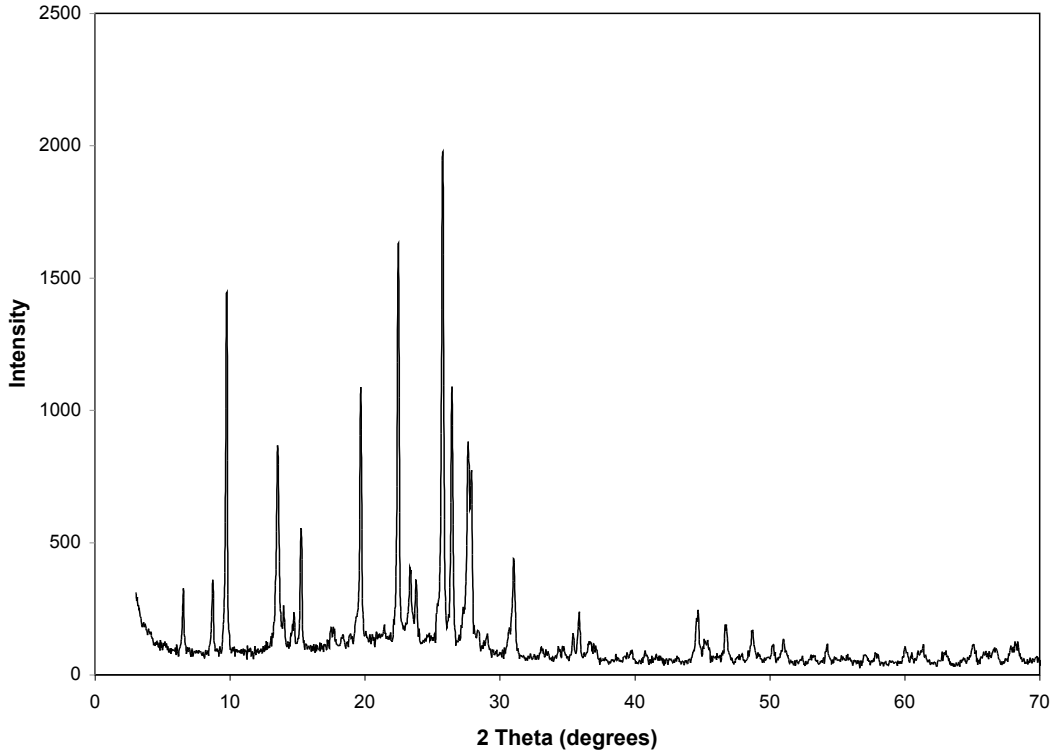

Figure 6. XRD pattern for H-MOR (Si/Al = 11.1).

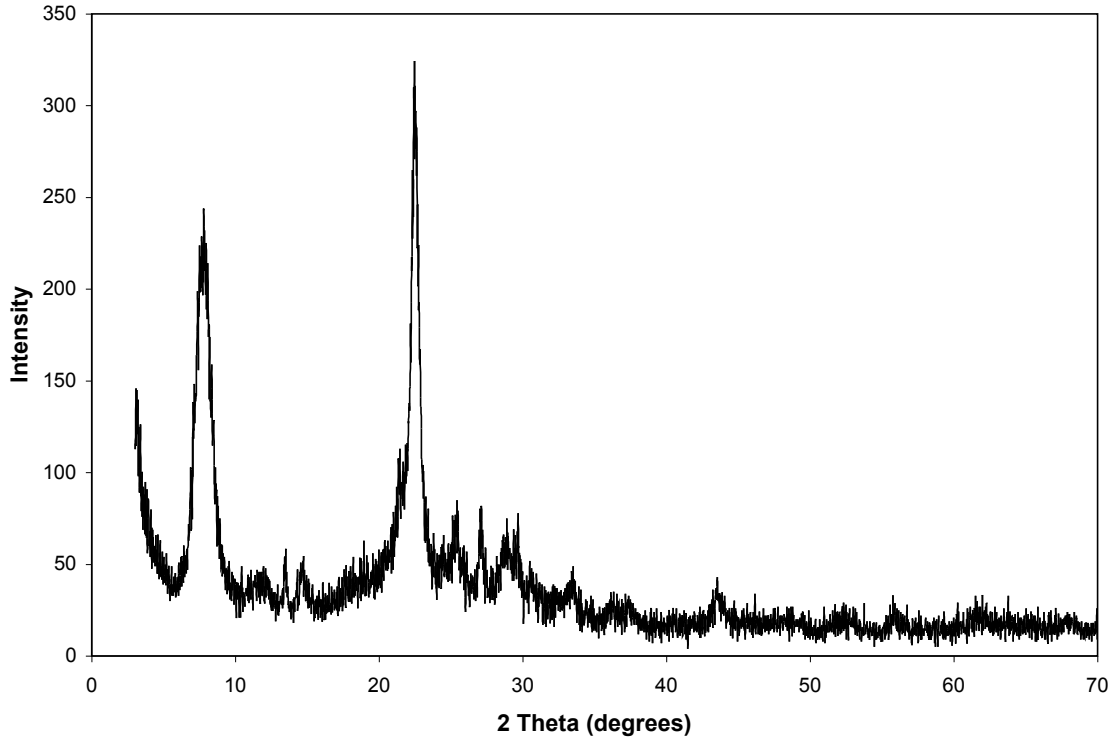

Figure 7. XRD pattern for H-BEA (Si/Al = 12).

1.3 Overview of methanol-to-hydrocarbons over zeolite catalysts

The methanol-to-hydrocarbons (MTH) process was first discovered by Mobile Research Laboratories in 1976, when methanol fed over zeolites led to the formation of methylated aromatics, and olefins and alkanes with preference towards branched isomers. [6] The selective formation of olefins or branched alkanes is particularly attractive as valuable precursors to polymers or as gasoline surrogates (namely 2,2,3 trimethylbutane, or triptane, which has an octane number of 112), respectively. [7,8] Methanol is also a versatile feedstock as it can be derived from any gasifiable carbon source, including coal, [9,10] biomass, [11,12] and natural gas, [13] via synthesis gas, which is a mixture of carbon monoxide and hydrogen from partial oxidation reactions, over Cu/ZnO catalysts (Equation 1 below). [14,15]

(1) $CO + 2\ H_2 \rightarrow CH_3OH$

The dehydration of two methanol molecules to form ethylene and water has been discounted as the predominant initiator of the MTH process due to an observed lengthening of the catalytic induction period as methanol and the zeolite catalyst were intensively purified. [16] This indicates that hydrocarbon impurities within methanol, or equivalently dimethyl ether (DME), or the zeolite catalysts are responsible for acting as CH_3* acceptors, which then undergo further chemical transformations to form the observed aromatic, olefin, and alkane products. The widely-accepted indirect "hydrocarbon pool" mechanism by Dahl and Kolboe, [17] indicates that aromatics and olefins [18-20] that are entrained within the zeolite micropores act as scaffolds for forming and breaking carbon-carbon bonds, with size restrictions dictated by the interior dimensions of the pore network. [21-24] Therefore, the observed product distribution of MTH is both a function of zeolite structure and the constituency of the aromatic and olefin hydrocarbon pools, and the extent to which these hydrocarbons methylate, cyclize, crack, and dealkylate (Figure 8).

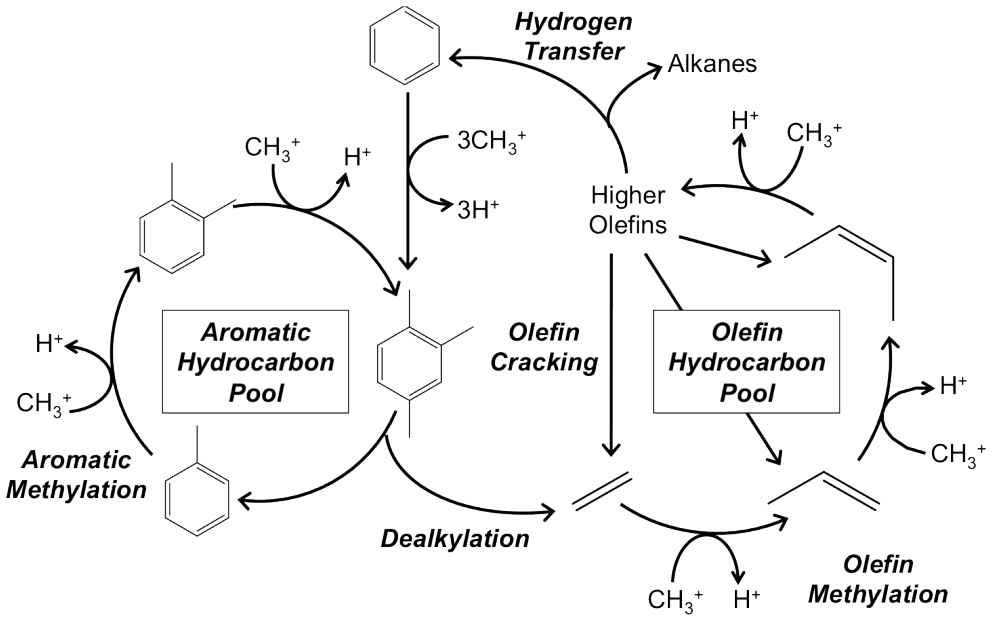

Figure 8. Dual olefin and aromatic methylation cycle that comprises the hydrocarbon pool mechanism for MTH on zeolite catalysts. Successive methylation steps upgrade olefins to higher homologues, which may crack or generate aromatics and alkanes via hydrogen-transfer steps. These aromatics are successively

methylated to form higher methylbenzenes and subsequently eliminate alkyl groups to form lower polymethylbenzenes (PMBs) and light olefins.

This work will attempt to describe and quantify the propagation of the olefin and aromatic methylation cycles through the isolation and determination of elementary step kinetics at differential conversions. The effects of zeolite and reactant structure on methylation rates, in addition to kinetic modeling, isotopic, and surface titration studies are used to determine mechanism of olefin and aromatic methylation and the active surface derivative of methanol or DME that is responsible for methylation.

Chapter 2: Kinetics and mechanism of olefin methylation reactions on zeolites

2.1 Introduction

Processing synthetic fuels and commodity chemical precursors from alternative carbon sources is a necessity in light of the depletion of global petroleum reserves. A methanol-based platform has become a dedicated topic of research as it is readily synthesized via the catalytic conversion of synthesis gas, [14,15] which is formed through the oxidative conversion of a variety of carbon-based feedstocks, including coal, [9,10] natural gas, [13] and biomass. [11,12] Acid-catalyzed conversion of methanol-to-hydrocarbons (MTH) can be used to produce hydrocarbons in the gasoline range, [7,8,16,17,25-34] aromatics [35-37] and light olefins [20,38-41] starting from either methanol or dimethyl ether (DME) although typically not with high selectivity. [6,25,42,43]

There has been much debate over the past 30 years regarding two aspects of the MTH reaction: the origin of the first C-C bond from the C_1 reactants and the mechanism by which the MTH reaction propagates. A broad consensus has emerged in the recent literature concerning the inability of zeolite-adsorbed C_1 species to couple directly into hydrocarbons at rates relevant for steady state MTH catalysis. The presence of persistent surface-bound C_1 methoxide species in zeolites has been described by Wang and Hunger using infrared spectroscopy and ^{13}C MAS NMR studies. [44] Waroquier et al. [45-47] have shown, through a series of theoretical studies, that energy barriers for C-H bond activation on surface-bound methoxide species are prohibitively large (242 kJ mol^{-1}) compared to indirect mechanistic routes involving the methylation of unsaturated hydrocarbons (<94 kJ mol^{-1}). [16,37] Isotopic distributions in product olefins in the ^{13}C-methanol methylation of aromatics have shown that all ethene and majority propene are formed through the cracking of arenes on H-ZSM-5, H-MOR, and H-BEA catalysts, and not direct coupling of C_1 species. [37] Experiments have also shown that the catalyst induction period is sensitive to hydrocarbon impurity concentrations in methanol. [16,30] These results show that over zeolite and zeotype catalysts the methylation of unsaturated hydrocarbons proceeds in the absence of direct ethylene formation from methanol

coupling. Haw et al. [48] report a binomial distribution of unlabeled:tri-labeled:hexa-labeled dimethyl ether in the product stream using a 1:1 mixture of unlabeled and d_6 dimethyl ether on SAPO-34 at 523 K clearly demonstrating the activation of C-O bonds, but no C-H bond cleavage as would be necessary in the formation of direct C_1 coupling products.

An early reaction mechanism for MTH outlined by Dessau and LaPierre [26,49] entails: (i) methylation of olefinic species to form higher homologues, (ii) formation of arenes and alkanes through hydrogen transfer steps, (iii) methylation of arenes to form methylbenzenes, and (iv) cracking reactions that form smaller olefinic species. Later work from Dahl and Kolboe stressed the importance of a co-catalytic "hydrocarbon pool," consisting of entrained organic species within the zeolite framework that act as a methylation and cracking center and are responsible for the generation of ethylene and propylene in the observed MTH product distribution. [17,50,51] Several theoretical and isotopic labeling studies have confirmed the importance of this indirect hydrocarbon pool mechanism. [17,22,28,30,37,41,50-57]

Extensive theoretical and experimental studies have focused on the role of entrained aromatic compounds - mainly polymethylbenzenes, as naphthenic species were calculated to have too high an energy barrier to compete over CHA frameworks using ONIOM derived energies and geometries (170 kJ mol^{-1} compared to 129 kJ mol^{-1}) [36]- as potential hydrocarbon pool organic co-catalysts. The gem-methylation of a methylbenzene species allows for one of three events to occur: (i) the elimination of the geminal hydrogen to complete the methyl substitution, (ii) elimination of a methyl hydrogen to allow for side-chain methylation (side-chain mechanism), [41,55] or (iii) the collapse from a 6-membered to a 5-membered ring, generating a branched alkyl substituent (paring mechanism). [21,22,28] These alkyl groups are then susceptible to cracking, forming the observed C_2-C_4 olefins in the product distribution and occluded lower methylbenzenes. The predominant occluded polymethylbenzenes and their methylated cation intermediates have also been directly observed using *in-situ* ^{13}C MAS NMR [22] and GCMS analysis of the hydrocarbon pool via HF digestion of the reacted zeolite/zeotype catalyst. [21,22] These studies have shown that large-pore zeolites and zeotype materials (like H-BEA and H-SAPO-34) operate via an aromatic hydrocarbon

pool consisting mostly of pentamethylbenzene and hexamethylbenzene while di-, tri-, and tetra- methylbenzenes dominate the aromatic hydrocarbon pool of medium-pore H-ZSM-5. [21,22]

Recently, computational [18,19,58] and experimental [20,24,40] studies have begun to focus on the viability and reactivity of an olefin hydrocarbon pool. The kinetic induction period observed and the inability to explain the primary product selectivity in MTH catalysis led several researchers early on to propose that a relatively inefficient mechanism leads to the formation of the first C-C bond followed by olefin chain growth and cracking. [26] Chen et al. [59] initially reported the auto-catalytic effect of olefinic compounds in MTH. Langner et al. [60] noted that co-feeding a small amount of higher alcohols led to an 18-fold reduction in the induction period. These initial studies all point to a catalytic role for olefin methylation where an existing olefin molecule is repeatedly methylated by methanol to form higher homologues. Lesthaeghe et al. [18] have shown through van der Waals corrected ONIOM calculations over 48T zeolite clusters that the energy barriers for olefin methylation are of similar magnitude (60 – 80 kJ mol^{-1}) to those for methylation of lower methylbenzenes in H-ZSM-5, thereby suggesting that the contribution of the alkene hydrocarbon pool towards the observed product distribution is significant. A reaction scheme for a "dual cycle" mechanism is outlined in Figure 8 of chapter 1; the two hydrocarbon pools undergo inter-conversion on H-ZSM-5 as demonstrated in recent isotopic studies from Olsbye et al. [37,61] where the authors show that 25-50% of the carbon in product ethylene and propylene originate from co-fed toluene in the presence of ^{13}C methanol, implying ethylene and propylene are formed primarily from dealkylation reactions of arene species.

Through the selective operation of one cycle of the dual cycle mechanism, the product selectivity of MTH chemistry can be systematically controlled. The arene methylation cycle is largely suppressed over H-ZSM-22 (a one dimensional, 10-member ringed channel zeolite) because arene methylation operates under space-limiting conditions while olefin methylation does not. [20,40,52,62] In this special case, propylene and higher-order olefins, which are the major products of the olefin cycle, are selectively produced over ethylene and alkanes/arenes, which arise from the formation and

dealkylation of arenes. [52] The complex role that the dual olefin-arene methylation cycle plays in the observed catalytic rate and selectivity for MTH implies that it is difficult to isolate one hydrocarbon pool cycle over another. Reduced methylation barriers with increasing olefin chain length, the subsequent isomerization of hydrocarbon products, and formation of olefinic species from both methylation and cracking reactions at conversions relevant for practice of MTH make quantitative evaluation of kinetic parameters of olefin methylation on zeolites experimentally challenging. The difficulty in isolating kinetically-relevant steps is evidenced by the sparse reporting of reaction rates and kinetic parameters for MTH reactions. [8,38,39,58]

In this work, methylation kinetics of ethylene and propylene were measured on proton form MFI, MOR, BEA, and FER zeolites at low olefin conversions (<0.2%) and high DME:olefin ratios (15-60:1). We report that the kinetics of olefin methylation are consistent with a mechanism involving a surface predominantly covered by DME derived species (0 order kinetics) that react with olefinic species in kinetically relevant steps (1st order kinetics). A systematic decrease in activation barriers was noted with increasing substitution of the olefin. These data show that MFI, MOR, BEA and FER zeolites propagate the olefin methylation cycle to varying extents and thereby explain the marked diversity in selectivity and yield for C_1 homologation using different zeolites.

The identity of the reactive C_1 surface species on the zeolitic Brønsted acid site responsible for the methylation of olefins and arenes determines the MTH reaction behavior under varying operating conditions. The reactant state for olefin methylation is either explained as a surface methyl group reacting with a gas-phase olefin, [44] or through the formation of a methanol/olefin co-adsorbed complex. [19,63,64] This report aims to elucidate the nature of the methylating surface species on zeolites via experimental evidence and energetic arguments in an effort to complete the mechanistic picture of the olefin methylation reaction cycle in MTH.

2.2 Materials and Methods

2.2.1 Catalyst preparation

FER, MFI, MOR, and BEA zeolite samples (silicon to aluminum ratios were determined by ICP-OES elemental analysis performed at Galbraith Laboratories) from Zeolyst were sieved in their NH_4^+ form to obtain aggregate particle sizes between 180 and 425 μm (40-80 mesh). Treatment in dry air (1.67 cm^3 s^{-1} NTP, ultrapure, Minneapolis Oxygen) during a 0.0167 K s^{-1} temperature ramp to 773 K and holding for 4 h thermally decomposed NH_4^+ to H^+ and $NH_{3(g)}$. Protonated zeolite samples used in this study are denoted as H-FER, H-MFI, H-MOR, and H-BEA. Chiang et al. [3] performed DME titration experiments of zeolite acid sites over the H-FER, H-MFI, and H-MOR samples used in this study and have shown that 0.5 DME molecules are adsorbed per acid site. From this information, we conclude that the Brønsted acid site concentration in these samples is nearly identical to the aluminum concentration determined by ICP-OES, which also excludes the presence of a significant fraction of Lewis acidic aluminum centers in these framework materials. [3]

2.2.2 Steady-state catalytic reactions of DME and light olefins

Steady-state olefin methylation reactions were carried out in a 9.52 mm OD packed-bed stainless steel tube reactor at atmospheric pressure and differential conversions (<0.2%). Catalyst samples (0.005 - 0.260 g) were supported between quartz wool plugs under isothermal conditions using a furnace (National Electric Furnace FA120 type) regulated by a Watlow Temperature Controller (96 Series). Catalyst temperature was monitored using a K-type thermocouple threaded through a coaxial thermal well penetrating the catalyst bed. Samples were treated in flowing He (1.67 cm^3 s^{-1}, ultrapure, Minneapolis Oxygen) at 773 K (0.0334 K s^{-1} temperature ramp) for 4 h prior to cooling to reaction temperatures (353 – 473 K). A mixture of dimethyl ether (DME), argon, and methane (50:49:1; Praxair certified standard grade) (0.26 – 0.62 bar) was combined with a C_2H_4 (Matheson Tri-Gas, chemical purity grade) or C_3H_6 (50:50 mixture with argon; Praxair certified standard grade) (0.005 – 0.03 bar) stream and He to

maintain a total flow rate of 1.67 cm^3 s^{-1}. Reaction order dependencies were determined by varying either DME or olefin flow rates in the feed stream while keeping the other constant and adjusting He flow to compensate for the change in overall reactant flow rate. Reactor effluent composition was monitored via gas chromatography (Agilent 7890) through a methyl-siloxane capillary column (HP-1, 50.0 m x 320 μm x 0.52 μm) connected to a flame ionization detector and a packed column (Supelco HAYSEP DB packed column, 12 ft) connected to a thermal conductivity detector.

2.2.3 Introduction of d_6-DME in ethylene methylation reactions on H-MFI

Isotopic experiments were performed on the experimental set-up described above. A 0.42 cm^3 s^{-1} total flow of ethylene (0.03 bar) and a mixture of 50:49:1 DME:Ar:CH_4 (0.67 bar) with balance helium was passed over 100 mg of H-MFI for 4.6 h at 393 K. At steady-state reaction conditions, DME pressure was reduced to 0.17 bar and 0.15 bar d_6 DME (Isotec, 99.9 at% isotopic purity) was introduced into the reaction system. Product mass distributions were monitored using an online mass spectrometer (MKS Cirrus 200 Quadrupole mass spectrometer system) and ethylene methylation rates were monitored using gas chromatographic protocols described above.

2.3 Results and Discussion

2.3.1 Ethylene Methylation

Steady-state ethylene methylation reactions were run at differential conversions (<0.2%) to maintain low propylene concentrations, inhibiting secondary and further reactions. Figure 1 shows that every zeolite probed in this study obeys a first-order dependence of the propylene formation rate on the partial pressure of ethylene. Propylene formation rates on all zeolites are independent of DME partial pressure (Figure 9). These data are consistent with a mechanism involving a zeolite surface predominantly covered with a DME-derived species that reacts with ethylene to form propylene in the rate-limiting step. Our observations are consistent with the first-order rate dependence in

ethylene and zero-order dependence in methanol partial pressure reported by Svelle et al. [38]over H-MFI at 623 K. These authors extrapolated rates to zero conversion because at the higher temperatures used in their study, secondary products were observed, however, under the low temperature and high DME pressure conditions used in this study, no secondary reactions are observed.

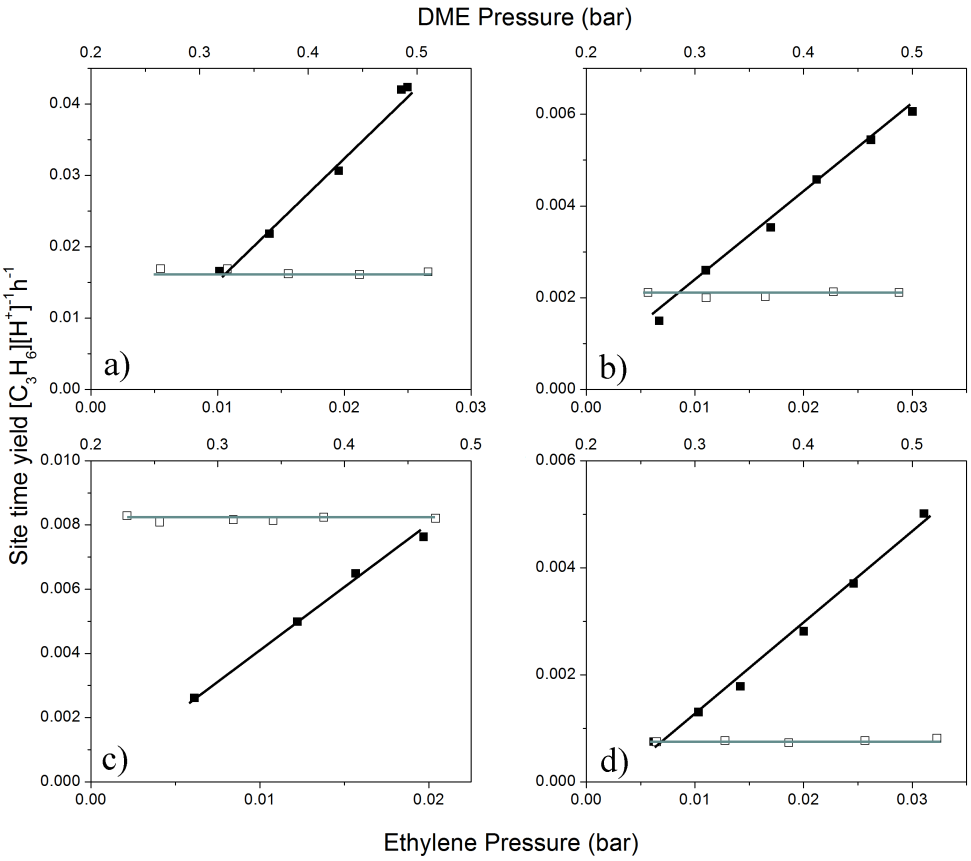

Figure 9. Dependence of the propylene formation rate on ethylene partial pressure (closed symbols) and DME partial pressure (open symbols). Ethylene pressure was varied from 0.005 – 0.034 bar, and DME pressure was varied from 0.21 – 0.52 bar DME. (a) H-BEA at 365 K (b) H-FER at 370 K (c) H-MFI at 370 K and (d) H-MOR at 380 K.

Activation barriers and temperature-normalized rate constants were obtained from Arrhenius plots generated from reaction rate data at various temperatures (Figure 10). Measured rate constants for ethylene methylation show a clear trend from ethylene pressure dependent studies (Note: data sets reported in figure 1 were obtained at

temperatures between 365 and 380 K making direct comparisons possible) and from temperature dependent studies: $k_{BEA}>k_{MFI}>k_{FER}>k_{MOR}$ (Table 2). A comparison of the activation energy of H-MFI obtained in this report shows good agreement with previously reported values for reactions of methanol and ethylene at 623 K (94 kJ mol^{-1} compared to 109 kJ mol^{-1}, respectively), [38] and theoretical studies using hybrid MP2:DFT calculations on clusters using corrections from periodic DFT calculations (104 kJ mol^{-1}) [63] and a simplified cluster with a harmonic oscillator approximation for zeolite framework bonds (94 kJ mol^{-1}). [58]

Sample (Si/Al)	E_a (kJ mol^{-1})	k_{373} (h^{-1} bar^{-1})	A (h^{-1} bar^{-1})
H-FER (10)	84	0.21	1×10^{11}
H-MFI (40)	94	0.35	3×10^{9}
H-MOR (11)	61	0.08	4×10^{7}
H-BEA (12)	62	0.79	3×10^{8}

Table 2. A comparison of kinetic parameters for ethylene methylation over proton form zeolites.

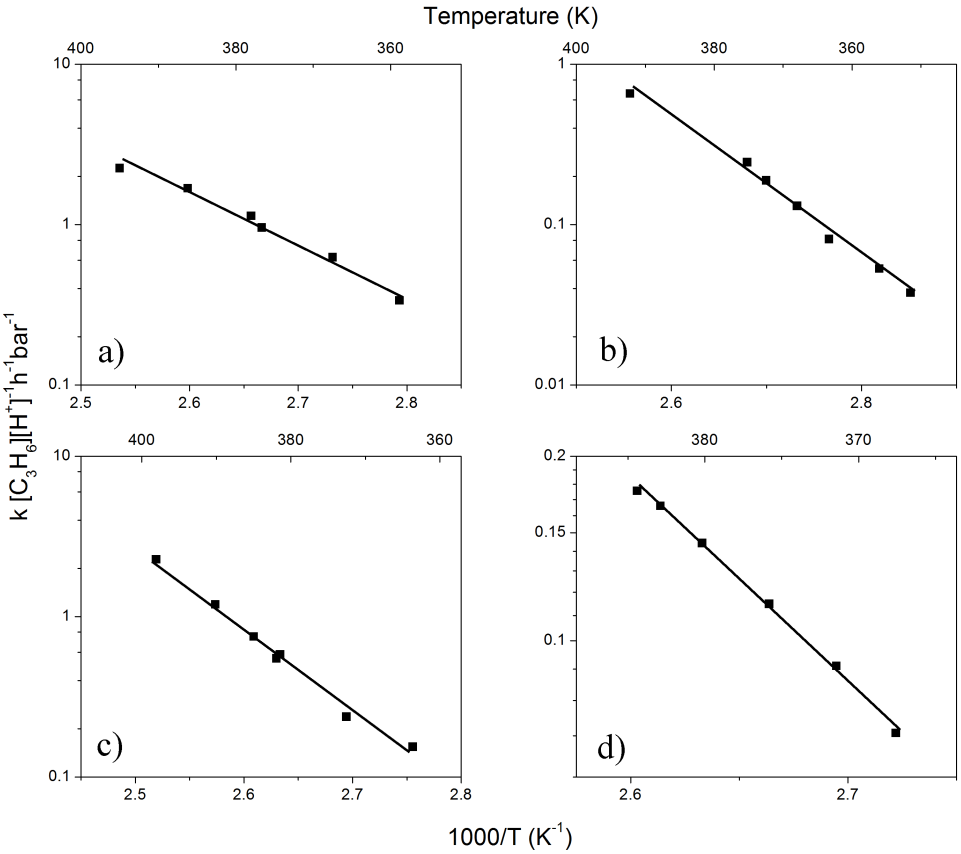

Figure 10. Temperature dependence of the first-order rate constant for propylene formation in ethylene methylation reactions (0.02 bar C_2H_4 and 0.31 bar DME, T = 360 – 400 K). (a) H-BEA (b) H-FER (c) H-MFI and (d) H-MOR.

2.3.2 Propylene Methylation

An analogous set of experiments to those conducted for ethylene methylation was performed for propylene methylation over H-MFI, H-BEA, H-FER, and H-MOR zeolites. Reaction rates for butene formation increase linearly with increasing propylene partial pressure, and are independent of the DME partial pressure (Figure 11). Svelle et al. [39] have reported similar trends for propylene and methanol partial pressures for the methylation of propylene to butenes with methanol on H-ZSM-5 at 523 K. We show that

first order dependence in propylene and zero order dependence in dimethyl ether describes the kinetics of propylene methylation across various zeolites.

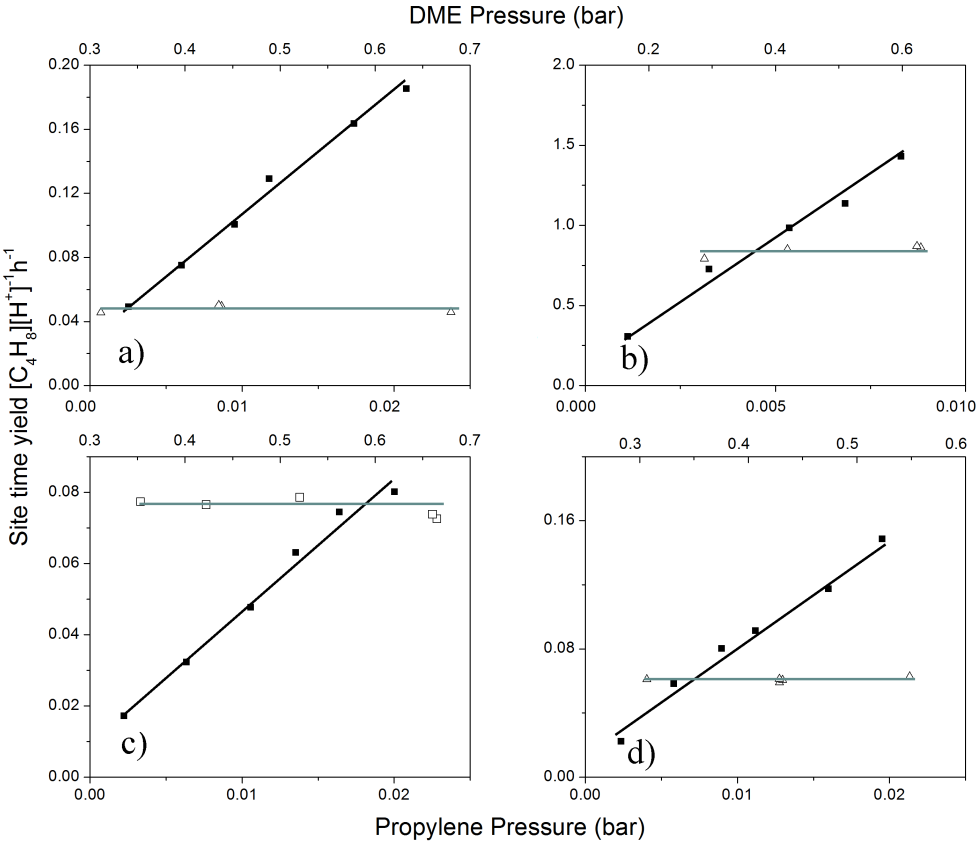

Figure 11. Dependence of the butene formation rate on propylene partial pressure (closed symbols) and DME partial pressure (open symbols). Propylene pressure was varied from 0.002 – 0.023 bar, and DME pressure was varied from 0.30 – 0.69 bar DME. a) H-BEA at 355 K b) H-MFI at 404 K c) H-MOR at 404 K and d) H-FER at 420 K.

A variety of temperatures were required to maintain butene conversions below 0.2% as secondary reactions became significant, particularly on H-BEA. In light of this fact, data shown in the pressure dependence studies are not directly comparable as they were in the case of ethylene methylation. Arrhenius plots generated from propylene methylation rate data at various temperatures show that these catalysts exhibit similar

activation energies, but rate constants at 413 K vary by a factor of 30 (Figure 12 and Table 3).

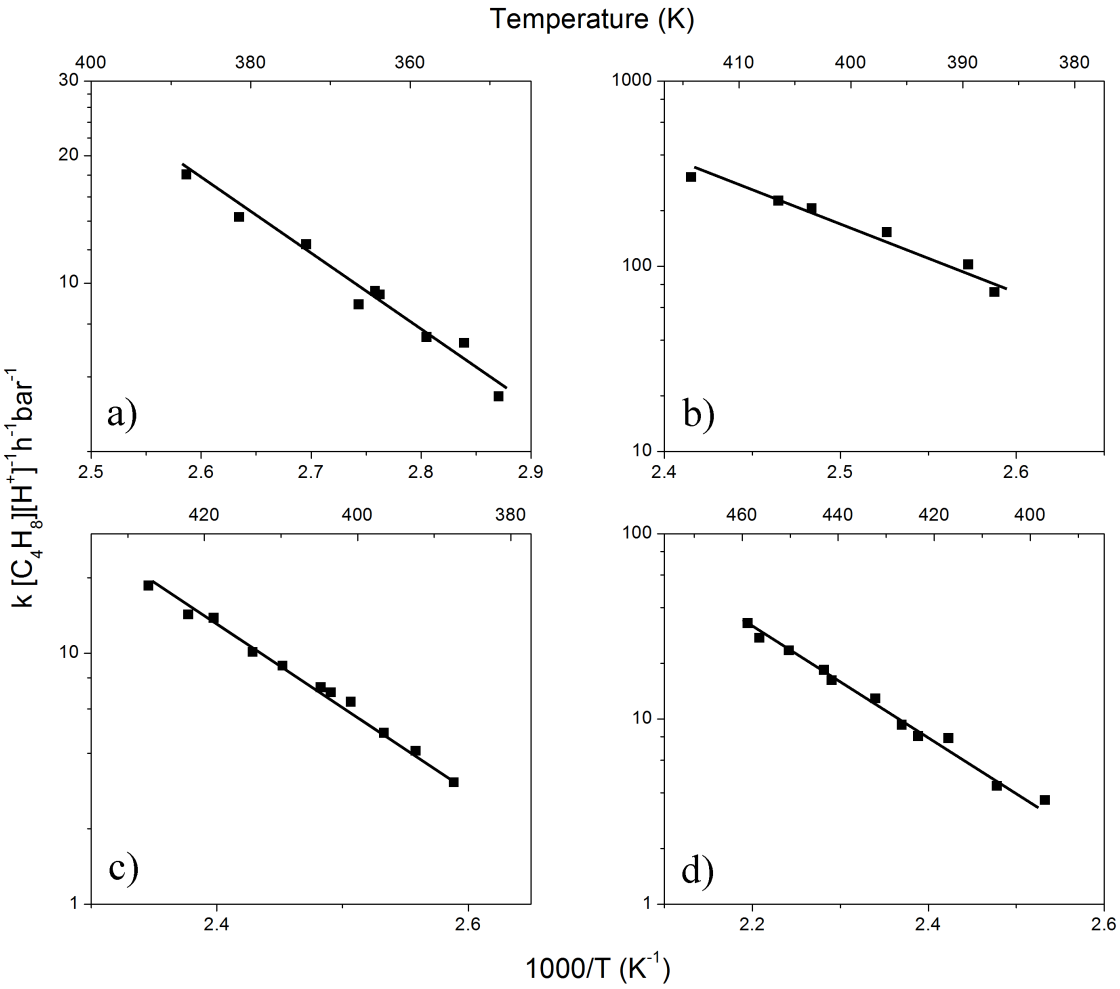

Figure 12. Temperature dependence of the first-order rate constant for butene formation in propylene methylation reactions (0.01 bar C_3H_6 and 0.62 bar DME, T = 345 – 430 K). a) H-BEA b) H-MFI c) H-MOR and d) H-FER.

A comparison of the activation energy of H-MFI obtained in this report shows good agreement with previously reported values for methylation of propylene at 623 K with methanol (61 kJ mol^{-1} compared to 69 kJ mol^{-1}, respectively), [39] and theoretical studies using hybrid MP2:DFT calculations on clusters using corrections from periodic DFT calculations (64 kJ mol^{-1}) [63] and a simplified cluster with a harmonic oscillator approximation for zeolite framework bonds (62 kJ mol^{-1}). [58] The reaction rate constant calculated for propylene methylation over H-BEA is within a factor of two compared to

the first-order rate constant calculated from the propylene methylation rate reported by Simonetti et al. (1.5×10^{-2} compared to 7.4×10^{-3} mol [mol Al s bar]$^{-1}$ at 473 K). [8]

Sample (Si/Al)	E_a (kJ mol^{-1})	k_{413} (h^{-1} bar^{-1})	A (h^{-1} bar^{-1})
H-FER (10)	57	6.5	1×10^{8}
H-MFI (40)	61	190.2	2×10^{10}
H-MOR (11)	58	13.1	3×10^{8}
H-BEA (12)	54	131.2	8×10^{12}

Table 3. A comparison of kinetic parameters for propylene methylation over proton form zeolites

The pressure dependence studies discussed above show that olefin methylation proceeds via the same mechanism regardless of olefin chain length and zeolite topology, making the comparison of rate constants and activation parameters across these variables valid. Structures MFI and BEA systematically show higher rates of olefin methylation compared to FER and MOR frameworks for both ethylene and propylene. Our results for olefin methylation kinetics on different zeolites reported in Tables 1 and 2 are in agreement with those reported by Svelle et al. [38,39] for H-ZSM-5 by tracking ^{13}C methanol methylation of C_2-C_4 olefins at 623 K. The data reported in Tables 1 and 2 show that olefin methylation rate constants increase and activations energies decrease systematically for higher-order olefins. These trends are consistent with those expected for carbocation stability with increasing alkyl substitution. Pre-exponential factors observed in this study are upper-bound by those outlined by Dumesic et al. [65] for Eley-Rideal mechanisms on surfaces ($<10^{12}$ h^{-1}bar^{-1}).

2.3.3 Mechanism of olefin methylation reactions: co-adsorbed species or surface CH_3 groups

An outstanding question pertaining to the methylation of olefins is the identity of the active DME-derived species on the zeolite surface that is responsible for the

methylation of olefins. Surface species that have been investigated to exist at zeolite Brønsted acid sites under olefin methylation conditions include:

(i) a co-adsorbed DME/methanol and olefin complex
(ii) methanol dimers, and
(iii) surface-bound methoxide groups

In a series of papers, Svelle et al. [19,64] have shown that the heats of co-adsorption for DME/methanol and an olefin are largely influenced by the choice of methylating agent (97 kJ mol^{-1} for DME/C_3H_6 co-adsorption compared to 114 kJ mol^{-1} for methanol/C_3H_6 co-adsorption) and not the olefin (111 kJ mol^{-1} and 114 kJ mol^{-1} for C_2H_4 and C_3H_6, respectively at 298 K) using combined DFT and ab-initio calculations on 4T model zeolite clusters. The relative importance of the choice of methylating agent was confirmed experimentally as a factor of 2.5 increase in the rate of propylene methylation was observed when feeding DME compared to methanol at 523 K over H-ZSM-5. [64] Theoretical studies carried out on H-ZSM-5 by Sauer et al. [63] using hybrid MP2:DFT calculations with periodic boundary conditions have also shown that the adsorption of methanol is stronger than that of subsequent co-adsorption with an olefin (-115 for methanol adsorption compared with -37 and -53 kJ mol^{-1} for C_2H_4 and C_3H_6 co-adsorption, respectively) and a ~2 kJ mol^{-1} difference was observed when ethylene was co-adsorbed with methanol in a purely silaceous framework compared to a framework containing Brønsted acid sites, indicating that van der Waals interactions with the zeolite pore walls are the dominant factor in ethylene adsorption as opposed to adsorbing at a Brønsted acid site. Work from Mirth and Lercher [66] shows that toluene/methanol co-adsorption complexes decompose first by loss of toluene at 473 K under 10^{-6} mbar vacuum, followed by the incomplete desorption of methanol using temperature programmed desorption techniques monitored via infrared spectroscopy and mass spectrometry. These studies clearly show that the major contribution to the heat of adsorption of DME/methanol and olefin co-adsorbed complexes arise from the initial adsorption of the methylating agent.

Lee and Gorte have shown that the differential heat of adsorption for methanol on H-ZSM-5 (ΔH_{ads} = -115 kJ mol^{-1}) does not change significantly for loadings up to 2 methanol molecules per acid site using microcalorimetry experiments at 400 K. [67] Waroquier et al. [45] have reported an enthalpy of adsorption, ΔH_{ads} = -73.3 kJ mol^{-1} and an activation barrier, E_{act} = 98 kJ mol^{-1} for the formation methanol dimers on model H-ZSM-5 at 720 K using ONIOM calculations over 30T and 46T clusters. Methanol activation studies performed by Blaszkowski and van Santen using self-consistent non-local corrected DFT have shown that the adsorption of a single methanol molecule on a Brønsted acid site has a ΔH_{ads} = -75 kJ mol^{-1} and the formation of methanol dimers has an enthalpy of adsorption, ΔH_{ads} = -121-130 (1T vs 3T cluster) kJ mol^{-1}. [68] With similar adsorption energies to those reported for methanol-alkene co-adsorbed species (-111-152 for ethylene and -114-168 for propylene) [19,63,64] and observed 2 methanol-per-site loadings from microcalorimetric measurements taken at 400 K, [67] the formation of methanol dimer species is not insignificant when considering mechanistic steps from physisorbed states. Work from Stich et al. [69] has shown that the activation of methanol is most facile in the absence of external hydrogen bonding using first principle molecular dynamics simulations. This suggests that methanol dimers would be inadequate methylating agents for olefins as their mutual hydrogen bonding results in enhanced species stability.

Unlike surface-bound higher alkoxides, surface-bound methoxide species are unable to desorb due to the lack of a β-H. [44,70] This results in a highly stable intermediate species, observed via high-temperature *in situ* infrared spectroscopy studies to exist in vacuum at 673 K before surface-bound C-H stretches diminished in coke formation. [71] Bosacek [72] and Hunger et al. [44] have experimentally observed surface methoxide species on H-ZSM-5 using solid-state ^{13}C MAS NMR at 473 K in and continuous flow setups, [44] and infrared spectroscopy studies have also reported the formation of surface-bound methoxides using deuterated methanol. [73] The reactivity of observed surface-bound methoxide species has been probed using methanol (forming DME), water (forming methanol), and ammonia (forming methylamines) over zeolites H-Y and H-ZSM-5 and zeotype H-SAPO-34. [44] Theoretical studies utilizing DFT, ab-initio, and mixed methods

(ONIOM) over small 3T-5T clusters have reported 215, [74] 217, [75] and 223 [46] kJ mol^{-1} barriers toward the dehydration of a physisorbed methanol molecule on a zeolite acid site to form a surface-bound methoxide species and water. It is these high barriers that have led to the conclusion that mechanisms involving methoxide species are unfavorable to those proceeding via associative mechanisms of co-adsorbates. In recent work, Boronat et al. [76] have studied the formation of surface methoxide species on 121-130 atom clusters of MOR from DME and methanol in both 12 membered-ring and 8 membered-ring environments using DFT-D methods. When dispersion interactions within the MOR framework are taken into consideration, activation barriers for surface methoxide formation are 8 kJ mol^{-1} and 12 kJ mol^{-1} from methanol and DME, respectively, concluding that computational studies done using small clusters result in inordinately high activation barriers for the formation of surface methoxide species. [76]

Co-feed DME and d_6 DME experiments at steady-state olefin methylation reaction conditions were done to provide mechanistic insight regarding the nature of the active surface species and the role of C-H bonds in the rate-determining step. Unreacted DME and d_6 DME scrambling about C-O bond was observed by the presence of a 1.2:1.5:1 distribution of d_0:d_3:d_6 isotopic distribution in the product stream. Similar observations were made using a 1:1 d_0:d_6 DME feed in the absence of the MTH reaction (yielding a 1:2:1 d_0:d_3:d_6 isotopic distribution) by Haw et al. at 523K. [48] Significant scrambling about the C-O bond at the reaction conditions reported herein proves that fast and reversible formation of surface-bound methoxides occurs during olefin methylation reaction conditions. A co-adsorbed mechanism would only break the DME C-O bond in direct association with an adsorbed olefin. The olefin methylation rate decreased by a factor of 1.3 in the presence of a 1.2:1 d_0:d_6 DME feed compared to purely unlabeled reagents. This observed rate difference is consistent with a positive secondary kinetic isotope effect, indicating the transition from an sp^3 to sp^2 hybridized methyl species in the generation of the activated complex without the cleavage of a C-H bond. [77]

From these experimental results, we propose two possible mechanisms that proceed via a planar methyl transition state (Figures 13 and 14). One of these mechanisms postulates the formation of a cyclopropyl cation intermediate (Figure 13).

These species have been proposed to explain cracking and hydroisomerization selectivity towards branched hydrocarbons and low yields to light olefins in solid acid catalyzed reactions. [78-80] The reaction mechanism may also proceed through the direct addition of a surface-bound methoxide to an olefin, generating the n+1 alkoxide (Figure 14). Both of these routes would be rate limiting in the methylation step and necessarily exclude the direct breaking of C-H bonds, as this would yield a primary kinetic isotope effect. Increasing rates and decreasing activation energies with increasing carbon substitution can be explained with increasing cyclopropyl [78-80] and carbocation [7,8] stabilization via electron-donating and hyperconjugative effects from alkyl substituents.

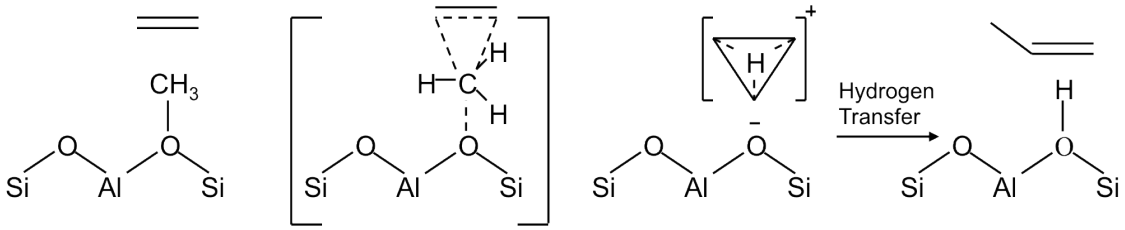

Figure 13. Proposed ethylene methlyation scheme involving the addition of a surface-bound methoxide group to ethylene to form a propoxide intermediate via a planar CH3+ group. Deprotonation at the β-position forms propylene and regenerates a zeolitic *Brønsted acid site.*

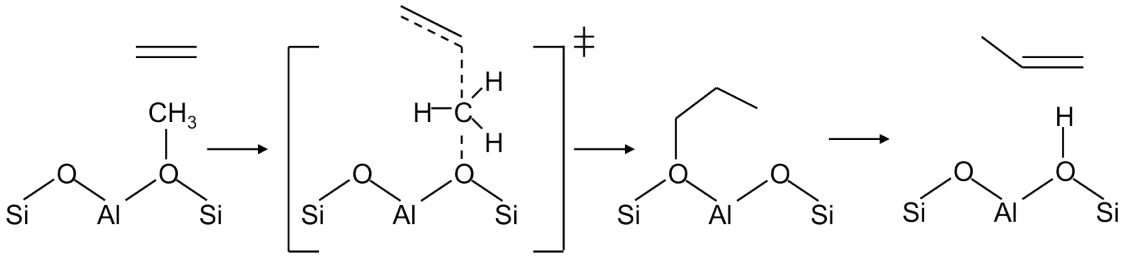

Figure 14. Proposed ethylene methlyation scheme involving the addition of a surface-bound methoxide group across the olefinic double bond to form a cyclopropyl cation intermediate. Rapid hydrogen transfer, deprotonation, and ring collapse form propylene and regenerate a zeolitic Brønsted acid site.

The proposed cyclopropyl mechanism explains *in situ* infrared spectroscopic observations by Yamazaki et al. [71] of the selective regeneration of zeolite active sites on H-ZSM-5 from hydrogen originating from methanol/DME in d_3-methanol methylation of olefins, as the cyclopropyl intermediate can only be protonated by the hydrogen-rich

surface methoxide group. While the cyclopropyl mechanism explains the experimental results reported herein and the observations by Yamazaki et al., [71] other zeolites may proceed through cyclopropyl or carbocationic intermediates as outlined in scheme 2.

Our studies in this report show that olefin methylation reactions proceed via similar mechanistic routes on proton form BEA, MFI, FER, and MOR zeolites; however, these reactions are propagated to varying extents by different zeolites thereby providing an initial hypothesis for the marked diversity in C_1 homologation selectivity and yield observed with varying structure. [81] Our findings also evidence that surface methoxide groups are formed under methylation reaction conditions and that the transition state of the rate-limiting step proceeds via an sp^2 hybridized configuration generated from an sp^3 hybridized precursor state without breaking C-H bonds consistent with these surface-bound methoxide species being responsible for the methylation of olefins.

2.4 Conclusions

Rate constants for ethylene and propylene methylation over H-MFI, H-BEA, H-MOR, and H-FER at temperatures < 473K in excess DME and ~0.2% conversion have shown that H-BEA and H-MFI propagate the olefin methylation cycle of the hydrocarbon pool mechanism to a greater extent than H-MOR and H-FER. Observed rate constants and activation parameters for H-MFI and H-BEA coincide with those previously reported at higher temperatures and conversions. [8,38,39] Rate constants were found to be systematically higher and activation energies were found to be systematically lower for C_3H_6 methylation compared to C_2H_4 methylation for every zeolite framework studied, showing that increased olefin substitution affords an increased stabilization of reaction intermediates and/or transition states. Pressure dependence experiments show a first order rate dependence on olefin partial pressure and a zero order rate dependence on DME partial pressure over all frameworks studied, consistent with a zeolite surface predominately covered with DME-derived species reacting with an olefin. Temperature dependence studies yielded pre-exponential factors consistent with Eley-Rideal kinetics, also in line with an activated DME-derived surface species reacting with an olefin. [65]

Steady-state ethylene methylation in the presence of un-labeled and d_6 DME has shown that the scission and formation of the DME C-O bond is fast compared to olefin methylation reactions through the statistical distribution of d_0:d_3:d_6 DME in the unreacted feed, indicating the facile formation of surface methoxide species on the zeolite surface. A secondary kinetic isotope effect was observed with the introduction of d_6 DME into the reaction system, consistent with a planar transition state for surface methyl species from a tetrahedral precursor in the absence of C-H/C-D bond cleavage. These experimental observations are consistent with a mechanism for olefin methylation on all zeolites involving the formation of surface methoxide groups that react with olefins.

Acknowledgements

This work was supported by the Abu Dhabi-Minnesota Institute for Research Excellence (ADMIRE); a partnership between the Petroleum Institute of Abu Dhabi and the Department of Chemical Engineering and Materials Science of the University of Minnesota. Acknowledgment is also made to the donors of the American Chemical Society Petroleum Research Fund for partial support of this research. The authors would also like to thank Yong Sam Ng for his contributions to the reaction studies presented herein.

Chapter 3: Kinetics of butene isomer methylation with dimethyl ether over zeolite catalysts

3.1 Introduction

The mechanism underlying the methanol to hydrocarbons (MTH) process over acidic zeolites has been a topic of debate since its discovery by Mobil in 1977. [6,25] The failure of direct methanol C-C coupling to explain prolonged induction periods with increasing methanol purity, [16] product isotopomer distributions in labeling experiments, [29,48,61] and high activation barriers for ylide formation via computational methods [45-47] supports an indirect "hydrocarbon pool" mechanism first proposed by Stein and Kolboe. [17,50,51] This mechanism states that unsaturated hydrocarbons trapped within the zeolite framework undergo methylation, dealkylation, and hydrogen transfer reactions to generate the observed MTH products over zeolite and zeotype materials, in effect, acting as co-catalysts. Olefins and aromatics have been shown to be present within the zeolite framework under MTH reaction conditions through spectroscopic [27,82] and analytical [21,22,83] techniques. Experiments co-feeding propene or toluene with DME over MFI at 548 and 623 K have shown that olefins increase product selectivity to C_4 to C_7 aliphatic hydrocarbons and aromatics increase selectivity to methylbenzenes and ethene. The overall product selectivity over MFI can be selected using varying mole fractions of both propene and toluene in 4 kPa co-feed stream. [84]

Aromatic methylation and subsequent dealkylation determine product selectivity towards aromatics and light olefins for MTH reactions, as observed via $^{12}C/^{13}C$ methanol switching experiments over SAPO-34, [85] BEA, [21,22] and MFI. [24] These experiments allowed the authors to attribute the differences in propene/ethene selectivity to differences in the degree of methylation of the aromatic hydrocarbon pool. Polymethylbenzenes comprise the major aromatic species entrained within the zeolite framework as observed by *in-situ* ^{13}C MAS NMR [22] and via GCMS analysis of the HF digest from the spent zeolite/zeotype catalyst. [21,22,24,85] These studies showed that larger pore BEA[16,17] and SAPO-34 [85] have penta- and hexa- methylbenzenes as the most active

methylation and dealkylation species, while MFI [21,22,24,85] showed higher alkylation activity for di- tri- and tetra- methylbenzenes.

Dessau and La Pierre [26,49,86] proposed a methylation cycle of olefins over MFI. The slow methylation of ethene and the promotion of longer-chain olefins to aromatics were included in their model from primary product reaction studies performed by monitoring product selectivity at high space velocities. Chen et al. [59] noted that co-feeding olefins led to the increased production of higher olefins in MTH reactions and occurred much faster than ethene formation. Langner et al. [60] noted that the induction period observed for MTH reactions could be decreased by up to 18 fold through the addition of alcohols, which rapidly dehydrate to olefins at 473K over acid catalysts. Medium channel TON has been shown to selectively methylate olefins in the absence of cyclization and dealkylation reactions. [20] Ethene methylation reactions run over this framework showed that propene and subsequent olefins selectively added carbon from ^{13}C labeled methanol at 623 K. [20] Experimental work on MFI by Svelle et al. [38,39] has shown that, at 623 K and 1:1 methanol and olefin pressures, rate constants and activation energies can be obtained by extrapolating reaction rates to infinite space velocities for ethene, propene, and 1-butene. These studies found that the methylation rate constant increases as olefin substitution increases concurrently with a systematic decrease in the apparent activation energy. Pressure dependence studies found that the reaction rate is independent of methanol partial pressures, but monotonically increases with olefin pressures. [38,39] Computational modeling of these reaction systems based on hybrid MP2:DFT on clusters with periodic corrections [63] and simplified clusters using a harmonic oscillator approximation for zeolite framework bonds [18,58] has verified these reaction parameters based on mechanisms involving the co-adsorption of methanol and an olefin at a single zeolite acid site. The co-adsorption mechanism considers methylation reactions to proceed through the decomposition of a methanol-olefin co-adsorbed complex. An alternative mechanism involves the initial dehydration of methanol/DME to form surface methyl groups and subsequent reactions of these methyl groups with olefins. The existence and persistence of surface methoxides on zeolites has been clearly demonstrated by FTIR [71] and ^{13}C MAS NMR [44,87] studies at 453 K and above, consistent

with the inability of surface CH_3 groups to desorb from the surface except by reaction. The discrepancy between theoretical results and spectroscopic studies is indicative of the ongoing debate arising from the two mechanisms, and a basis to explain the origins of these conflicting observations is necessary to elucidate the identity of the methylating agent. [88]

This work aims to systematically quantify rate constants and activation energies for butene methylation over zeolites of varying structures, continuing work that explored zeolite topology effects on ethene and propene methylation. [89,90] Based on the elementary-step rate parameters reported herein, rate constants increase substantially as intermediate carbocation substitution increases. In addition, high butene pressure experiments were performed to test the kinetic behavior of methylation reactions based on predictions for the co-adsorbed mechanism and the surface methoxide-mediated mechanism, and titration of DME-derived intermediates subsequent to butene methylation reactions enabled the identification of surface intermediates present during steady-state olefin methylation.

3.2 Materials and methods

3.2.1 Catalyst preparation

Zeolites FER, MFI, MOR, and BEA were obtained from Zeolyst in their NH_4^+ form and ICP-OES elemental analysis performed by Galbraith Laboratories was used to determine the aluminum content of each material (See Table S.1 in the Supplementary Information for results from elemental analysis, DME titration experiments, N_2 adsorption experiments, and XRD). Zeolites were sieved to aggregate sizes between 180 and 425 μm and treated in dry air (1.67 $cm^3\ s^{-1}$ NTP, ultrapure, Minneapolis Oxygen) with a 0.0167 K s^{-1} temperature ramp to 773 K and holding for 4 h to obtain the H^+ counter-ion. Protonated zeolite catalysts used in this study are referred to as H-FER, H-MFI, H-MOR, and H-BEA.

3.2.2 Steady-state catalytic conversion of DME and butene isomers

Steady-state methylation reactions of 1-butene, *trans*-2-butene, *cis*-2-butene, and isobutene were performed in a 10 mm inner diameter packed-bed quartz reactor at atmospheric pressure and differential conversions (<0.1% pentene + hexene formation). Catalysts were supported on a quartz frit inside the reactor, and the temperature was controlled using a furnace (National Electric Furnace FA120 type) connected to a Watlow Temperature Controller (96 series). Catalyst temperatures were measured using a K-type thermocouple at the bottom of a well penetrating the catalyst bed. Samples (0.005 – 0.010 g, diluted in quartz sand) were treated in flowing He (1.67 cm^3 s^{-1}, ultrapure, Minneapolis Oxygen) at 773 K (0.0334 K s^{-1} temperature ramp) for 4 h prior to cooling to reaction temperatures (258 – 333 K). A mixture of dimethyl ether (DME), argon, and methane (50:49:1; Praxair certified standard grade) (0.15 – 0.98 bar) was combined with C_4H_8 (Sigma-Aldrich, >99%) (0.001 – 0.03 bar) stream and He to maintain a total flow rate of 1.67 cm^3 s^{-1} (*trans*-2-butene*, cis*-2-butene, and 1-butene) or 0.84 cm^3 s^{-1} (isobutene). Reaction order dependencies were determined by varying either DME or olefin flow rates in the feed stream while keeping the other constant and adjusting He flow to compensate for the change in overall reactant flow rate. Reactor effluent composition was monitored via gas chromatography (Agilent 7890) through a methyl-siloxane capillary column (HP-1, 50.0 m x 320 μm x 0.52 μm) connected to a flame ionization detector and a packed column (Supelco HAYSEP DB packed column, 12 ft) connected to a thermal conductivity detector.

3.2.3 In-situ titration of surface species present during olefin methylation

Steady state methylation of *cis*-2-butene with 200 mg BEA at 273 and 282 K and 0.03 bar olefin in the presence of 0.6 bar DME was maintained for 2 hours prior to switching to 0.83 cm^3 s^{-1} He. Temperature was increased to 423 K at a rate of 0.25 K s^{-1} and held for 0.5 h, followed by introduction of 0.08 cm^3 s^{-1} water using a syringe pump. Effluent compositions were monitored online using an MKS Cirrus quadrupole mass spectrometer and quantified using Ar as an internal standard.

3.3 Results and discussion

We have systematically examined the kinetics and mechanism of butene isomer methylation to quantitatively assess the dependence of reaction rates, rate constants, and activation energies on olefin substitution and zeolite pore structure. These studies were performed in the absence of olefin isomerization, oligomerization, and hydride transfer reactions. Arguments regarding the identity of the DME-derived methylating agent on the zeolite surface are included based on derived kinetics and direct titration of surface intermediates.

3.3.1 Effect of zeolite topology on 1-butene methylation

DME and 1-butene pressure dependence studies were performed over zeolites BEA, MOR, MFI, and FER. The rate of methylation is first order in 1-butene pressure and zero order in DME (Figure 15), showing similar trends to those observed for ethene and propene methylation. [89,90] Work from Svelle et al. [38,39] has also observed these same pressure dependencies for MFI at 623 K and equal pressures of ^{13}C methanol and olefin (50 mbar) by extrapolating rates to zero contact times. These results indicate that 1-butene methylation proceeds via the formation of an active DME-derived species, followed by the rate-limiting addition of the activated C_1 to the olefin. Arrhenius plots of temperature dependence studies (Figure 16) show that rate constants for 1-butene methylation vary by an order of magnitude for different zeolite frameworks, namely MFI and BEA have higher rate constants than MOR and FER, consistent with rate constants for ethene and propene methylation previously reported [89,90] (Table 4). Apparent activation energies remain relatively constant between frameworks, indicating that pore wall stabilization of adsorbed species is either (i) offset by transition state destabilization or (ii) small compared to other contributions to the activation barrier. DFT+D models using the PBE exchange-correlation functional of ethene methylation over many zeolite frameworks have shown that activation energies and heats of physisorption vary among zeolites to different extents. [91] It is the balance of these two values that encompass

variations in methylation rates among different zeolites structures The activation energy of 1-butene methylation over MFI, 44 kJ mol^{-1}, is in good agreement with the previously reported experimental value of 45 kJ mol^{-1}, [39] MP2:DFT calculated value of 48 kJ mol^{-1}, [63] and a value of 45 kJ mol^{-1} calculated using ONIOM methods. [58] Furthermore, an extrapolation of the experimental rate constant in this account is within a factor of 0.7 with the previously determined value of 3.6 x 10^4 h^{-1} bar^{-1} at 623 K. [39]

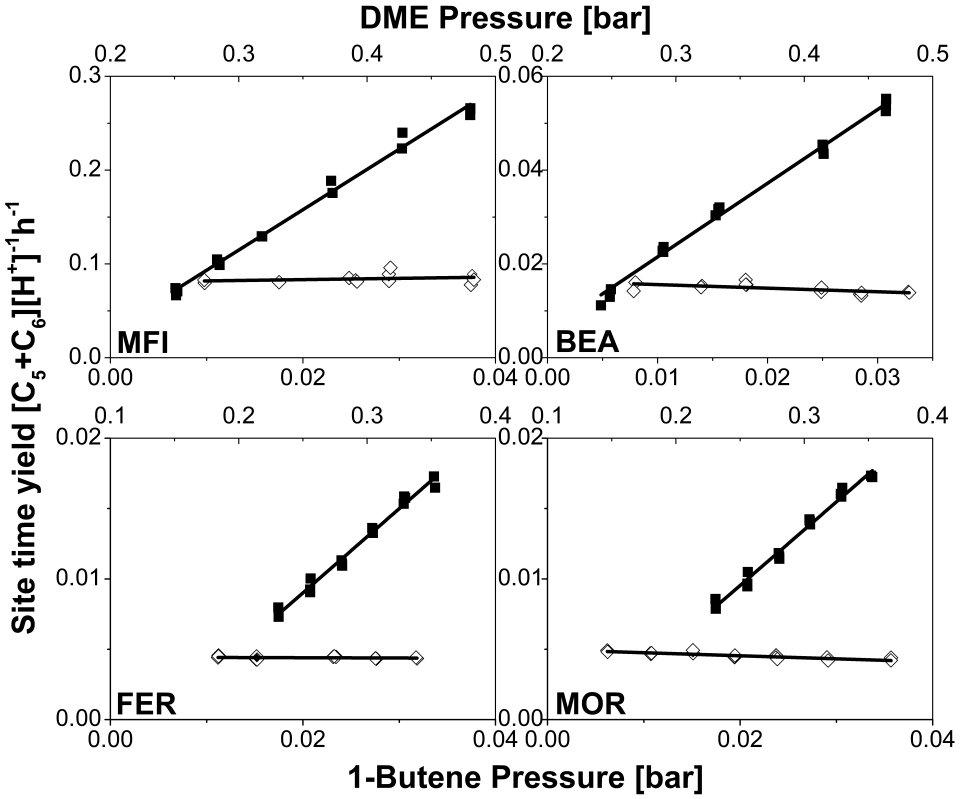

Figure 15. 1-butene methylation olefin and DME pressure dependence plots. (■) 1-butene pressure dependence. (◇) DME pressure dependence.

3.3.2 Effect of butene isomer on methylation reactions over zeolites BEA and MFI

Temperature, olefin pressure, and DME pressure dependence experiments were performed for the three other butene isomers: *cis*-2-butene, *trans*-2-butene, and isobutene over MFI and BEA, shown in Figures 17 and 18, respectively. These zeolites were chosen as consistently higher reaction rates are noted on MFI and BEA compared to

MOR and FER. A compilation of our data in Table 4 shows that the 2-butene isomers have similar activation barriers toward methylation. The rate of methylation of 1-butene is on the order of propene at 373 K. [89,90]

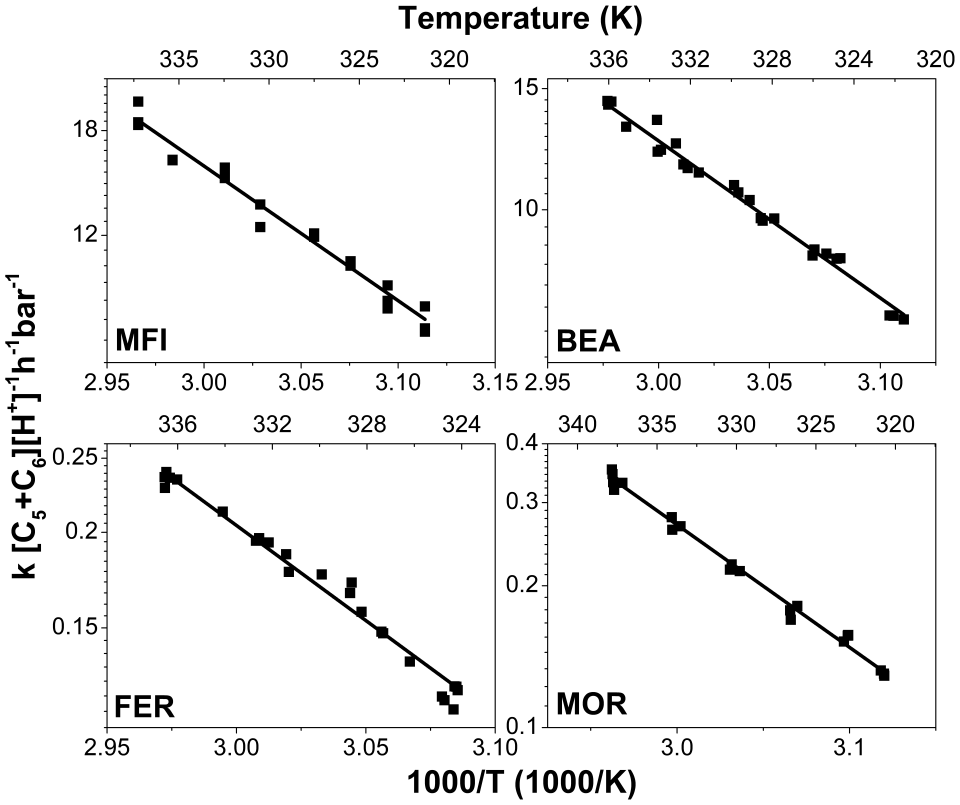

Figure 16. Arrhenius plots for 1-butene methylation from temperature dependence studies.

The rate constant for isobutene methylation exceeds those for all other isomers by an order of magnitude at 373 K. These data suggest that the rate of methylation is directly related to the degree of substitution about the double bond, which stabilizes intermediate carbocations through inductive electron donation. The ranking of carbocation or cyclopropyl-type intermediates is as follows: primary (C_2H_4) < secondary (C_3H_6,) < secondary (1-C_4H_8, *trans*-2-C_4H_8, *cis*-2-C_4H_8) < tertiary (*iso*-C_4H_8). The role of olefin methylation [8] and zeolite structure [7] in the overall reaction network leading to selective 2,2,3 trimethylbutane formation has shown that the formation of branched alkanes arises

due to increased carbocation stability of reactive intermediates and proceeds over BEA with the highest rate.

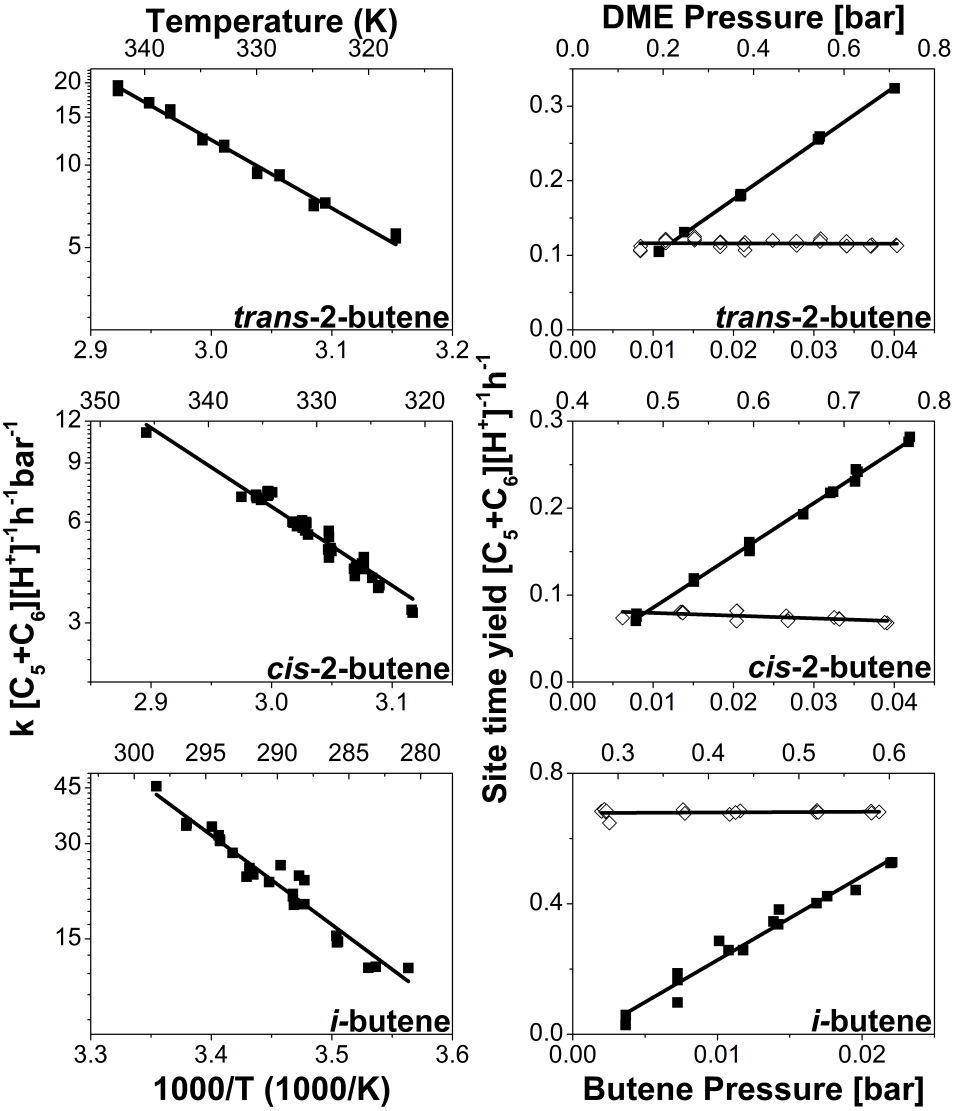

Figure 17. Kinetics of butene methylation over MFI for different isomers. Temperature dependence (left) and (■) olefin pressure dependence, (◇) DME pressure dependence (right).

Propene and butene isomer methylation reactions with ^{13}C DME over BEA at 473 K were performed by Simonetti et al. [8] using isotope tracing. These experiments yielded rates, when taken as first-order rate constants at 473 K, within the range of 24 $h^{-1}bar^{-1}$ for isobutene methylation to 49 $h^{-1}bar^{-1}$ for 1-butene methylation for C_3 and C_4 co-feeds. We attribute the conflicting observations regarding the methylation rate of isobutene to the

difference in reaction conditions and, specifically, the presence of hydride transfer. Isobutene is the only isomer capable of forming a tertiary carbocation upon methylation at the most kinetically favored position in the absence of hydride transfer (Figure 19). Comparing rate constants in Table 4 and the carbenium ion-like transition states formed, compounds with similar bond order about the carbocation have similar rate constants toward methylation with an order of magnitude gap between subsequent groups.

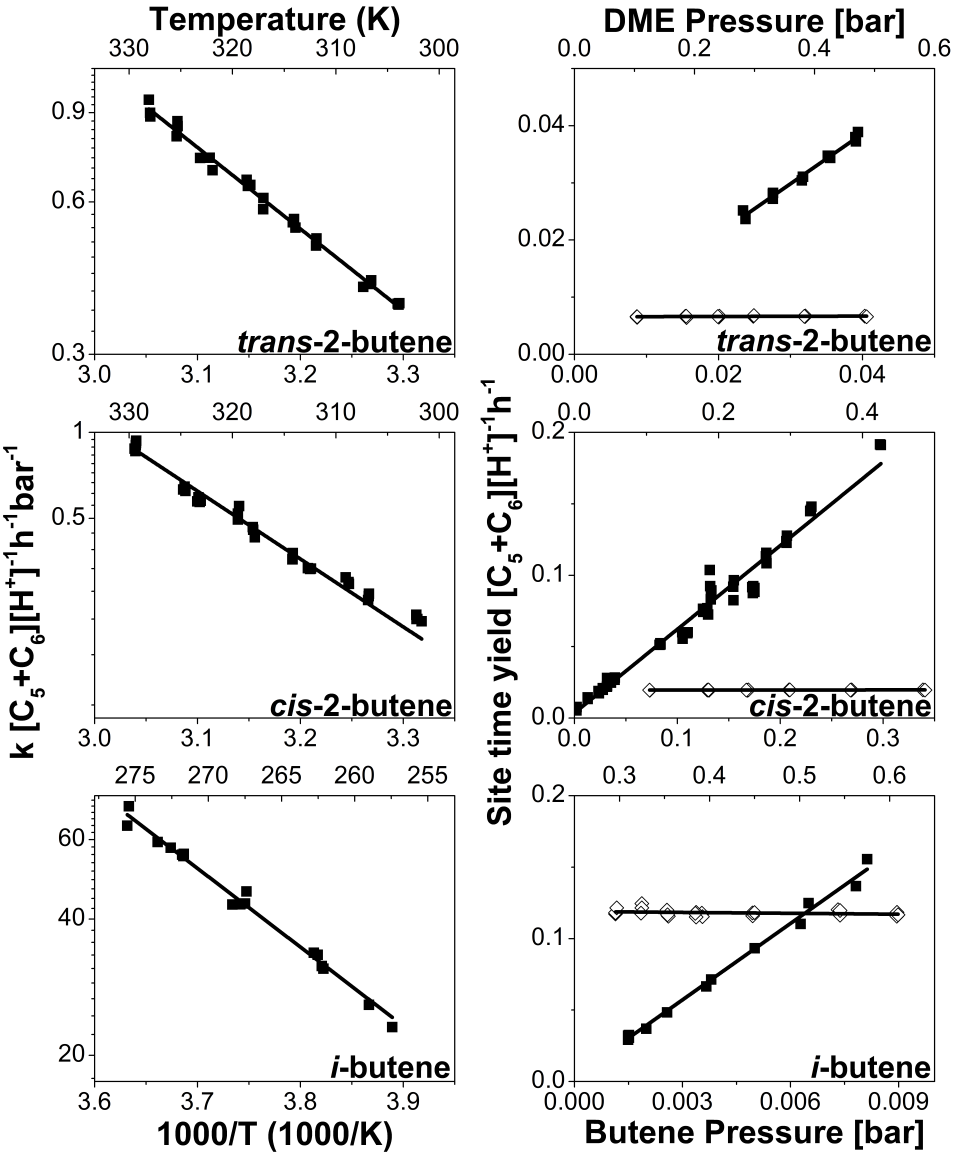

Figure 18. Kinetics of butene methylation over BEA for different isomers. Temperature dependence (left) and (■) olefin pressure dependence, (◇) DME pressure dependence (right).

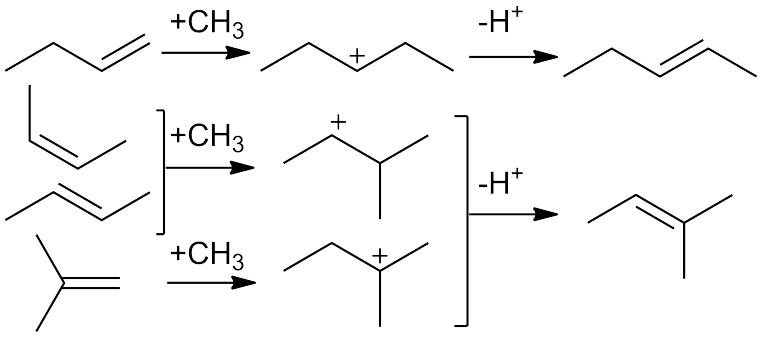

Figure 19. Methylation pathway for butene isomers.

	C_2H_4*		C_3H_6*		1-C_4H_8		*trans*-2-C_4H_8		*cis*-2-C_4H_8		*i*-C_4H_8	
	k	**Ea**	**k**	**Ea**	**k**	**Ea**	**k**	**Ea**	**k**	**Ea**	**k**	**Ea**
BEA	0.12	64±2	2.8	54±2	72.5	45±3	63.7	29±1	17.5	42±1	2995	34±1
MOR	0.01	61±3	0.20	58±4	1.8	49±1	-	-	-	-	-	-
MFI	0.06	98±3	3.7	62±3	89.1	44±2	74.2	46±1	40.6	49±1	3509	56±3
FER	0.03	84±2	0.12	57±2	1.2	50±3	-	-	-	-	-	-

Table 4. Rate parameters for C_2-C_4 olefin methylation over zeolites. All k values reported are in h^{-1} bar^{-1} and normalized to 373 K. Activation energies are reported in kJ mol^{-1}. * Reported previously.[36,37]

3.3.3 Reaction rate expression derivation for butene methylation

The identity of the surface species responsible for methylation reactions on zeolites remains a topic of debate in the field of MTH. [88] Two possible species are considered to be active for the methylation of olefins: a complex involving a physisorbed methanol/DME molecule on a Brønsted acid site with a subsequently physisorbed olefin, or a chemisorbed methoxide bound directly to the zeolite lattice.

The co-adsorbed mechanism has been used to explain experimental observations [64] and used as a theoretical basis for computational studies. [45,63,64] This mechanism postulates an active co-adsorbed complex between the methylating agent and a co-fed olefin on a zeolite acid site. The energy associated with the formation of co-adsorbed complexes has been shown to mostly derive from the interaction of the methylating agent, i.e. methanol or DME, with the zeolite acid center. Svelle et al. [63] have reported the

heat of adsorption of ethylene onto a physisorbed methanol molecule differs by only 2 kJ mol^{-1} between a purely silaceous framework and with one containing Al using hybrid MP2:DFT calculations with periodic boundary conditions. This suggests that the addition of ethylene onto the physisorbed methylating agent is not driven by ionic interactions with methanol, but rather van der Waals interactions with the zeolite pore walls. The differential heat of adsorption with the addition of an olefin onto a physisorbed methanol is -37 and -53 kJ mol^{-1} for C_2H_4 and C_3H_6 co-adsorption, respectively. [63] In contrast, Blaszkowski and van Santen [68] have shown that the adsorption of a single methanol molecule on a Brønsted acid site has an enthalpy of adsorption, ΔH_{ads} = -75 kJ mol^{-1} and the formation of methanol dimers has a ΔH_{ads} = -121-130 (1T vs 3T cluster) kJ mol^{-1} using self-consistent non-local corrected DFT. The similar contributions to the adsorption energy from a co-adsorbed olefin and a second methanol molecule indicate that methanol dimers are potentially in competition with co-adsorbed species, as methanol does not exhibit a significant change in the heat of adsorption, ΔHads = -115 ± 5 kJ/mol, on MFI until loadings above 2 molecules per Al are achieved, as observed by microcalorimetry at 400K. [67] Molecular dynamics simulations have shown that methanol dimers are considered inactive for the methylation of olefins due to their enhanced stabilization through mutual H-bonding. [69] Methylation via co-adsorbed complexes is traditionally viewed as being less energetically taxing compared to the activated formation of a methoxide, yielding barriers around 100 kJ mol^{-1} for ethylene methylation [63] compared to barriers between 215 - 223 kJ mol^{-1} for the formation of surface methoxides. [45,74,75] A recent study by Boronat et al. [76] has shown that dispersion effects play an important role in the stabilization of methoxide species by using 121-130 atom clusters with DFT-D dispersion corrections, yielding intrinsic barriers of 39-150 kJ mol^{-1} for 12-membered ring channels in MOR.

A formal derivation of rate equations is provided to further understand the kinetic behavior of the two proposed active surface species. It is assumed in each derived rate expression that only one surface species is responsible and the others act to inhibit the rate by occupying acid sites. Equation (1) below outlines the site balance used for both rate models, based on the discussion provided above:

(1) $$[H^+]_0 = H^* + H{\cdot}CH_3OCH_3^* + H{\cdot}CH_3OH^* + H{\cdot}Dimer^* + H{\cdot}CH_3OCH_3{\cdot}O_n^* + H{\cdot}CH_3OH{\cdot}O_n^* + CH_3^* + CH_3{\cdot}O_n^*$$

The terms in equation (1) refer to unoccupied acid sites; physisorbed DME, methanol, methanol dimers, DME/olefin and MeOH/olefin co-adsorption complexes; and chemisorbed methoxy groups and an olefin adsorbed on a methoxide, respectively. The accompanying rate equation for co-adsorbed complex mediated olefin methylation is given in equation (2).

(2)

(i)	$CH_3OCH_3 + H^* \leftrightarrow H{\cdot}CH_3OCH_3^*$	K_a
(ii)	$H{\cdot}CH_3OCH_3^* + O_n \leftrightarrow H{\cdot}CH_3OCH_3{\cdot}O_n^*$	K_C
(iii)	$H{\cdot}CH_3OCH_3{\cdot}O_n^* \rightarrow O_{n+1} + H^* + CH_3OH$	k_C
(iv)	$CH_3OH + H^* \leftrightarrow H{\cdot}CH_3OH^*$	K_a'
(v)	$H{\cdot}CH_3OH^* + O_n \leftrightarrow H{\cdot}CH_3OH{\cdot}O_n^*$	K_C'
(vi)	$H{\cdot}CH_3OH^* + CH_3OH \leftrightarrow H{\cdot}Dimer^*$	K_D
(vii)	$H{\cdot}CH_3OH{\cdot}O_n^* \rightarrow O_{n+1} + H^* + H_2O$	k_C'
(viii)	$H{\cdot}CH_3OCH_3^* \leftrightarrow CH_3OH + CH_3^*$	K_M
(ix)	$H{\cdot}CH_3OH^* \leftrightarrow H_2O + CH_3^*$	K_M'
(x)	$CH_3^* + O_n \leftrightarrow CH_3{\cdot}O_n^*$	K_O

Where O_n refers to a general olefin consisting of n-carbons and O_{n+1} refers to the methylated olefin, or butene and pentene in this report, respectively

The mechanism described in equation (2) provides two potential reactions to generate a methylated olefin, corresponding to co-adsorbed complexes generated from DME and methanol. Assuming decomposition of these complexes occur on kinetically similar time scales, as reported by Svelle et al. [64] where the rate of DME methylation of propene is ~2.5 times that of methanol when comparing saturated rates at (625 K, 20 mbar C_3H_6 25 – 75 mbar DME or CH_3OH, 100 mL min^{-1} flow) and 5 times that of

methanol based on B3LYP/6-31G(d) + ZPE energy calculations and quasi-IRC techniques, the rate-limiting step is represented by equation (3):

$$\frac{Rate_c}{[H^+]_0} = k_c[H \bullet CH_3OCH_3 \bullet O_n{*}] + k_c'[H \bullet CH_3OH \bullet O_n{*}] \quad (3)$$

Under high DME pressure conditions, the methanol co-adsorbed complex contributes a negligible amount to the overall reaction rate, yielding the fully derived form provided in the Appendix. Considering a zeolite surface covered in co-adsorbed complexes with DME, the rate equation reduces to the following form:

$$\frac{Rate_C}{[H^+]_0} = k_C \quad (4)$$

The surface methoxide-mediated mechanism is represented by the following sequence of reaction steps:

(5)

(i)	$CH_3OCH_3 + H^* \leftrightarrow H{\cdot}CH_3OCH_3^*$	K_a
(ii)	$H{\cdot}CH_3OCH_3^* \leftrightarrow CH_3OH + CH_3^*$	K_M
(iii)	$CH_3^* + O_n \leftrightarrow CH_3{\cdot}O_n^*$	K_O
(iv)	$CH_3{\cdot}O_n^* \rightarrow O_{n+1} + H^*$	k_M
(v)	$CH_3OH + H^* \leftrightarrow H{\cdot}CH_3OH^*$	K_a'
(vi)	$H{\cdot}CH_3OH^* \leftrightarrow H_2O + CH_3^*$	K_M'
(vii)	$H{\cdot}CH_3OCH_3^* + O_n \leftrightarrow H{\cdot}CH_3OCH_3{\cdot}O_n^*$	K_C
(viii)	$H{\cdot}CH_3OH^* + O_n \leftrightarrow H{\cdot}CH_3OH{\cdot}O_n^*$	K_C'
(ix)	$H{\cdot}CH_3OH^* + CH_3OH \leftrightarrow H{\cdot}Dimer^*$	K_D

The rate-determining step has the following form, with the fully derived equation reported in the Appendix:

$$\frac{Rate_M}{[H^+]_0} = k_M[CH_3 \bullet O_n{*}] \quad (6)$$

Assuming a zeolite surface covered in methoxide species, the rate equation reduces to the following form:

(7) $$\frac{Rate_M}{[H^+]_0} = K_O k_M P_O$$

A distinguishing feature between these rate expressions is the rate behavior at high olefin pressures. Saturation of surface sites with both DME and olefin concurrently is only possible for the co-adsorbed mechanism, while the surface methoxide mechanism predicts first order rate dependence in either DME or olefin but never saturated in both. Running steady-state *cis*-2-butene methylation at 308 K over BEA with olefin pressures ranging from 0.2 - 30 kPa in the presence of 20 kPa DME maintains linear behavior, indicating that saturation of the BEA surface with a co-adsorbed complex does not occur under these conditions, if these species are formed at all (Figure 18).

The relative stability of physisorbed intermediates compared to surface methoxides provides a basis for probing the identity of the surface species. Surface methoxides have been shown to be thermally stable species as they are able to persist in vacuum at 673 K, monitored via *in-situ* IR spectroscopy, before surface-bound C-H stretches diminish during coke formation. [71] This enhanced stability arises from the absence of mechanisms for surface C_1 species to desorb unlike their higher homologues, which can generate an olefin via β-elimination. [44,70] These species have also been directly observed using solid-state ^{13}C MAS NMR under vacuum [87] and continuous flow [44] conditions on MFI at 473 K. In this report, the temperature of a 200 mg BEA sample was increased to 423 K in 1.67 $cm^3\ s^{-1}$ He after steady state cis-2-butene methylation. The steady state rate constant, when extrapolated to 373 K using the activation energy calculated from temperature dependence studies, was 20.4 $h^{-1}bar^{-1}$, which coincides with the 17.5 $h^{-1}bar^{-1}$ found at higher temperatures and 5 mg BEA (Table 4). Increasing the temperature in He was done to remove residual physisorbed species removed from the zeolite surface and isolate the reaction intermediate. Water was added in excess using a syringe pump to probe the existence and number of residual methoxides via the formation of methanol, based on reactivity studies performed by Wang et al. [44] who reacted methanol (forming DME), water (forming methanol), and ammonia (forming methylamines) with methoxides from zeolites H-Y and H-ZSM-5 and zeotype H-SAPO-34. Methanol liberated with H_2O amounted to 1.02 ± 0.03 and 1.01 ± 0.04 molecules per

Al in BEA for 273 and 282 K experiments, respectively, indicating that the BEA surface is entirely covered in reactive DME-derived surface species at 423 K in He consistent with surface methoxide stability (Figure 20).

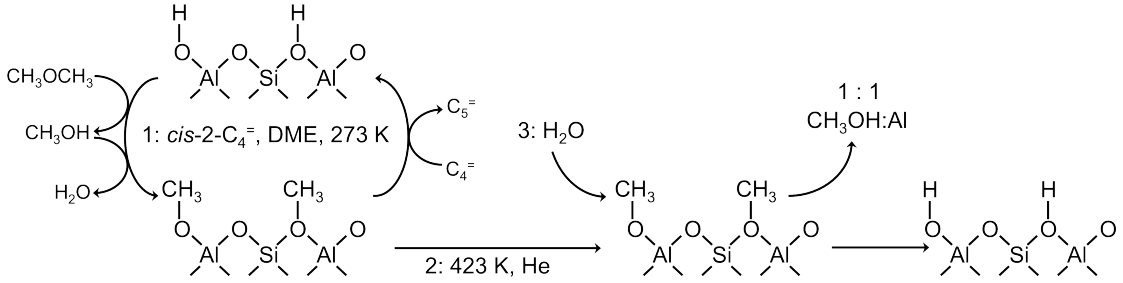

Figure 20. Post-olefin methylation titration of surface species with H_2O on zeolite BEA.

Our studies show that 1-butene methylation reaction rates are first order in olefin pressure and zero order in DME pressure over zeolites BEA, MFI, FER, and MOR. These pressure dependencies are also observed for butene isomers over MFI and BEA, consistent with observations made for ethene and propene methylation that olefin methylation reactions proceed through the same mechanism regardless of the olefin or framework. [89,90] Zeolite pore structures and olefins are distinguished by the varying extents to which they propagate the olefin hydrocarbon pool by different zeolites. The extent olefins propagate the hydrocarbon pool can be classified by the degree of substitution about the most stable carbenium ion-like transition state available based on measured rate constants. High olefin pressure studies and direct titration of methylation intermediates provide further evidence that surface methoxides are the species responsible for methylating olefins to their higher homologues.

3.4 Conclusions

The rate of dimethyl ether methylation of 1-butene at temperatures below 350 K in excess DME at differential conversions is independent of DME partial pressure and first order in olefin pressure. This is consistent with results reported for higher conversions with methanol [39] and lighter olefins, [38,39,89] and agrees with a mechanism

involving the rapid formation of DME-derived methylating agents reacting with 1-butene in the rate limiting step. These pressure dependencies hold for all butene isomers over BEA and MFI, and rate constants scale with the stability of the intermediate carbenium ion formed. Temperature dependence experiments show good agreement with previous studies [38,39,58,63] and little variation between zeolite frameworks.

Methylation reactions with a high *cis*-2-butene to DME ratio (up to 1.5) provide evidence that even in conditions with excess olefin, the reaction rate maintains a first order dependence in olefin and zero order dependence in DME. This indicates saturation of the rate in olefin and DME, as predicted for the co-adsorbed complex mediated mechanism, would require higher olefin to DME ratios than those probed in this study. Surface species were titrated with H_2O at 423 K in He in a 1:1 ratio with Al. These titrations were performed by first replacing reactant flows with He during steady-state *cis*-2-butene methylation over BEA, followed by increasing the temperature to 423 K. The surface species were shown to persist in a 1:1 ratio with Al at 423 K under He flow consistent with NMR [44] and reaction studies [70] of surface methoxide stability and observed zero order rate dependencies on DME pressure. These experiments give evidence toward an olefin methylation cycle that proceeds through carbenium ion-like transition states, formed by reaction with surface methoxide species on zeolite acid sites.

Acknowledgements

The authors acknowledge financial support from The Dow Chemical Company and the National Science Foundation (CBET 1055846)

Chapter 4: Kinetics and mechanisms of benzene, toluene, xylene methylation over H-MFI

4.1 Introduction

Since its discovery in 1977 by Mobil, [6,25,32] consensus on the mechanism governing the methanol-to-hydrocarbons (MTH) process over zeolite or zeotype catalysts has remained elusive. Despite this, aspects of the MTH chemistry have garnered agreement among researchers. Direct C-C coupling of methanol in MTH has been largely regarded as negligible compared to indirect methylation of olefin and aromatic impurities, as shown via increasing induction periods through rigorous reactant purification, [16] isotopic studies, [29,48,61] and high activation barriers for direct coupling. [45-47] The development of indirect mechanisms [26,49,86] has lead to the widely accepted "hydrocarbon pool" mechanism, [17,50,51] which describes the growth, dealkylation, and interconversion of olefin [20,38-40] and aromatic species [22,27-30,37,52-54,56,57] within the confined inorganic framework as being responsible for observed product distributions. Recent work has described the role and contributions of constituent reactions pertinent to MTH chemistry, indicating that the relative rates of these steps yields particular termination products from olefin and aromatic hydrocarbon pools, which can be quantified to determine which cycle is relatively more productive. [84,92]

The use of aromatic co-feeds as a means of studying the evolution of the aromatic hydrocarbon pool has been extensively reported, mainly in using isotopically-labeled reagents to track the pathways available for chemical transformations of aromatics, in particular, their role in the formation of light olefins. [21,22,24,37,93] For example, Mikkelsen et al. [37] have shown through observed isotopic distributions in product olefins in the ^{13}C-methanol methylation of aromatics that all ethene and majority propene are formed through the cracking of arenes on H-ZSM-5, H-MOR, and H-BEA catalysts, and not direct coupling of C_1 species. [37] Switching experiments have shown the relative incorporation rates of ^{13}C methanol, when switched from a ^{12}C methanol feed indicates that aromatics track with ethene and olefins track with propene, indicating that ethene originates from the aromatic hydrocarbon pool, and that the methylation of propene is

mostly responsible for the formation of higher olefins over SAPO-34, [23] BEA, [21,93] and MFI. [24] The predominant methylbenzenes responsible for the formation of light olefins has been shown to be zeolite framework dependent, and specifically for MFI to comprise $C_8 - C_{10}$ aromatics.

The investigation and quantitation of the kinetics of aromatic methylation has been a relatively recent focus, and allows for the direct comparison of reaction rates and activation energies between the aromatic and olefin hydrocarbon pools. The kinetics of ^{13}C benzene methylation with ^{12}C methanol over H-ZSM-5 has shown that benzene methylation and propene methylation proceed with similar rates and reactant pressure dependencies at 673K. [94] Recent studies have also quantified the effects of pore size and degree of methylation of co-feed aromatics on the formation rate of light hydrocarbons and higher aromatics. [95] DFT calculations using a co-adsorbed methanol and toluene precursor over 4T clusters have shown that activation barriers for toluene methylation are of the order of 180 – 195 kJ mol^{-1}. [19,64,96,97] Barriers calculated using hybrid ONIOM methods on 46 T clusters of MFI are ~ 163 kJ mol^{-1}, showing that framework effects are important in stabilizing MTH intermediates and transition states. [28] Reaction rates for the methylation of benzene over H-ZSM-5 and H-BEA were determined using 17 mbar benzene and 37 mbar ^{13}C methanol at 623 K and contact times below 0.009 h which minimized the effects of secondary reactions by extrapolating these values to zero contact time. [94] Comparison of benzene methylation rate parameters with propene methylation [39] run at similar reaction conditions have shown that activation energies (58 and 69 kJ mol^{-1}) and first-order rate constants (4.8 and 4.5 x 10^{-3} mol g^{-1} h^{-1} $mbar^{-1}$) are similar, and thus the aromatic and olefin hydrocarbon pools are both contributors to the product distribution observed over H-ZSM-5.

The goal of this work is to quantify rate constants and activation energies for BTX methylation over H-ZSM-5 and mesoporous self-pillared pentasil (H-SPP), and compare kinetics and mechanisms to previous work investigating the methylation of $C_2 - C_4$ olefins [89,90,98] to quantify the relative propagation rates of these two cycles over MFI frameworks. Elementary-step aromatic methylation of benzene, toluene, *para*-xylene, and *ortho*-xylene was investigated to also probe the surface species present and active during

aromatic methylation reactions. The effect of mesoporosity on observed rates and mechanisms is also presented to determine the role of adsorption and diffusion on observed kinetic parameters.

4.2 Materials and Methods

4.2.1 Catalyst preparation

Zeolite H-ZSM-5 (MFI, Zeolyst, Si/Al = 42.6) and self-pillared pentasil (MFI, Si/Al = 75, 2 – 7 nm mesopores. sample preparation and characterization described elsewhere [99]) were pressed, crushed, and sieved to 180 to 425 μm aggregate sizes. Catalysts were then treated in dry air (1.67 cm^3 s^{-1} NTP, ultrapure, Minneapolis Oxygen) at 773 K for 8 h. Thermal treatment in air was repeated to regenerate self-pillared pentasil (H-SPP) samples between reactions to conserve sample.

Catalysts were diluted in quartz sand (Sigma Aldrich) to 1 g total mass and supported on a quartz frit within a 10 mm quartz U-shaped reactor tube where isothermal reaction conditions were maintained using a National Electric FA120 furnace connected to a 96 Series Watlow temperature controller. Catalyst temperatures were measured using a K-type thermocouple located in a thermowell penetrating the center of the catalyst bed. Samples were treated in flowing He (1.67 cm^3 s^{-1}, ultrapure, Minneapolis Oxygen) at 773 K (0.033 K s^{-1} temperature ramp) for 4 h prior to cooling to reaction temperatures.

4.2.2 Steady-state aromatic methylation reactions

Benzene, toluene, *para*-xylene, and *ortho*-xylene methylation reactions with DME were performed using 1.67 cm^3 s^{-1} total reactant flow rates with 0.68 bar DME (Matheson, CP grade), 0.01 bar aromatic (Sigma Aldrich, 99.9% purity), and 0.03 bar CH_4 (Minneapolis O_2, CP grade) as an internal standard. Methylation reactions over H-ZSM-5 used 50 mg of catalyst at 373 K for benzene, 10 mg catalyst at 403 K for toluene, and 1 mg catalyst at 473 K for xylene to maintain <0.1 % aromatic conversion. Methylation over H-SPP used 1 mg catalyst at 473 K for benzene and xylene, and 433 K

for toluene co-feeds. Pressure dependence reactions were run from 0.002 – 0.05 bar aromatic, and 0.29 to 0.68 bar DME while keeping the partial pressure of the other constant by adjusting He flow rates to maintain 1.67 cm^3s^{-1} total flow. Products were monitored using an Agilent 5890 gas chromatograph equipped with an HP-1 capillary column attached to an FID detector.

4.2.3 Post-reaction zeolite surface titration with H_2O

Steady-state methylation reactions were run over 200 mg H-SPP (in the absence of quartz sand diluent) at 358 K for benzene, 343 K for toluene, and 353 K for para-xylene co-feeds. After 7.2 ks time-on-stream, flow over the catalyst was switched to 1.67 cm^3 s^{-1} He for 1.8 ks to purge residual and reactor temperature was increased to 423 K at a rate of 0.17 K s^{-1} to remove physisorbed species from the catalyst surface. Flow to the reactor was then switched to 10 kPa H_2O in He with a total flow of 1.67 cm^3 s^{-1} to remove chemisorbed $*CH_3$ species as methanol. Effluent compositions were monitored and quantified using an online Cirrus MKS quadrupole mass spectrometer using CH_4 as an internal standard.

4.2.4 In-situ d_6 DME/DME switching

Steady-state methylation reactions over H-SPP were performed at identical catalyst weights, total flow rates, and reaction temperatures as described in the H_2O titration section, with the exception of using 0.20 bar DME pressure instead of 0.68 bar DME. After 7.2 ks time-on-stream, DME composition was changed to 0.10 bar d_0 DME and 0.10 bar d_6 DME for 3.6 ks prior to returning to 0.2 bar d_0 DME. Reaction rates were monitored via GC, and effluent composition was monitored via online MS.

4.3 Results and discussion

The kinetics of benzene, toluene, *para*-xylene, and *ortho*-xylene methylation have been systematically studied to derive reactant pressure and temperature dependencies of the reaction rate at differential reaction conditions in the absence of secondary products.

Based on these pressure dependencies and rate equations, mechanistic inferences have been made in conjunction with isotopic [89,90] and surface titration [98] methods used previously to obtain a description of the effect of aromatic substitution on methylation rates and pathways.

4.3.1 Benzene methylation on H-ZSM-5

The methylation of benzene with DME yielded first-order pressure dependence in benzene and zero-order dependence in DME (Figure 21, panel A and B). These pressure dependencies are consistent with the rapid formation and complete surface coverage of DME-derived species that react with benzene in the rate-determining step, as observed for $C_2 - C_4$ methylation with DME or methanol. [38,39,89,90,98] First-order rate constants and activation energies (Table 5) show an identical activation energy and a rate constant within a factor of 0.72 of studies that were performed with 0.037 bar methanol and 0.017 bar benzene at 623 K over H-ZSM-5, where parameters were derived by extrapolating conversions to zero contact time with the catalyst. [94]

		H-ZSM-5		**H-SPP**	
		Ea (kJ/mol)	**k_{373} (h bar)$^{-1}$**	**Ea (kJ/mol)**	**k_{373} (h bar)$^{-1}$**
Benzene		58 ± 3	6.8	58 ± 2	8.3
Toluene		52 ± 4	48.1	47 ± 3	31.4
***Para*-xylene**	**0.05 bar**	-	-	44 ± 4	12.5
	0.003 bar	62 ± 3	13.4	62 ± 3	10.1
***Ortho*-xylene**	**0.05 bar**	-	-	34 ± 3	3.0
	0.003 bar	62 ± 4	3.1	63 ± 4	4.0

Table 5. Apparent activation energies and rate constants at 373 K for aromatic methylation reactions over H-ZSM-5 and H-SPP. Listed pressures denote xylene reactant pressure at which temperature dependence reactions were run

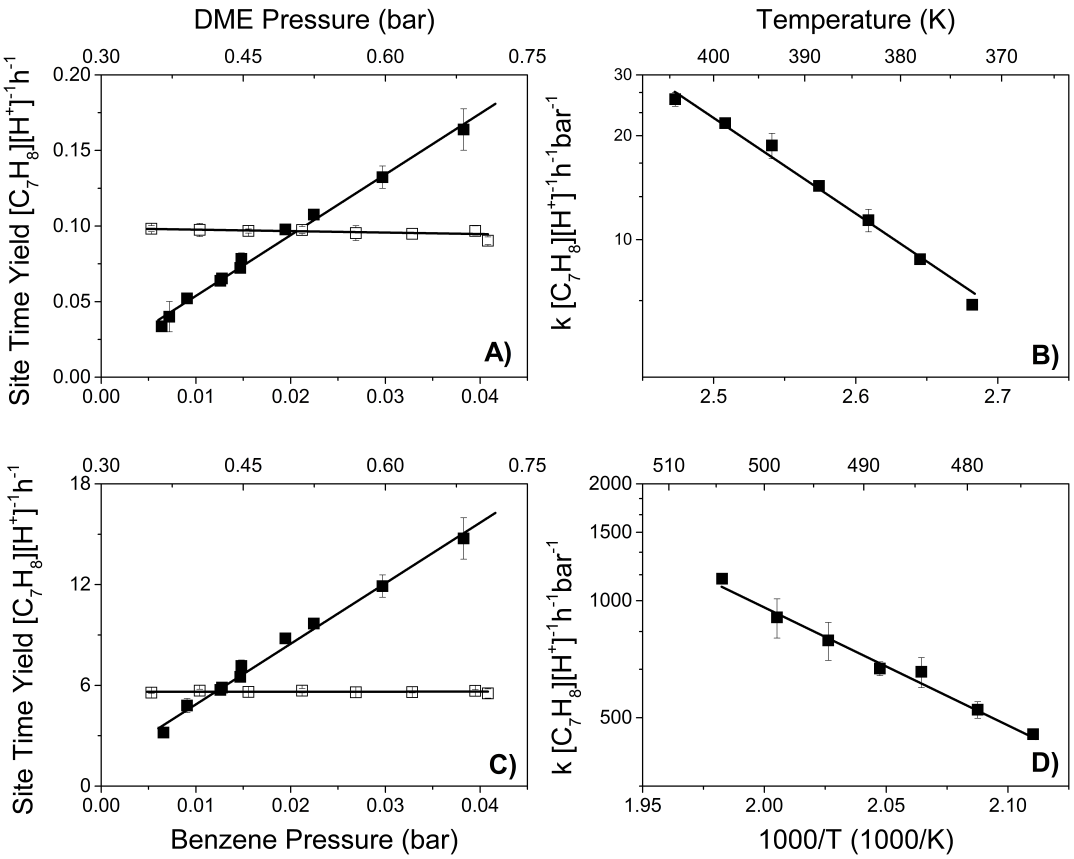

Figure 21. DME methylation of benzene over H-ZSM-5, 50 mg at 373 K, (A and B) and H-SPP, 1 mg at 473 K (C and D). Benzene pressure dependence (■) and DME pressure dependence (□) are shown in the left panels, temperature dependence is shown in the panels to the right.

A comparison with DFT calculations performed using hybrid functionals [58,63] and previous experimental studies [39,89] shows that benzene methylation proceeds with similar apparent activation barriers (62 – 77 kJ mol^{-1}) and rate constants (3.7 – 5.8 [C_4H_8][H^+]h^{-1}bar^{-1} at 373 K) as propene methylation. Similar apparent rate behavior between propene and benzene could be explained through similarities in the local structure of the two molecules, namely, the secondary substitution about the carbon formed upon methylation in the absence of additional alkyl substituents to inductively donate electron density. This result is not intuitive on the basis that apparent barriers include adsorption enthalpies, which are calculated to be -94 kJ mol^{-1} at the wB97x-D/6-31 +g(d) level of theory [94] for benzene and -53 kJ mol^{-1} using MP2/DFT with periodic boundary conditions [63] for

propene on H-ZSM-5, indicating a greater intrinsic barrier for benzene methylation by ~40 kJ mol^{-1} compared to that of propene. Experimental enthalpies of adsorption by generating adsorption isochores in low dead-volume systems estimate that benzene has a heat of adsorption of -55 to -75 kJ mol^{-1} on H-ZSM-5, depending on unit cell loading; [100,101] however these values represent an upper bound compared to propene adsorption and this study reflects adsorption on a Brønsted acid site rather than co-adsorbing on surface-bound methanol-derived species.

4.3.2 Toluene methylation on H-ZSM-5

Toluene methylation with DME over H-ZSM-5 showed first-order dependence in aromatic and zero-order dependence in DME partial pressures in agreement with benzene kinetics, indicating that the zeolite surface is completely covered with DME-derived species, which react with toluene in the rate-determining step (Figure 22). The first-order rate constant for toluene methylation on H-ZSM-5 (Table 5) is a factor of 1.5 larger compared to a first-order rate constant calculated from previously reported rates at 373 K, where Vinek et al. [102] co-fed 2.5 kPa toluene and 3.5 kPa methanol over H-ZSM-5 at 373 – 773 K. Vinek et al. [102] also reported activation energies of 52 – 85 kJ mol^{-1}, which is in good agreement with 68 kJ mol^{-1} derived from toluene methylation in a simulated riser reactor, [103] 47 kJ mol^{-1} from a fixed fluidized bed reactor from 573 – 673 K, [104] and 52 kJ mol^{-1} reported in this work (Table 5).

The methylation of toluene proceeds with a rate constant of 48 $[Xylene][H^+]^{-1}h^{-1}bar^{-1}$ at 373 K and agrees well with *n*-butene methylation rate constants of 41 – 90 $[C_5+C_6][H^+]^{-1}h^{-1}bar^{-1}$, [98]and the activation barrier of 52 kJ mol^{-1} agrees with butene methylation barriers of 44 - 49 [98] and 48 [39] kJ mol^{-1} from previous experimental studies. The effective change in kinetics from benzene to toluene are similar to that of propene and 1-butene, respectively, indicating that the addition of a methyl group in these cases has a similar effect on stabilizing reaction intermediates, namely inductive electron donation, despite the different extended structure of aromatics compared to olefins.

Toluene heats of adsorption derived from equilibrium isochores over H-ZSM-5 [101] range between -60 to -80 kJ mol^{-1}, which is similar to *trans*-2-butene adsorption values of

-68 kJ mol^{-1} calculated using MP2/DFT with periodic boundary conditions. [63] This agreement makes direct comparison of apparent barriers between toluene and butene more relevant than for benzene and propene.

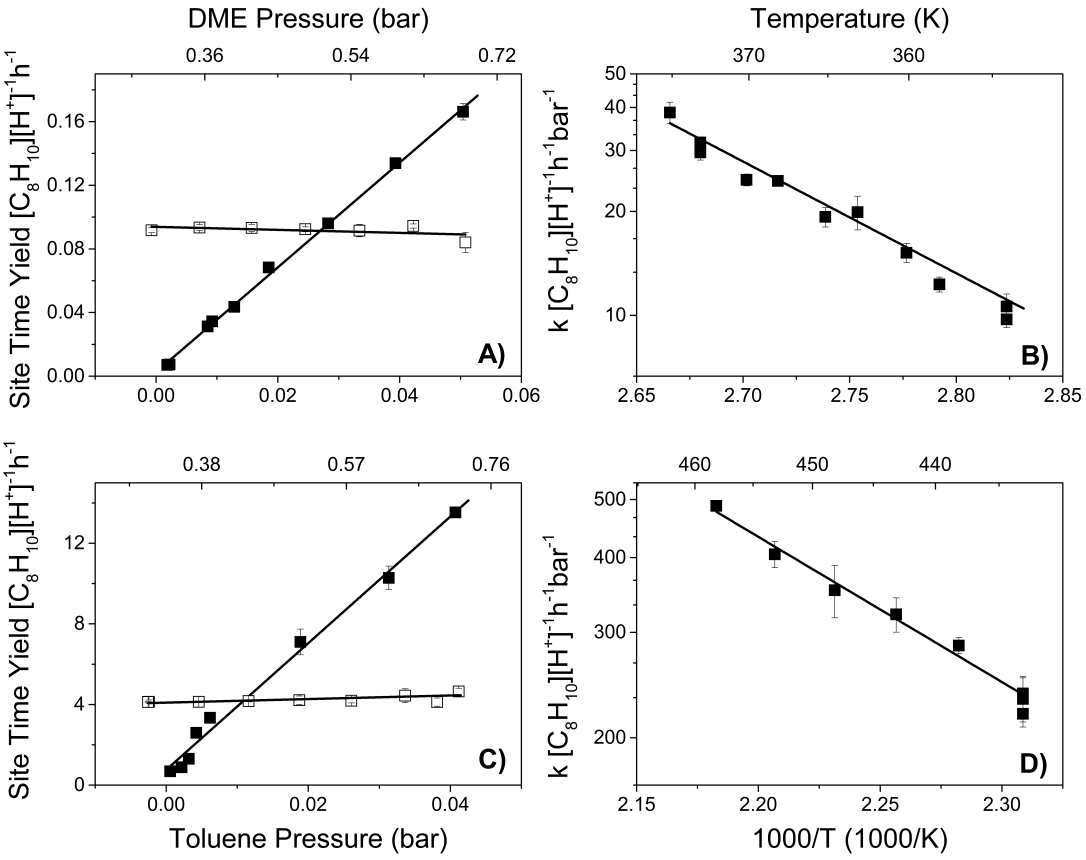

Figure 22. DME methylation of toluene over H-ZSM-5, 10 mg at 403 K, (A and B) and H-SPP, 1 mg at 433 K (C and D). Toluene pressure dependence (■) and DME pressure dependence (□) are shown in the left panels, temperature dependence is shown on the panels to the right.

4.3.3 A comparison of benzene and toluene methylation rates on H-MFI and mesoporous H-SPP

Aromatic and DME pressure dependencies and temperature dependencies for benzene and toluene methylation over H-SPP is shown on the bottom panels of Figures 21 and 22 for benzene and toluene, respectively. Rate constants agree within 50% and activation parameters within 10% (Table 5) between microporous and mesoporous MFI

samples. This indicates kinetic control for these systems and any effects of sterics or confinement are strictly limited to the micropores for benzene and toluene methylation.

4.3.4 Ortho- and para-xylene methylation

The results of xylene methylation are presented in Figure 23, with kinetic parameters reported in Table 5. While methylation rate constants increased from benzene to toluene methylation reactions over H-ZSM-5, the marked decrease in xylene methylation rate constants is not intuitive, as increasing methyl substitution about the aromatic ring is expected to further increase intermediate carbocation stability. Ahn et al. [95]have recently reported that the rate of methylation from toluene, to *para*-xylene, to 1,2,4-trimethylbenzene decreases from 35, to 22, to 3.7 [10^{-2} mol (mol H s)$^{-1}$] when feeding 1.2 kPa toluene and 0.3 kPa methanol, a 4:1 aromatic to methanol ratio, at 673 K over H-ZSM-5 at 45 – 58 % conversion. The decrease in methylation rate was ascribed to diffusion limitations in xylenes and larger aromatics in the medium pore zeolites, where these species would mostly dealkylate to lower methylbenzenes with more favorable diffusion properties as opposed to directly leaving the zeolite framework. While reaction rates for para- and ortho- xylene are independent of DME pressure, as in the case of benzene and toluene methylation, xylene methylation rates saturate with respect to xylene partial pressure at the reaction conditions presented in this study (Figures 21-23). The origin of this behavior could arise from (i) diffusion limitations (ii) a change in the rate-determining step, or (iii) a change in the predominant surface species prior to the rate-determining step.

4.3.5 Diffusion of aromatics in H-ZSM-5

The diffusion of aromatic molecules in zeolites has been extensively studied using spectroscopy, [105,106] experimental methods, [100,101,107-114] and theoretical calculations. [115,116]The effect of coking on diffusion in zeolites has shown that coking has little effect on the selectivity towards *para*-xylene during toluene methylation reactions on H-ZSM-5 using IR spectroscopy and reaction rate measurements. [105]A model for a zero-length column (ZLC) experimental system, developed by Ruthven and Vidoni, [109]has allowed

for this experimental technique to account for combined kinetic effects of surface resistance and internal diffusion limitations to mass transfer.

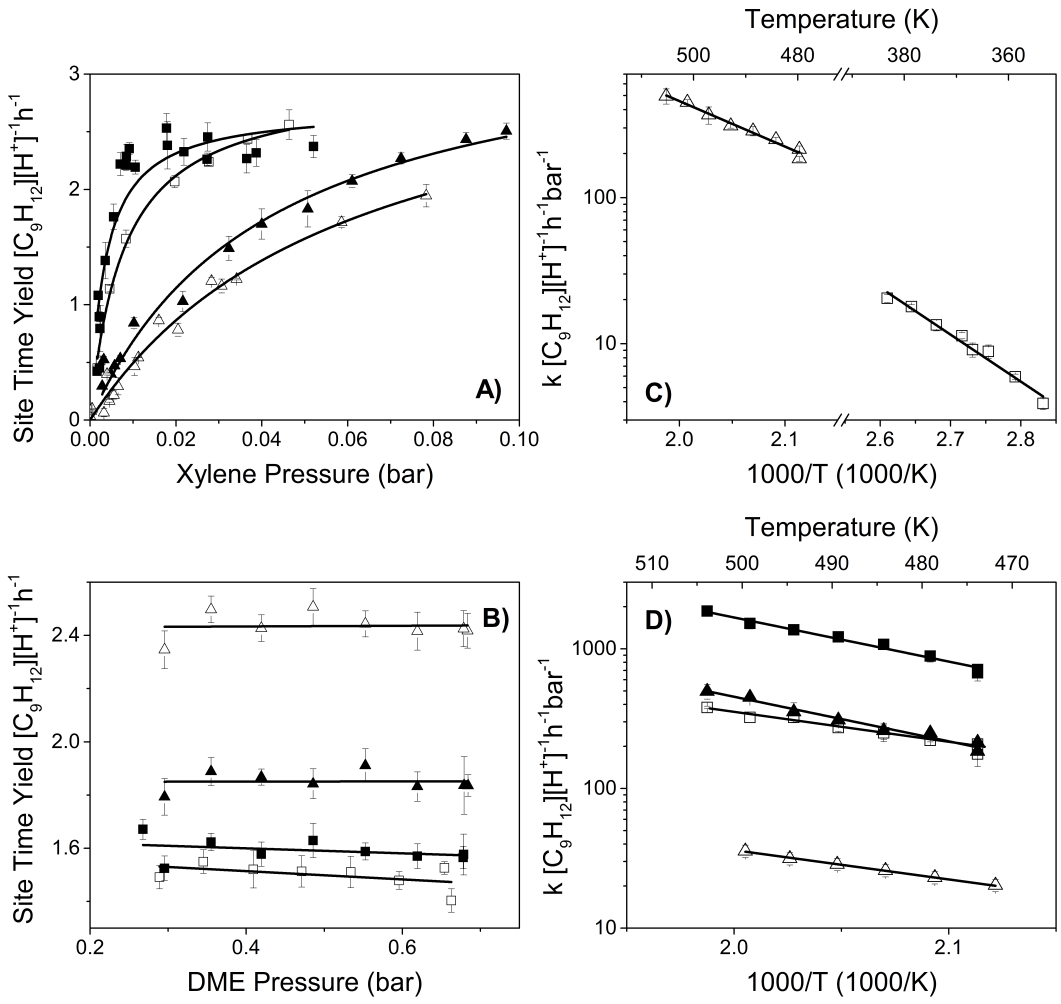

Figure 23. Xylene pressure dependencies for *para*-xylene over H-MFI(□) and H-SPP(■), and *ortho*-xylene over H-MFI(Δ) and H-SPP(▲). B) DME pressure dependencies for *para*-xylene over H-MFI(□) and H-SPP(■), and *ortho*-xylene over H-MFI(Δ) and H-SPP(▲). C) Temperature dependence of DME methylation of *para*-xylene over 1 mg H-ZSM-5 (□) and *ortho*-xylene over 1 mg H-ZSM-5 (Δ). D) Temperature dependence of DME methylation over 1 mg H-SPP at 0.002 bar *para*-xylene (■), and 1 mg H-SPP at 0.05 bar *para*-xylene (□), and 1 mg SPP at 0.002 bar *ortho*-xylene (▲), and 1 mg SPP at 0.05 bar *ortho*-xylene (Δ).

Diffusion coefficients for benzene, *ortho*- and *para*-xylene over H-ZSM-5 and silicalite using ZLC have been calculated using this model for MFI frameworks. [107,108]Calculating thiele moduli using these values, and toluene diffusivities obtained via TGA, [114]at relevant reaction temperatures and rate constants reported in Table 5 yield the most diffusion-limited case of *ortho*-xylene methylation $\varphi = 0.19$ using 1 μm crystallite sizes, which indicates that the rate constants reported in this work are dictated by reaction kinetics. Thiele moduli calculations are confirmed by the experimental observation that mesoporous and microporous H-SPP and H-ZSM-5 samples saturate at nearly identical rates for xylene methylation and indicate rate independence with respect to critical diffusion length, and therefore, operate outside of diffusion limitations.

4.3.6 Temperature dependence for ortho-xylene and para-xylene in linear and saturated rate regimes

Temperature dependence studies were carried out on H-SPP at 0.003 bar and 0.05 bar *para*- and *ortho*- xylene pressures. These pressures correspond to linear and saturated regimes in the xylene pressure dependent data, which we ascribe to a zeolite surface predominately covered in surface methoxides and xylene molecules adsorbed on methoxides, respectively. These inferred surface species and experimental evidence for their presence and reactivity will be discussed in studies presented below. High-pressure regimes yielded apparent activation barriers of 34 to 44 kJ mol^{-1} and low-pressure regimes 63 to 62 kJ mol^{-1} for *ortho*- and *para*-xylene, respectively (Table 5). While first-order rate constants between high and low-pressure regimes are within 25% at 373 K, the differences in activation barriers indicate that this agreement is coincidental, as a different a choice in reference temperature would cause these values to diverge. Differing apparent barriers for methylation at saturated pressures compared to linear regimes indicates that the rate-determining elementary step is different. Considering the same bond to be broken in both cases, the intrinsic activation barrier would remain constant, requiring the saturated regime to have a more stabilized surface species prior to the rate-determining step compared to surface species present in low-pressure regimes.

4.3.7 Post-reaction zeolite surface titration with H_2O for benzene, toluene, and para-xylene methylation

Resolving active surface derivatives of DME or methanol for methylation reactions is a continuing debate in the MTH literature, specifically, the formation of co-adsorption complexes from physisorbed reactants or a stepwise mechanism through the formation of a surface methoxide species. [88] Computational methods have reported consistent results [18,28,58,63] with kinetic measurements [38,39] by modeling methylation reactions via the co-adsorption mechanism. However, FTIR [71]and ^{13}C MAS NMR [44,87] at 453 K and above, and computational studies [75,76] provide evidence for the existence of surface methoxides on the zeolite surface. These surface methoxides are unable to desorb, due to the absence of a β-hydrogen, except via reaction, and their stability has been noted up to 673 K under vacuum. [44,70,71] The titration of chemisorbed methoxides on the surface of H-SPP was performed in a similar fashion to previous studies on *cis*-2-butene methylation over H-BEA. [98]The experimental setup is outlined in Figure 24 and the results of these chemical titration studies are reported in Table 6. Upon interaction with water, 0.95 – 0.98 CH_3OH:Al was evolved after benzene, toluene, and *para*-xylene methylation at two different reactant partial pressures, indicating that, at these conditions, the surface is predominantly covered by surface methoxide species ($*CH_3$).

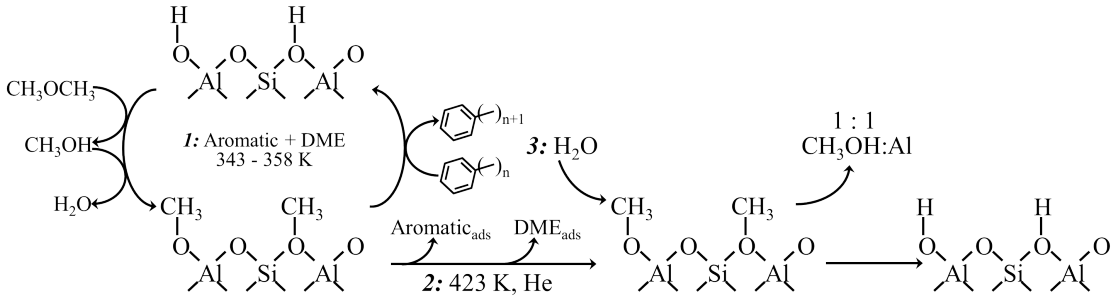

Figure 24. Three steps involved in the titration of surface species generated in aromatic methylation experiments on H-SPP, where n = 0,1,2.

4.3.8 In-situ d_6 DME/DME switching for benzene, toluene, and para-xylene methylation:

H-SPP samples were exposed to a 50:50 mixture of d_0/d_6 DME after steady-state operation in the absence of deuterated DME. Results for these studies are shown in Table 6 and indicate that the rate-determining step for all BTX methylation reactions involve the formation of a C-C bond in the transition state as observed via secondary kinetic isotope effects ranging from 1.25 – 1.35 k_H/k_D.

		CH_3*/Al[a]	Effluent DME Content[b]			k_H/k_D[b]
			d_0	d_3	d_6	
Benzene		0.95 ± 0.06	1	1.69	0.86	1.25 ± 0.08
Toluene		0.96± 0.07	1	1.52	0.82	1.35 ± 0.06
***Para*-xylene**	**0.05 bar**	0.98 ± 0.08	1	0.04	0.84	1.34 ± 0.04
	0.003 bar	-	1	0.23	0.85	1.31 ± 0.05

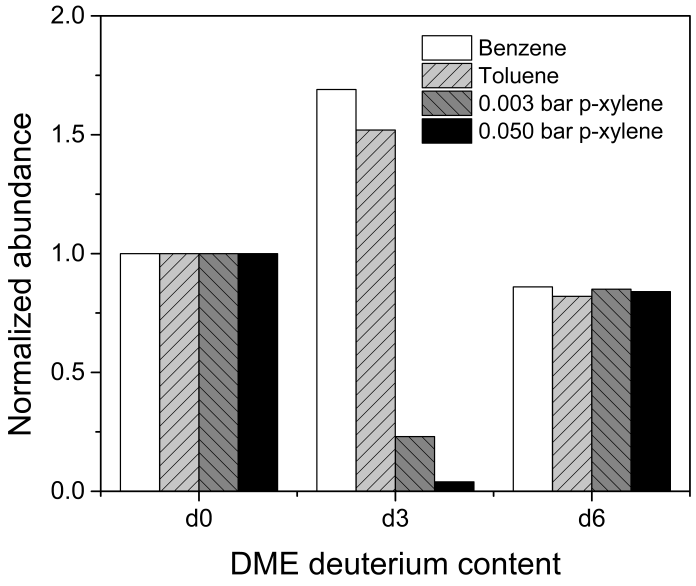

Table 6. Results for (a) post-reaction water titration experiments and (b) isotopic switching experiments over H-SPP. Deuterium distributions in effluent DME are normalized to d_0 (m/z = 46) abundances.

Benzene and toluene methylation reactions showed a near-binomial distribution of d_0:d_3:d_6 DME (1:2:1), consistent with results from ethene methylation.[89] *Para*-xylene methylation showed ~15% of the C-O bond scrambling observed in effluent DME compared to benzene and toluene methylation using 0.003 bar partial pressure of *para*-xylene, and almost no scrambling in the presence of 0.05 bar *para*-xylene. This indicates that surface methoxides are hindered from reacting with other gas-phase DME molecules to facilitate C-O scrambling, which is consistent with *para*-xylene blocking these sites through co-adsorption, which would be expected to exacerbate at higher xylene partial pressures.

4.3.9 Rate equation for BTX methylation systems

The linear pressure dependence of benzene and toluene methylation rates on aromatic pressure and rate independence with respect to DME over MFI indicates a mechanism similar to that previously described for $C_2 - C_4$ olefins over MFI, BEA, MOR, and FER.[89,90,98]The elementary steps involved for benzene and toluene methylation are described in Equation 1, and shown in (Figure 25, bottom):

(i)	$CH_3OCH_3 + H^* \leftrightarrow H{\cdot}CH_3OCH_3^*$	K_{ads}
(ii)	$H{\cdot}CH_3OCH_3^* \leftrightarrow CH_3OH + CH_3^*$	K_M
(iii)	$CH_3^* + Ar_n \rightarrow Ar_{n+1} + H^*$	k

Where Ar_n represents an aromatic with n methyl groups, or 0, 1 and 2 for benzene, toluene, and xylene, respectively and k is the apparent rate constant. The related per-proton rate equation for this sequence of elementary steps is:

(2)

$$\frac{Rate}{[H^+]_O} = \frac{K_{ads}K_M k[Ar_n]\frac{[DME]}{[CH_3OH]}}{1 + K_{ads}[DME] + K_{ads}K_M\frac{[DME]}{[CH_3OH]}}$$

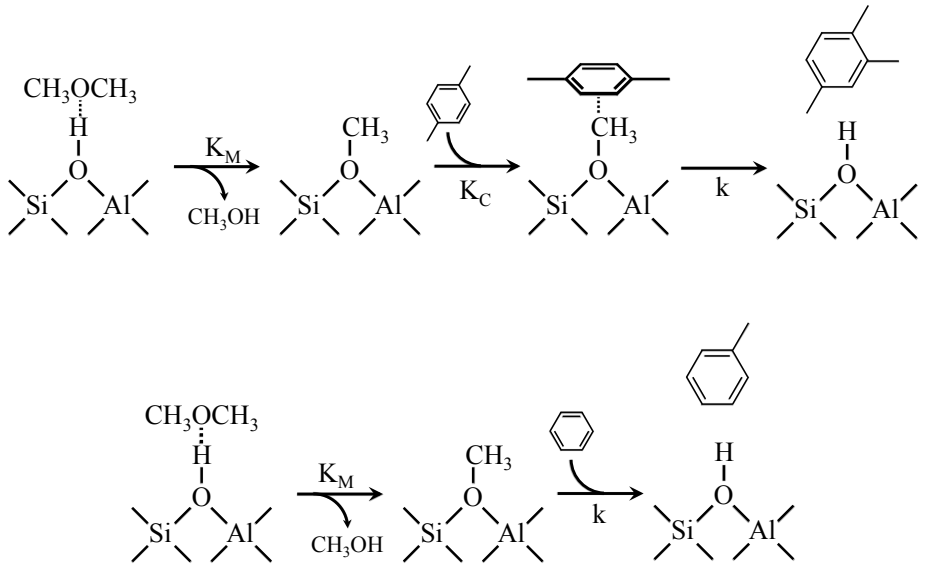

Figure 25. Proposed mechanisms for *para*-xylene and *ortho*-xylene (top) and benzene and toluene (bottom) methylation with DME.

Assuming inhibition by methanol is negligible due to its trace quantities observed compared to DME and that methanol is also active for methylation reactions, and the surface is predominately covered by surface methoxides as observed from surface titration studies, Equation (2) simplifies to:

(3)

$$\frac{Rate}{[H^+]_O} = k[Ar_n]$$

This model fits rate data presented in Figures 21 and 22 for all partial pressures of DME and benzene/toluene measured, as well as observed secondary kinetic isotope effects and surface titration studies.

Based on the observations that (i) the reaction rate simultaneously saturates in xylene and DME pressures for both *para*- and *ortho*-xylene, (ii) the saturated rate for *para*-xylene and *ortho*-xylene methylation does not change appreciably from H-ZSM-5 samples to H-SPP samples, and (iii) observed kinetic isotope effects, we postulate that this system is kinetically-limited and the rate-determining step involves a surface species derived from DME and xylene, but still involves the breaking/formation of a C-C bond. Equation 4 outlines a mechanism, which involves the formation of a surface methoxide and the adsorption of a subsequent xylene molecule prior to the rate-determining step (Figure 25, top).

(4)	(i)	$CH_3OCH_3 + H^* \leftrightarrow H{\cdot}CH_3OCH_3^*$	K_{ads}
	(ii)	$H{\cdot}CH_3OCH_3^* \leftrightarrow CH_3OH + CH_3^*$	K_M
	(iii)	$CH_3^* + Xylene \leftrightarrow Xylene{\cdot}CH_3^*$	K_c
	(iv)	$Xylene{\cdot}CH_3^* \rightarrow TMB + H^*$	k

The related rate equation for this sequence of elementary steps is:

(5)

$$\frac{Rate}{[H^+]_O} = \frac{K_{ads}K_MK_ck[Xylene]\frac{[DME]}{[CH_3OH]}}{1 + K_{ads}[DME] + K_{ads}K_M\frac{[DME]}{[CH_3OH]} + K_{ads}K_MK_c[Xylene]\frac{[DME]}{[CH_3OH]}}$$

Considering the negligible formation of methanol compared to DME as observed in reactor effluents, and the predominant surface species to be surface methoxides or co-adsorbed methoxides with xylene, equation 2 simplifies to:

(6)

$$\frac{Rate}{[H^+]_O} = \frac{K_ck[Xylene]}{1 + K_c[Xylene]}$$

Non-linear fitting of equation 6 to the pressure dependent data are plotted in figure 3 and the parameter fits are presented in Table 3. The zero-order rate constant for *para*-xylene saturates at 2.7 – 2.9 $[TMB][H+]^{-1}h^{-1}$, and for *ortho*-xylene at 3.5 $[TMB][H+]^{-1}h^{-1}$. Co-adsorption equilibrium constants are higher for *para*-xylene compared to *ortho*-xylene, and H-SPP samples increase this value compared to H-MFI samples. Higher K_c values indicate a stronger binding of xylene onto the surface methoxide.

		K_c	k_{473} ($[TMB][H^+]^{-1}h^{-1}$)
***Para*-xylene**	**H-ZSM-5**	130 ± 20	2.9 ± 0.5
	H-SPP	290 ± 70	2.7 ± 0.8
***Ortho*-xylene**	**H-ZSM-5**	17 ± 3	3.5 ± 0.7
	H-SPP	24 ± 4	3.5 ± 0.6

Table 7. Parameter fitting results for equation 3 modeling xylene pressure dependent data.

4.3.10 Adsorption effects of aromatics in MFI structures

The distinct aromatic pressure dependence behavior exhibited by xylenes compared to benzene and toluene arises, in part, due to stronger surface adsorption. Brogaard et al. [117]have reported using self-consistent DFT with BEEF-vdW and RPBE functionals and periodic boundary conditions that for MFI structures, adsorption enthalpies of -59, -73, and -78 kJ mol^{-1} for benzene, toluene, and *para*-xylene, respectively. When compared to experimental adsorption enthalpies of -55, -80, and -96 kJ mol^{-1}, [118]the computation results progressively underestimated adsorbants with higher degrees of substitution because of underestimates in the van der Waals interactions between methyl groups and the inorganic framework. [117] Aromatic compounds studied (benzene through tetracene) were found to prefer occupation of channel intersections, however, benzene and toluene were the only adsorbents that had a relative preference to adsorb into the more-restricted sinusoidal channels compared to adsorption in straight channels. [117] This indicates that for xylenes and larger aromatics, accessibility to sinusoidal channels is restricted. These results are supported by IR measurements by Armaroli et al. [106]that show benzene, toluene, *para*-xylene, and *ortho*-xylene completely

occupy the acid sites of H-ZSM-5, but *meta*-xylene only partially occupies surface acid sites at room temperature, indicating restricted access to a fraction of these sites, which would be expected to exacerbate with bulkier surface methoxides in place of Brønsted acid sites and could lead to similar behavior in *para*- and *ortho*-xylene.

This restricted accessibility has also been noted experimentally by calorimetric studies obtaining adsorption isotherms for *para*-xylene on H-ZSM-5, noting a phase transition in the zeolite structure at 300 K, [119] thermogravimetric analysis citing 210 and 180 J mol^{-1} K^{-1} entropy differences for *para*-xylene and benzene adsorption, respectively. [120] X-ray diffraction studies for *para-,* [121]*ortho*-, and *meta*-xylene isomers [122] in silicalite have noted missing symmetries indicative of aromatic occupation of sinusoidal channels, in addition to distorting the MFI straight channels to induce a monoclinic to orthorhombic transition at room temperature for aromatic loading greater than three molecules per unit cell. The preferential occupation of straight channels over sinusoidal channels has been noted to lead to significant kinetic differences in *para*-xylene isomerization compared to *ortho*- and *meta*-xylene isomers over H-ZSM-5, which were mostly invariant with the addition of MgO and CaO on a 1:1 basis with Al, indicating that occupation effects play a larger role than sterics in this system. [123] As adsorption is an equilibrium process that is dependent on aromatic pressure in the gas phase, enhanced adsorption on H-SPP compared to H-MFI could be explained by enhanced access to less favored adsorption sites with less effect of sterics from neighboring molecules, allowing for the achievement of a saturated zeolite surface at lower aromatic partial pressures.

The methylation of xylene on MFI is distinct from elementary-step methylation reactions of olefins, benzene, and toluene in that, in the absence of diffusion limitations, rate saturation is achieved relative to both xylene and DME partial pressures. This phenomenon is attributed to the saturation of the zeolite surface with xylene molecules adsorbing on a surface methoxide, owing to highly negative enthalpies of adsorption. Differences between *para*- and *ortho*- xylene may arise because of a resistance to surface saturation due to varying degrees of difficulty in interacting with Brønsted acid centers located in MFI sinusoidal pores. Higher xylene pressures drive the co-adsorption equilibrium towards adsorbed species until the surface is effectively saturated with

xylene molecules adsorbed on to surface *CH_3 species. Comparing H-SPP, containing 2 – 7 nm mesopores, with 1 μm crystallite H-ZSM-5 it is observed that xylene pressure at which rate saturation is achieved is lower for H-SPP. This is ascribed to improved tortuosity effects toward active site accessibility due to a higher fraction of accessible sites being exposed on the one-unit cell thick zeolite sheets.

4.4 Conclusions

The rate of methylation of benzene and toluene with DME at temperatures below 503 K at differential conversions is first-order dependent in aromatic pressure and independent of DME pressure, indicating the rapid formation of DME-derived species covering the zeolite surface reacting with the aromatic in the rate-determining step. The kinetics of benzene methylation are consistent with previous studies at higher temperatures with rates extrapolated to zero contact time [94] and toluene methylation activation energies are consistent with previous kinetic studies. [102,103] Benzene and toluene methylation proceed with similar rates and activation energies as propene and 1-butene methylation, respectively, on H-ZSM-5. A comparison with H-SPP show no significant difference between microporous and mesoporous samples (minimum factor of 150 difference in critical diffusion length) thereby demonstrating that transport restrictions do not play a role in benzene and toluene methylation under the reaction conditions reported in this research.

Methylation of *para*- and *ortho*-xylene show a shift in surface species population from surface methoxides to co-adsorbed xylene on surface methoxides, as observed from differing apparent activation energies at low and high partial pressures of xylene. These reactions were run in the absence of isomerization and diffusion limitations, and the formation of surface methoxides for all methylation reactions is consistent with post-reaction titration experiments with water liberating 1:1 methanol molecules per zeolite Al. Inhibited DME isotopic exchange is observed for para-xylene methylation only, indicative of co-adsorbed xylene molecules blocking the methoxide species from further reaction with DME. Observed secondary kinetic isotope effects for benzene, toluene, and

xylene methylation studies over H-MFI show that the rate-determining step is the same across these aromatics, and it consistent with similar observation for ethylene methylation. [89] These experiments explain the distinct behavior of xylene methylation from benzene and toluene methylation over microporous and mesoporous MFI on a mechanistic basis.

Acknowledgements

The authors acknowledge financial support from The Dow Chemical Company and the National Science Foundation (CBET 1055846)

Chapter 5: Unpublished results—Pentene β-scission over H-MFI and H-BEA

5.1 Introduction

The MTH process is comprised of many reactions that play a critical role in the observed product distribution. So far, this work has been concerned with carbon-carbon bond forming reactions, however the decomposition of higher olefins and higher methylbenzenes also plays an important role in determining product distributions of the MTH process, namely, the formation of light olefins. Previous research that has studied the kinetics of olefin β-scission, conducted by Buchanan et al., [124] has shown that the cracking of olefins occurs on a much faster time scale than their alkane counterparts.

There are three possible reactions through which an olefin can proceed upon interacting with a zeolite acid site: (i) β-scission to form stoichiometric ratios of olefin fragments, (ii) isomerization of one olefin species to another through either the migration of the double-bond or the rearrangement of methyl side groups, and (iii) bimolecular oligomerization of two olefins into one olefin of double the carbon chain length (Figure 26), and its potential cracking products.

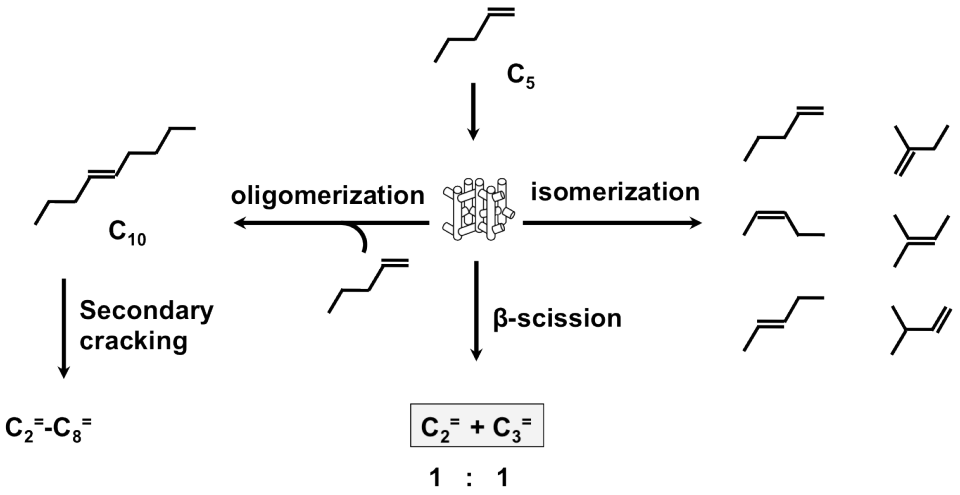

Figure 26. Possible reactions of 1-pentene with H-MFI

Quantifying olefin β-scission reactions either requires the complete isolation of β-scission from both oligomerization and isomerization reactions, or the instance where

isomerization is quantifiable either through direct measurement of individual isomers or through modeling isomerization as being thermodynamically equilibrated. The latter case would require calculating the mole fraction of each isomer, y_j, is calculated from an individual isomer's Gibbs free energy of formation and used in the equations (1) and (2) as defined by Alberty et al. [125]

(1) $$\Delta G_T{}^o(T) = -RT \ln \left[\sum_{j=1}^{N_j} \exp\left(-\frac{\Delta G_j{}^o(T)}{RT}\right)\right]$$

(2) $$y_j = \exp\left(\frac{\Delta G_T{}^o(T) - \Delta G_j{}^o(T)}{RT}\right)$$

where $\Delta G_j{}^o(T)$ is the Gibbs free energy of formation for isomer j and temperature T; N_j is the number of isomers.

The kinetics of 2-pentene and 2-methyl-2-butene over zeolites H-MFI and H-BEA are discussed in this work and the relationship between the rate constant and extent of isomer equilibration in relation to observable and theoretical products is addressed.

5.2 Materials and methods

Steady-state olefin cracking was carried out in a 10 mm inner diameter packed-bed quartz reactor at atmospheric pressure and differential conversions (<0.5% product formation) and reaction temperatures above 703 K for H-BEA and 773 K for H-MFI. H-MFI and H-BEA zeolites (Zeolyst) were supported on a quartz frit at the bottom of the reactor, and the temperature was controlled using a furnace (National Electric Furnace FA120 type) connected to a Watlow Temperature Controller (96 series), which was measured using a K-type thermocouple placed in a well penetrating the catalyst bed. Samples (0.0003g, diluted in quartz sand) were pretreated in flowing He (1.67 cm^3s^{-1}, ultrapure, Minneapolis Oxygen) at a 773 K (0.067 Ks^{-1} temperature ramp for 6 hours. A mixture of methane and argon (1:99, Matheson) was combined with 2-pentene or 2-methyl-2-butene (Sigma-Aldrich, analytical grade), which was introduced via a syringe pump (kdScientific) at approximately 1.3 x 10^{-2} kPa olefin, and He to obtain a total flow

rate of 3.35 cm^3s^{-1}. Reactor effluent composition was monitored via gas chromatography (Agilent 7890) through a methyl-siloxane capillary column (HP-1, 50.0 m x 320 μm x 0.52 μm) connected to a flame ionization detector.

5.3 Results and discussion

5.3.1 Kinetics of pentene β-scission over H-MFI and H-BEA

Pentene β-scission reactions were operated at high temperatures (>723 K), low catalyst weights (0.3 mg), and low pentene pressures (1.3 x 10^{-2} kPa) to avoid olefin oligomerization and subsequent secondary cracking. [126] Pressure dependent studies showed a first-order behavior dependence on the rate of 1:1 ethene and propene formation with pentene pressure, indicating that (i) the surface coverage of pentene on the zeolite surface is low, and (ii) that oligomerization and secondary cracking are not significant at these conditions (Figures 27 and 28).

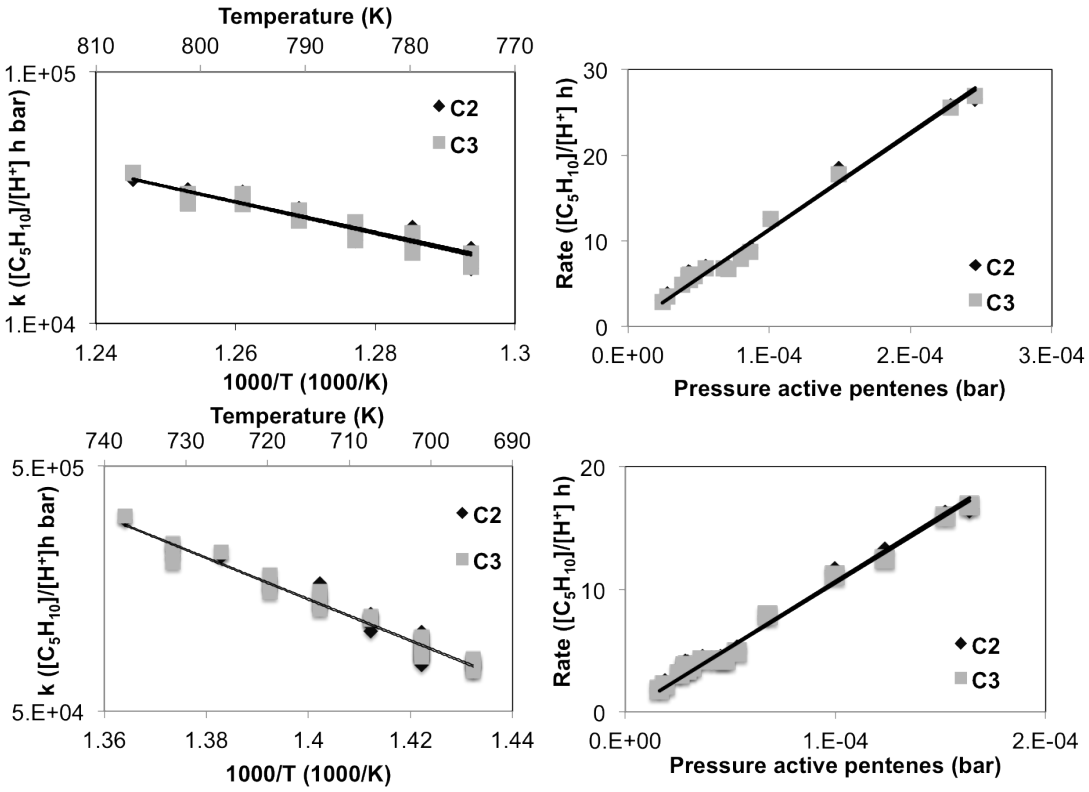

Figure 27. Ethene and propene formation from 2-pentene over H-MFI (Top) at T > 773 K and H-BEA at T > 723 K (bottom). Temperature dependence in left panels, 2-pentene pressure dependence in right panels.

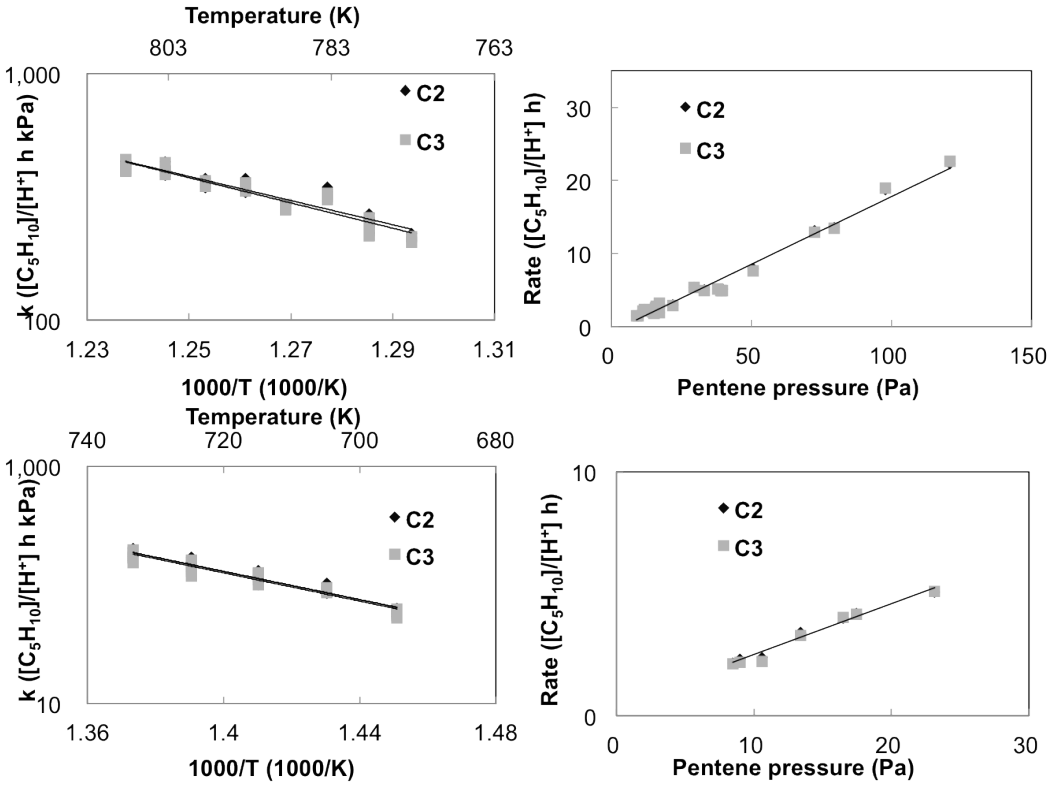

Figure 28. Ethene and propene formation from 2-methyl-2-butene over H-MFI (Top) at T > 773 K and H-BEA at T > 723 K (bottom). Temperature dependence in left panels, 2-methyl-2-butene pressure dependence in right panels.

Rate constants and activation energies for 2-pentene and 2-methyl-2-butene β-scission are provided in Table 9 and show that H-BEA has a higher rate constant and activation energy compared with H-MFI. This could be explained through the stabilization of reactants, intermediates, or transition states in H-MFI to via increased van der Waals forces in its smaller pore network compared to H-BEA, leading to a decrease in the apparent activation barrier. Comparison of pentene β-scission rate constants over MFI with those previously reported [124] show a difference within a factor of two (~5.3 compared to 9.5 s^{-1} bar^{-1}), indicating good agreement with literature.

		All pentenes		2-m-2-butene corrected	
		Ea (kJ/mol)	k_{783} $(s\ bar)^{-1}$	Ea (kJ/mol)	k_{783} $(s\ bar)^{-1}$
2-pentene	**H-MFI**	120 ± 11	5.5	-	11.4
	H-BEA	162 ± 15	88	-	112
2-methyl-2-butene	**H-MFI**	99 ± 14	5.0	-	13.8
	H-BEA	135 ± 12	40	-	99

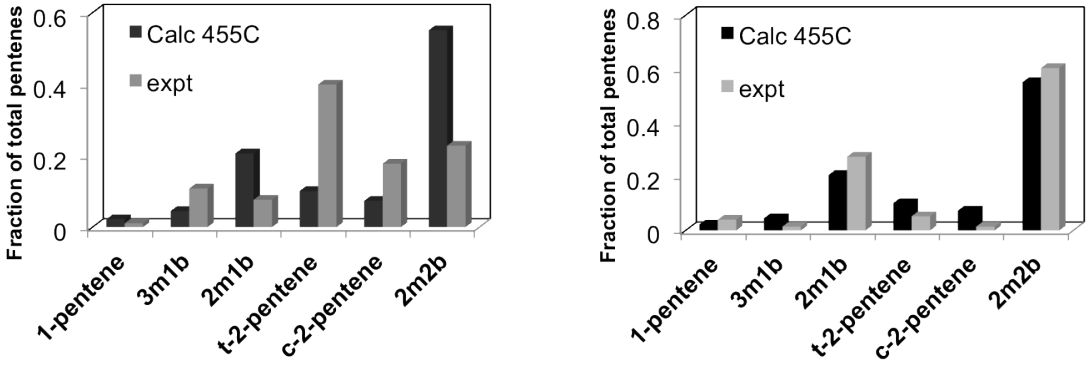

Table 8. First-order rate constants at 783 K and activation energies for 2-pentene and 2-methyl-2-butene β-scission over H-MFI and H-BEA. Plots: theoretical and experimental isomer distribution for effluent C_5 for 2-pentene feed (left) and 2-methyl-2-butene feed (right) at reaction temperatures.

5.3.2 Effect of isomerization on β-scission reactions

In this study, as also observed in a previous study, [124] the isomerization of olefins occurs on a faster time scale than β-scission reactions over H-MFI at the reaction conditions used. In this case, the pentene isomers measured in the effluent matched the predicted thermodynamic equilibrium distribution of isomers, as can be seen from good agreement between 2-methyl-2-butene and 2-pentene rate constants. H-BEA cracks 2-pentene and 2-methyl-2-butene at rates that differ by over a factor of two, favoring 2-pentene methylation.

When comparing the six isomers of pentene, only 2-methyl-2-butene lacks a carbon-carbon bond in the β position relative to the double bond of the olefin (Figure 29). This means that there is no reasonable pathway for 2-methyl-2-butene to form ethene and propene, as observed in the products. The isomer distributions of the reactor effluent from 2-pentene and 2-methyl-2-butene cracking over H-BEA are shown in Table 8 and indicate that the isomer distribution is not thermally equilibrated as in the case of H-MFI.

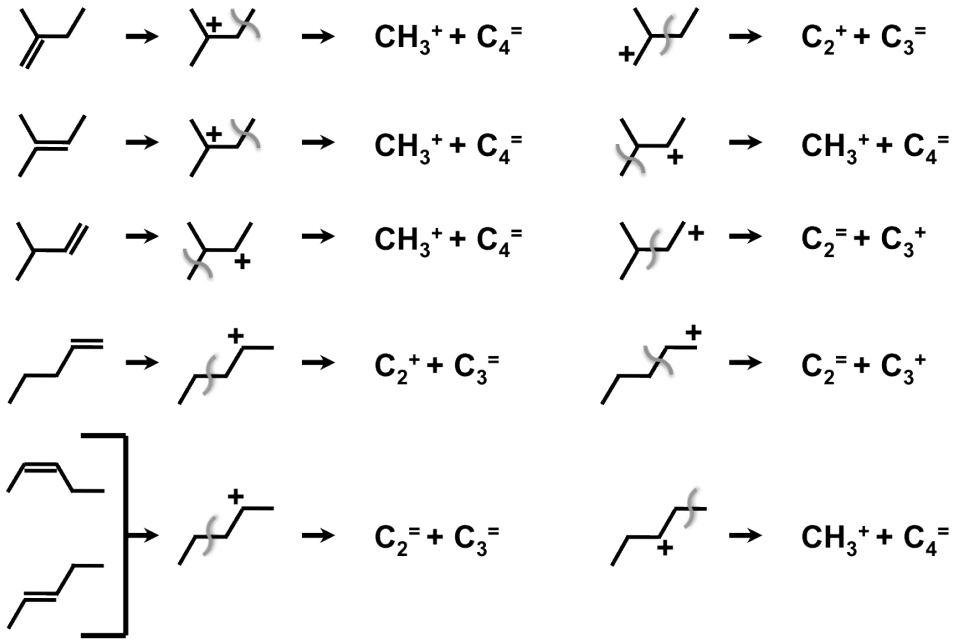

Figure 29. The six isomers of pentene, possible intermediate carbocations upon protonation with a zeolite Brønsted acid site, and the expected cracking products based on cleavage of the β carbon-carbon bond (indicated in gray).

The incomplete isomerization of pentenes in H-BEA can accounted in the calculation of rate constants when considering the inability of 2-methyl-2-butene to generate ethene or propene. When 2-pentene is used as a reactant, 77.2% of pentenes have a viable pathway to form the observed products, and only 39.6% when 2-methyl-2-butene is reacted. The corrected pentene pressures for active reactants are shown in Table 8, and can account for the discrepancy in rate constants between the two reactants in H-BEA (12% error compared to 55% error between the two values). This method is expected to only be viable for cracking systems where individual isomers can be separately quantified, otherwise, the only method of quantifying inactive isomers toward β-scission

would be to achieve and model an equilibrium distribution of isomers in the effluent stream at differential conditions.

Acknowledgements

The author would like to acknowledge Maria Chen for assisting in experiments and continuing this work.

Chapter 6: Appendix — Full derivation of co-adsorbed versus methoxide mechanisms in olefin methylation

6.1 Rate expression derivation for dimethyl ether to hydrocarbons systems

The site-balance in equation (1) refer to unoccupied acid sites; physisorbed DME, methanol, methanol dimers, DME/olefin and MeOH/olefin co-adsorption complexes; chemisorbed methoxy groups, and olefins adsorbed onto surface methoxides, respectively:

(1) $$[H^+]_0 = H^* + H{\cdot}CH_3OCH_3^* + H{\cdot}CH_3OH^* + H{\cdot}Dimer^*$$
$$+H{\cdot}CH_3OCH_3{\cdot}O_n^* + H{\cdot}CH_3OH{\cdot}O_n^* + CH_3^* + CH_3{\cdot}O_n^*$$

Derivations for both cases assume that only one type of site is responsible for methylation and all others inhibit the reaction through competitive population of zeolite active sites.

6.1.1 Co-adsorbed complex mediated route

The formation of dimethyl ether and methanol co-adsorption complexes with olefins and their decomposition into methylated products is described by the following reaction scheme:

(i)	$CH_3OCH_3 + H^* \leftrightarrow H{\cdot}CH_3OCH_3^*$	K_a
(ii)	$H{\cdot}CH_3OCH_3^* + O_n \leftrightarrow H{\cdot}CH_3OCH_3{\cdot}O_n^*$	K_C
(iii)	$H{\cdot}CH_3OCH_3{\cdot}O_n^* \rightarrow O_{n+1} + H^* + CH_3OH$	k_C
(iv)	$CH_3OH + H^* \leftrightarrow H{\cdot}CH_3OH^*$	K_a'
(v)	$H{\cdot}CH_3OH^* + O_n \leftrightarrow H{\cdot}CH_3OH{\cdot}O_n^*$	K_C'
(vi)	$H{\cdot}CH_3OH^* + CH_3OH \leftrightarrow H{\cdot}Dimer^*$	K_D
(vii)	$H{\cdot}CH_3OH{\cdot}O_n^* \rightarrow O_{n+1} + H^* + H_2O$	k_C'
(viii)	$H{\cdot}CH_3OCH_3^* \leftrightarrow CH_3OH + CH_3^*$	K_M
(ix)	$H{\cdot}CH_3OH^* \leftrightarrow H_2O + CH_3^*$	K_M'

(x) $CH_3^* + O_n \leftrightarrow CH_3 \cdot O_n^*$ K_O

The mechanism described in the scheme above provides two potential reactions to generate a methylated olefin, corresponding to co-adsorbed complexes generated from DME and methanol. The corresponding rate expression for this scheme is presented in Figure 26 (top).

Assuming decomposition of these co-adsorbed complexes occur on kinetically similar time scales, as reported by Svelle et al. [64] where the rate of DME methylation of propene is ~2.5 times that of methanol when comparing saturated rates (625 K, 20 mbar C_3H_6 25 – 75 mbar DME or CH_3OH, 100 mL min^{-1} flow) and 5 times that of methanol based on B3LYP/6-31G(d) + ZPE energy calculations and quasi-IRC techniques [5]:

$$\frac{Rate_c}{[H^+]_0} = k_c[H \bullet CH_3OCH_3 \bullet O_n^*] + k_c'[H \bullet CH_3OH \bullet O_n^*]$$

or

$$\frac{Rate_c}{[H^+]_0} = k_c[H \bullet CH_3OCH_3 \bullet O_n^*]$$; for high DME pressures and low conversions (DME>>MeOH).

The overall rate expression reduces to the equation below in the situation that DME and olefin are both in excess of zeolite acid sites, based on the assumption that the DME-olefin co-adsorbed complex predominates the surface:

$$\frac{Rate_C}{[H^+]_0} = k_C$$

6.1.2 Surface methoxide mediated route

The surface methoxide-mediated mechanism is represented by the following sequence of reaction steps:

(i) $CH_3OCH_3 + H^* \leftrightarrow H \cdot CH_3OCH_3^*$ K_a

(ii) $H \cdot CH_3OCH_3^* \leftrightarrow CH_3OH + CH_3^*$ K_M

(iii)	$CH_3^* + O_n \leftrightarrow CH_3 \cdot O_n^*$	K_O
(iv)	$CH_3 \cdot O_n^* \rightarrow O_{n+1} + H^*$	k_M
(v)	$CH_3OH + H^* \leftrightarrow H \cdot CH_3OH^*$	K_a'
(vi)	$H \cdot CH_3OH^* \leftrightarrow H_2O + CH_3^*$	K_M'
(vii)	$H \cdot CH_3OCH_3^* + O_n \leftrightarrow H \cdot CH_3OCH_3 \cdot O_n^*$	K_C
(viii)	$H \cdot CH_3OH^* + O_n \leftrightarrow H \cdot CH_3OH \cdot O_n^*$	K_C'
(ix)	$H \cdot CH_3OH^* + CH_3OH \leftrightarrow H \cdot Dimer^*$	K_D

Where O_n refers to a general olefin consisting of n-carbons and O_{n+1} refers to the methylated olefin, or butene and pentene in this report, respectively. The corresponding rate expression for this mechanism shown in Figure 26 (Bottom).

The overall rate expression reduces to the equation below in the situation that DME and olefin are both in excess of zeolite acid sites and the surface is predominately covered by surface methoxide species:

$$\frac{Rate_M}{[H^+]_0} = K_O k_M P_O$$

$$\frac{Rate_C}{[H^+]_0} = \frac{P_O(K_a K_C k_C P_{DME} + K'_a K'_C k'_C P_{MeOH})}{1 + K_a K_C P_{DME} P_O + K_a K_M \frac{P_{DME}}{P_{MeOH}} + K_a P_{DME} + K'_a P_{MeOH} + K'_a K_C P_{MeOH} P_O + K'_a K'_M \frac{P_{MeOH}}{P_{H_2O}} + K'_a K_D P_{MeOH}^2 + K_a K_M K_O \frac{P_{DME}}{P_{MeOH}} + K'_a K'_M K_O \frac{P_{DME}}{P_{MeOH}}}$$

$$\frac{Rate_M}{[H^+]_0} = \frac{K_O k_M P_O (K_a K_M \frac{P_{DME}}{P_{MeOH}} + K'_a K'_M \frac{P_{MeOH}}{P_{H_2O}})}{1 + K_a K_M \frac{P_{DME}}{P_{MeOH}} + K_a K_M K_O \frac{P_{DME}}{P_{MeOH}} P_O + K_a K_C P_{DME} P_O + K_a P_{DME} + K'_a P_{MeOH} + K_a K_M \frac{P_{MeOH}}{P_{H_2O}} + K'_a K'_M K_O \frac{P_{MeOH}}{P_{H_2O}} P_O + K'_a K'_C P_{MeOH} P_O + K'_a K_D P_{MeOH}^2}$$

Figure 30. Full rate expressions for the methylation of hydrocarbons through the co-adsorbed mechanism (top) or the surface methoxide mechanism (bottom).

Chapter 7: Bibliography

References

1. Baerlocher, C.; McCusker, L. B. *http://www.iza-structure.org/databases/* (accessed 01/28, 2009).

2. Cheung, P.; Bhan, A.; Sunley, G. J.; Iglesia, E. Selective carbonylation of dimethyl ether to methyl acetate catalyzed by acidic zeolites. *Angew. Chem. Int. Ed.* **2006**, *45*, 1617-1620.

3. Chiang, H.; Bhan, A. Catalytic consequences of hydroxyl group location on the rate and mechanism of parallel dehydration reactions of ethanol over acidic zeolites. *J. Catal.* **2010**, *271*, 251-261.

4. Chiang, H.; Bhan, A. Catalytic consequences of hydroxyl group location on the kinetics of n-hexane hydroisomerization over acidic zeolites. *J. Catal.* **2011**, *283*, 98-107.

5. Liu, D.; Bhan, A.; Tsapatsis, M.; Al Hashimi, S. Catalytic Behavior of Bronsted Acid Sites in MWW and MFI Zeolites with Dual Meso- and Microporosity. *ACS Catal.* **2011**, *1*, 7-17.

6. Chang, C. D.; Silvestri, A. J. Conversion of Methanol and Other O-Compounds to Hydrocarbons Over Zeolite Catalysts. *J. Catal.* **1977**, *47*, 249-259.

7. Ahn, J. H.; Temel, B.; Iglesia, E. Selective Homologation Routes to 2,2,3-Trimethylbutane on Solid Acids. *Angew. Chem. Int. Ed.* **2009**, *48*, 3814-3816.

8. Simonetti, D. A.; Ahn, J. H.; Iglesia, E. Mechanistic details of acid-catalyzed reactions and their role in the selective synthesis of triptane and isobutane from dimethyl ether. *J. Catal.* **2011**, *277*, 173-195.

9. Laurendeau, N. M. Heterogeneous Kinetics of Coal Char Gasification and Combustion. *Prog. Energy Combust. Sci.* **1978**, *4*, 221-270.

10. Wen, W. Y. Mechanisms of Alkali-Metal Catalysis in the Gasification of Coal, Char, Or Graphite. *Catal. Rev. Sci. Eng.* **1980**, *22*, 1-28.

11. Sutton, D.; Kelleher, B.; Ross, J. R. H. Review of literature on catalysts for biomass gasification. *Fuel Process. Technol.* **2001**, *73*, 155-173.

12. Asadullah, M.; Ito, S.; Kunimori, K.; Yamada, M.; Tomishige, K. Biomass gasification to hydrogen and syngas at low temperature: Novel catalytic system using fluidized-bed reactor. *J. Catal.* **2002**, *208*, 255-259.

13. Hickman, D. A.; Schmidt, L. D. Production of Syngas by Direct Catalytic-Oxidation of Methane. *Science* **1993**, *259*, 343-346.

14. Bowker, M.; Houghton, H.; Waugh, K. C. Mechanism and Kinetics of Methanol Synthesis on Zinc-Oxide. *J. Chem. Soc., Faraday Trans.* **1981**, *77*, 3023-3036.

15. Bowker, M.; Hadden, R. A.; Houghton, H.; Hyland, J. N. K.; Waugh, K. C. The Mechanism of Methanol Synthesis on Copper-Zinc Oxide Alumina Catalysts. *J. Catal.* **1988**, *109*, 263-273.

16. Song, W. G.; Marcus, D. M.; Fu, H.; Ehresmann, J. O.; Haw, J. F. An Oft-studied reaction that may never have been: Direct catalytic conversion of methanol or dimethyl ether to hydrocarbons on the solid acids HZSM-5 or HSAPO-34. *J. Am. Chem. Soc.* **2002**, *124*, 3844-3845.

17. Dahl, I. M.; Kolboe, S. On the Reaction-Mechanism for Propene Formation in the Mto Reaction Over Sapo-34. *Catal. Lett.* **1993**, *20*, 329-336.

18. Lesthaeghe, D.; Van der Mynsbrugge, J.; Vandichel, M.; Waroquier, M.; Van Speybroeck, V. Full Theoretical Cycle for both Ethene and Propene Formation during Methanol-to-Olefin Conversion in H-ZSM-5. *ChemCatChem* **2011**, *3*, 208-212.

19. Svelle, S.; Arstad, B.; Kolboe, S.; Swang, O. A theoretical investigation of the methylation of alkenes with methanol over acidic zeolites. *J. Phys. Chem. B* **2003**, *107*, 9281-9289.

20. Cui, Z.; Liu, Q.; Ma, Z.; Bian, S.; Song, W. Direct observation of olefin homologations on zeolite ZSM-22 and its implications to methanol to olefin conversion. *J. Catal.* **2008**, *258*, 83-86.

21. Bjorgen, M.; Olsbye, U.; Kolboe, S. Coke precursor formation and zeolite deactivation: mechanistic insights from hexamethylbenzene conversion. *J. Catal.* **2003**, *215*, 30-44.

22. Bjorgen, M.; Olsbye, U.; Petersen, D.; Kolboe, S. The methanol-to-hydrocarbons reaction: insight into the reaction mechanism from [C-12]benzene and [C-13]methanol coreactions over zeolite H-beta. *J. Catal.* **2004**, *221*, 1-10.

23. Arstad, B.; Kolboe, S. The reactivity of molecules trapped within the SAPO-34 cavities in the methanol-to-hydrocarbons reaction. *J. Am. Chem. Soc.* **2001**, *123*, 8137-8138.

24. Bjorgen, M.; Svelle, S.; Joensen, F.; Nerlov, J.; Kolboe, S.; Bonino, F.; Palumbo, L.; Bordiga, S.; Olsbye, U. Conversion of methanol to hydrocarbons over zeolite H-ZSM-5: On the origin of the olefinic species. *J. Catal.* **2007**, *249*, 195-207.

25. Chang, C. D.; Kuo, J. C. W.; Lang, W. H.; Jacob, S. M.; Wise, J. J.; Silvestri, A. J. Process Studies on Conversion of Methanol to Gasoline. *Ind. Eng. Chem. Process Des. Dev.* **1978**, *17*, 255-260.

26. Dessau, R. M. On the H-ZSM-5 catalyzed formation of ethylene from methanol or higher olefins. *J. Catal.* **1986**, *99*, 111-116.

27. Haw, J. F.; Nicholas, J. B.; Song, W. G.; Deng, F.; Wang, Z. K.; Xu, T.; Heneghan, C. S. Roles for cyclopentenyl cations in the synthesis of hydrocarbons from methanol on zeolite catalyst HZSM-5. *J. Am. Chem. Soc.* **2000**, *122*, 4763-4775.

28. McCann, D. M.; Lesthaeghe, D.; Kletnieks, P. W.; Guenther, D. R.; Hayman, M. J.; Van Speybroeck, V.; Waroquier, M.; Haw, J. F. A complete catalytic cycle for supramolecular methanol-to-olefins conversion by linking theory with experiment. *Angew. Chem. Int. Ed.* **2008**, *47*, 5179-5182.

29. Olsbye, U.; Bjorgen, M.; Svelle, S.; Lillerud, K. P.; Kolboe, S. Mechanistic insight into the methanol-to-hydrocarbons reaction. *Catal. Today* **2005**, *106*, 108-111.

30. Haw, J. F.; Song, W. G.; Marcus, D. M.; Nicholas, J. B. The mechanism of methanol to hydrocarbon catalysis. *Acc. Chem. Res.* **2003**, *36*, 317-326.

31. Haag, W. O.; Lago, R. M.; Rodewald, P. G. Aromatics, Light Olefins and Gasoline from Methanol - Mechanistic Pathways with ZSM-5 Zeolite Catalyst. *J. Mol. Catal.* **1982**, *17*, 161-169.

32. Chang, C. D. Hydrocarbons from Methanol. *Catal. Rev. Sci. Eng.* **1983**, *25*, 1-118.

33. Stocker, M. Methanol-to-hydrocarbons: catalytic materials and their behavior. *Microporous Mesoporous Mater.* **1999**, *29*, 3-48.

34. Campbell, S. M.; Jiang, X. Z.; Howe, R. F. Methanol to hydrocarbons: spectroscopic studies and the significance of extra-framework aluminium. *Microporous Mesoporous Mater.* **1999**, *29*, 91-108.

35. Arstad, B.; Kolboe, S.; Swang, O. Theoretical investigation of arene alkylation by ethene and propene over acidic zeolites. *J. Phys. Chem. B* **2004**, *108*, 2300-2308.

36. Hemelsoet, K.; Nollet, A.; Vandichel, M.; Lesthaeghe, D.; Van Speybroeck, V.; Waroquier, M. The Effect of Confined Space on the Growth of Naphthalenic Species in a Chabazite-Type Catalyst: A Molecular Modeling Study. *ChemCatChem* **2009**, *1*, 373-378.

37. Mikkelsen, O.; Ronning, P. O.; Kolboe, S. Use of isotopic labeling for mechanistic studies of the methanol-to-hydrocarbons reaction. Methylation of toluene with methanol over H-ZSM-5, H-mordenite and H-beta. *Microporous Mesoporous Mater.* **2000**, *40*, 95-113.

38. Svelle, S.; Ronning, P. A.; Kolboe, S. Kinetic studies of zeolite-catalyzed methylation reactions 1. Coreaction of [C-12]ethene and [C-13]methanol. *J. Catal.* **2004**, *224*, 115-123.

39. Svelle, S.; Ronning, P. O.; Olsbye, U.; Kolboe, S. Kinetic studies of zeolite-catalyzed methylation reactions. Part 2. Co-reaction of [C-12]propene or [C-12]n-butene and [C-13]methanol. *J. Catal.* **2005**, *234*, 385-400.

40. Cui, Z.; Liu, Q.; Song, W.; Wan, L. Insights into the Mechanism of Methanol-to-Olefin Conversion at Zeolites with Systematically Selected Framework Structures. *Angew. Chem. Int. Ed.* **2006**, *45*, 6512-6515.

41. Wang, C.; Wang, Y.; Lie, H.; Xie, Z.; Liu, Z. Catalytic activity and selectivity of methylbenzenes in HSAPO-34 catalyst for the methanol-to-olefins conversion from first principles. *J. Catal.* **2010**, *271*, 386-391.

42. Olah, G. A. Beyond oil and gas: The methanol economy. *Angew. Chem. Int. Ed.* **2005**, *44*, 2636-2639.

43. Olah, G. A. After oil and gas: methanol economy. *Catal. Lett.* **2004**, *93*, 1-2.

44. Wang, W.; Hunger, M. Reactivity of surface alkoxy species on acidic zeolite catalysts. *Acc. Chem. Res.* **2008**, *41*, 895-904.

45. Lesthaeghe, D.; Van Speybroeck, V.; Marin, G. B.; Waroquier, M. Understanding the failure of direct C-C coupling in the zeolite-catalyzed methanol-to-olefin process. *Angew. Chem. Int. Ed.* **2006**, *45*, 1714-1719.

46. Lesthaeghe, D.; Van Speybroeck, V.; Marin, G. B.; Waroquier, M. What role do oxonium ions and oxonium ylides play in the ZSM-5 catalysed methanol-to-olefin process? *Chem. Phys. Lett.* **2006**, *417*, 309-315.

47. Lesthaeghe, D.; Van Speybroeck, V.; Marin, G. B.; Waroquier, M. The rise and fall of direct mechanisms in methanol-to-olefin catalysis: An overview of theoretical contributions. *Ind. Eng. Chem. Res.* **2007**, *46*, 8832-8838.

48. Marcus, D. M.; McLachlan, K. A.; Wildman, M. A.; Ehresmann, J. O.; Kletnieks, P. W.; Haw, J. F. Experimental evidence from H/D exchange studies for the failure of direct C-C coupling mechanisms in the methanol-to-olefin process catalyzed by HSAPO-34. *Angew. Chem. Int. Ed.* **2006**, *45*, 3133-3136.

49. Dessau, R. M.; LaPierre, R. B. On the mechanism of methanol conversion to hydrocarbons over HZSM-5. *J. Catal.* **1982**, *78*, 136-141.

50. Dahl, I. M.; Kolboe, S. On the reaction mechanism for hydrocarbon formation from methanol over SAPO-34 .2. Isotopic labeling studies of the co-reaction of propene and methanol. *J. Catal.* **1996**, *161*, 304-309.

51. Dahl, I. M.; Kolboe, S. On the Reaction-Mechanism for Hydrocarbon Formation from Methanol Over Sapo-34 .1. Isotopic Labeling Studies of the Co-Reaction of Ethene and Methanol. *J. Catal.* **1994**, *149*, 458-464.

52. Teketel, S.; Olsbye, U.; Lillerud, K.; Beato, P.; Svelle, S. Selectivity control through fundamental mechanistic insight in the conversion of methanol to hydrocarbons over zeolites. *Microporous Mesoporous Mater.* **2010**, *136*, 33-41.

53. Wang, C.; Wang, Y.; Xie, Z.; Liu, Z. Methanol to Olefin Conversion on HSAPO-34 Zeolite from Periodic Density Functional Theory Calculations: A Complete Cycle of Side Chain Hydrocarbon Pool Mechanism. *J. Phys. Chem. C* **2009**, *113*, 4584-4591.

54. Kolboe, S.; Svelle, S.; Arstad, B. Theoretical Study of Ethylbenzenium Ions: The Mechanism for Splitting Off Ethene, and the Formation of a pi Complex of Ethene and the Benzenium Ion. *J. Phys. Chem. A* **2009**, *113*, 917-923.

55. Lesthaeghe, D.; Horre, A.; Waroquier, M.; Marin, G. B.; Van Speybroeck, V. Theoretical Insights on Methylbenzene Side-Chain Growth in ZSM-5 Zeolites for Methanol-to-Olefin Conversion. *Chem. -Eur. J.* **2009**, *15*, 10803-10808.

56. Lesthaeghe, D.; De Sterck, B.; Van Speybroeck, V.; Marin, G. B.; Waroquier, M. Zeolite shape-selectivity in the gem-methylation of aromatic hydrocarbons. *Angew. Chem. Int. Ed.* **2007**, *46*, 1311-1314.

57. Song, W. G.; Haw, J. F.; Nicholas, J. B.; Heneghan, C. S. Methylbenzenes are the organic reaction centers for methanol-to-olefin catalysis on HSAPO-34. *J. Am. Chem. Soc.* **2000**, *122*, 10726-10727.

58. Van Speybroeck, V.; Van der Mynsbrugge, J.; Vandichel, M.; Hemelsoet, K.; Lesthaeghe, D.; Ghysels, A.; Marin, G. B.; Waroquier, M. First Principle Kinetic Studies of Zeolite-Catalyzed Methylation Reactions. *J. Am. Chem. Soc.* **2011**, *133*, 888-899.

59. Chen, N. Y.; Reagan, W. J. Evidence of Auto-Catalysis in Methanol to Hydrocarbon Reactions Over Zeolite Catalysts. *J. Catal.* **1979**, *59*, 123-129.

60. Langner, B. E. Reactions of Methanol on Zeolites with Different Pore Structures. *Appl. Catal.* **1982**, *2*, 289-302.

61. Svelle, S.; Joensen, F.; Nerlov, J.; Olsbye, U.; Lillerud, K.; Kolboe, S.; Bjorgen, M. Conversion of methanol into hydrocarbons over zeolite H-ZSM-5: Ethene formation is mechanistically separated from the formation of higher alkenes. *J. Am. Chem. Soc.* **2006**, *128*, 14770-14771.

62. Cui, Z.; Liu, Q.; Baint, S.; Ma, Z.; Song, W. The role of methoxy groups in methanol to olefin conversion. *J. Phys. Chem. C* **2008**, *112*, 2685-2688.

63. Svelle, S.; Tuma, C.; Rozanska, X.; Kerber, T.; Sauer, J. Quantum Chemical Modeling of Zeolite-Catalyzed Methylation Reactions: Toward Chemical Accuracy for Barriers. *J. Am. Chem. Soc.* **2009**, *131*, 816-825.

64. Svelle, S.; Kolboe, S.; Swang, O.; Olsbye, U. Methylation of alkenes and methylbenzenes by dimethyl ether or methanol on acidic zeolites. *J. Phys. Chem. B* **2005**, *109*, 12874-12878.

65. Dumesic, J. A.; Rudd, D. F.; Aparicio, L. M.; Rekoske, J. E.; Trevino, A. A. *The Microkinetics of Heterogeneous Catalysis;* American Chemical Society: Washington D.C., 1993; , pp 315.

66. Mirth, G.; Lercher, J. A. Coadsorption of Toluene and Methanol on HZSM-5 Zeolites. *J. Phys. Chem.* **1991**, *95*, 3736-3740.

67. Lee, C. C.; Gorte, R. J.; Farneth, W. E. Calorimetric study of alcohol and nitrile adsorption complexes in H-ZSM-5. *J. Phys. Chem. B* **1997**, *101*, 3811-3817.

68. Blaszkowski, S. R.; van Santen, R. A. Theoretical study of the mechanism of surface methoxy and dimethyl ether formation from methanol catalyzed by zeolitic protons. *J. Phys. Chem. B* **1997**, *101*, 2292-2305.

69. Stich, I.; Gale, J. D.; Terakura, K.; Payne, M. C. Role of the zeolitic environment in catalytic activation of methanol. *J. Am. Chem. Soc.* **1999**, *121*, 3292-3302.

70. Cheung, P.; Bhan, A.; Sunley, G. J.; Law, D. J.; Iglesia, E. Site requirements and elementary steps in dimethyl ether carbonylation catalyzed by acidic zeolites. *J. Catal.* **2007**, *245*, 110-123.

71. Yamazaki, H.; Shima, H.; Imai, H.; Yokoi, T.; Tatsumi, T.; Kondo, J. N. Evidence for a "Carbene-like" Intermediate during the Reaction of Methoxy Species with Light Alkenes on H-ZSM-5. *Angew. Chem. Int. Ed.* **2011**, *50*, 1853-1856.

72. Bosacek, V. Formation of Surface-Bonded Methoxy Groups in the Sorption of Methanol and Methyl-Iodide on Zeolites Studied by C-13 Mas Nmr-Spectroscopy. *J. Phys. Chem.* **1993**, *97*, 10732-10737.

73. Ono, Y.; Mori, T. Mechanism of Methanol Conversion into Hydrocarbons Over Zsm-5 Zeolite. *J. Chem. Soc., Faraday Trans.* **1981**, *77*, 2209-2221.

74. Blaszkowski, S. R.; van Santen, R. A. The mechanism of dimethyl ether formation from methanol catalyzed by zeolitic protons. *J. Am. Chem. Soc.* **1996**, *118*, 5152-5153.

75. Zicovich-Wilson, C. M.; Viruela, P.; Corma, A. Formation of Surface Methoxy Groups on H-Zeolites from Methanol - a Quantum-Chemical Study. *J. Phys. Chem.* **1995**, *99*, 13224-13231.

76. Boronat, M.; Martinez, C.; Corma, A. Mechanistic differences between methanol and dimethyl ether carbonylation in side pockets and large channels of mordenite. *Phys. Chem. Chem. Phys.* **2011**, *13*, 2603-2612.

77. Streitwieser, J., A.; Jagow Jr., R. H.; Fahey, R. C.; Suzuki, S. Kinetic Isotope Effects in the Acetolyses of Deuterated Cyclopentyl Tosylates. *J. Am. Chem. Soc.* **1958**, *80*, 2326.

78. Sie, S. T. Acid-Catalyzed Cracking of Paraffinic Hydrocarbons .2. Evidence for the Protonated Cyclopropane Mechanism from Catalytic Cracking Experiments. *Ind. Eng. Chem. Res.* **1993**, *32*, 397-402.

79. Sie, S. T. Acid-Catalyzed Cracking of Paraffinic Hydrocarbons .3. Evidence for the Protonated Cyclopropane Mechanism from Hydrocracking Hydroisomerization Experiments. *Ind. Eng. Chem. Res.* **1993**, *32*, 403-408.

80. Sie, S. T. Acid-Catalyzed Cracking of Paraffinic Hydrocarbons .1. Discussion of Existing Mechanisms and Proposal of a New Mechanism. *Ind. Eng. Chem. Res.* **1992**, *31*, 1881-1889.

81. Mokrani, T.; Scurrell, M. Gas Conversion to Liquid Fuels and Chemicals: The Methanol Route-Catalysis and Processes Development. *Catalysis Reviews-Science and Engineering* **2009**, *51*, 1-145.

82. Ivanova, I. I.; Corma, A. Surface species formed and their reactivity during the alkylation of toluene by methanol and dimethyl ether on zeolites as determined by in situ C-13 MAS NMR. *J Phys Chem B* **1997**, *101*, 547-551.

83. Fu, H.; Song, W.; Haw, J. Polycyclic aromatics formation in HSAPO-34 during methanol-to-olefin catalysis: ex situ characterization after cryogenic grinding. *Catal. Lett.* **2001**, *76*, 89-94.

84. Ilias, S.; Bhan, A. Tuning the selectivity of methanol-to-hydrocarbons conversion on H-ZSM-5 by co-processing olefin or aromatic compounds, *J. Catal.* **2012**, *290*, 186-192.

85. Arstad, B.; Kolboe, S. The reactivity of molecules trapped within the SAPO-34 cavities in the methanol-to-hydrocarbons reaction. *J. Am. Chem. Soc.* **2001**, *123*, 8137-8138.

86. Dessau, R. M. Response to Comments on the H-Zsm-5 Catalyzed Formation of Ethylene from Methanol. *J. Catal.* **1987**, *103*, 526-528.

87. Bosacek, V. Formation of Surface-Bonded Methoxy Groups in the Sorption of Methanol and Methyl-Iodide on Zeolites Studied by C-13 MAS NMR-Spectroscopy. *J. Phys. Chem.* **1993**, *97*, 10732-10737.

88. Svelle, S.; Visur, M.; Olsbye, U.; Saepurahman; Bjorgen, M. Mechanistic Aspects of the Zeolite Catalyzed Methylation of Alkenes and Aromatics with Methanol: A Review
. *Top. Catal.* **2011**, *54*, 897-906.

89. Hill, I. M.; Hashimi, S. A.; Bhan, A. Kinetics and mechanism of olefin methylation reactions on zeolites. *J. Catal.* **2012**, *285*, 115-123.

90. Hill, I. M.; Hashimi, S. A.; Bhan, A. Corrigendum to "Kinetics and mechanism of olefin methylation reactions on zeolites". *J. Catal.* **2012**, *291*, 155.

91. Mazar, M. N.; Hashimi, S. A.; Bhan, A.; Cococcioni, M. *J. Phys. Chem. C* **2012**, *submitted*.

92. Ilias, S.; Bhan, A. Mechanism of the Catalytic Conversion of Methanol to Hydrocarbons. *ACS Catal.* **2013**, *3*, 18-31.

93. Bjorgen, M.; Olsbye, U.; Svelle, S.; Kolboe, S. Conversion of methanol to hydrocarbons: the reactions of the heptamethylbenzenium cation over zeolite H-beta. *Catal. Lett.* **2004**, *93*, 37-40.

94. Van der Mynsbrugge, J.; Visur, M.; Olsbye, U.; Beato, P.; Bjorgen, M.; Van Speybroeck, V.; Svelle, S. Methylation of benzene by methanol: Single-site kinetics over H-ZSM-5 and H-beta zeolite catalysts. *Journal of Catalysis* **2012**, *292*, 201-212.

95. Ahn, J. H.; Kolvenbach, R.; Al-Khattaf, S. S.; Jentys, A.; Lercher, J. A. Methanol usage in toluene methylation with medium and large pore zeolites. *ACS Catalysis* **2013**, *3*, 817-825.

96. Arstad, B.; Kolboe, S.; Swang, O. A theoretical investigation on the methylation of methylbenzenes on zeolites. *J. Phys. Chem. B* **2002**, *106*, 12722-12726.

97. Vos, A.; Rozanska, X.; Schoonheydt, R.; van Santen, R.; Hutschka, F.; Hafner, J. A theoretical study of the alkylation reaction of toluene with methanol catalyzed by acidic mordenite. *J. Am. Chem. Soc.* **2001**, *123*, 2799-2809.

98. Hill, I. M.; Ng, Y. S.; Bhan, A. Kinetics of Butene Isomer Methylation with Dimethyl Ether over Zeolite Catalysts. *ACS Catal.* **2012**, *2*, 1742-1748.

99. Zhang, X.; Liu, D.; Xu, D.; Asahina, S.; Cychosz, K. A.; Agrawal, K. V.; Al Wahedi, Y.; Bhan, A.; Al Hashimi, S.; Terasaki, O.; Thommes, M.; Tsapatsis, M. Synthesis of Self-Pillared Zeolite Nanosheets by Repetitive Branching. *Science* **2012**, *336*, 1684-1687.

100. Pope, C. G. Sorption of Benzene, Toluene, and Para-Xylene on ZSM-5. *J. Phys. Chem.* **1984**, *88*, 6312-6313.

101. Pope, C. G. Sorption of Benzene, Toluene, and Para-Xylene on Silicalite and H-ZSM-5. *J. Phys. Chem.* **1986**, *90*, 835-837.

102. Vinek, H.; Lercher, J. A. Production and Reactions of Xylenes over H-ZSM5. *J. Mol. Catal.* **1991**, *64*, 23-39.

103. Rabiu, S.; Al-Khattaf, S. Kinetics of Toluene Methylation over ZSM-5 Catalyst in a Riser Simulator. *Ind. Eng. Chem. Res.* **2008**, *47*, 39-47.

104. Odedairo, T.; Balasamy, R. J.; Al-Khattaf, S. Toluene Disproportionation and Methylation over Zeolites TNU-9, SSZ-33, ZSM-5, and Mordenite Using Different Reactor Systems. *Ind. Eng. Chem. Res.* **2011**, *50*, 3169-3183.

105. Cejka, J.; Zilkova, N.; Wichterlova, B.; Eder-Mirth, G.; Lercher, J. A. Decisive Role of Transport Rate of Products for Zeolite Para-selectivity: Effect of Coke Deposition and External Surface Silylation on Activity and Selectivity of HZSM-5 in Alkylation of Toluene. *Zeolites* **1996**, *17*, 265-271.

106. Armaroli, T.; Bevilacqua, M.; Trombetta, M.; Alejandre, A.; Ramirez, J.; Busca, G. An FT-IR Study of the Adsorption of Aromatic Hydrocarbons and of 2,6-lutidine on H-FER and H-ZSM-5 Zeolites. *Appl. Catal. A-Gen.* **2001**, *220*, 181-190.

107. Ruthven, D. M. Diffusion of Aromatic Hydrocarbons in Silicalite/HZSM-5. *Adsorption* **2007**, *13*, 225-230.

108. Ruthven, D. M.; Eic, M.; Richard, E. Diffusion of C8 Aromatic Hydrocarbons in Silicalite. *Zeolites* **1991**, *11*, 647-653.

109. Ruthven, D. M.; Vidoni, A. ZLC Diffusion Measurements: Combined Effect of Surface Resistance and Internal Diffusion. *Chem. Eng. Sci.* **2012**, *71*, 1-4.

110. Jentys, A.; Tanaka, H.; Lercher, J. Surface processes during sorption of aromatic molecules on medium pore Zeolites. *J Phys Chem B* **2005**, *109*, 2254-2261.

111. Gobin, O. C.; Reitmeier, S. J.; Jentys, A.; Lercher, J. A. Diffusion Pathways of Benzene, Toluene and P-xylene in MFI. *Microporous Mesoporous Mater.* **2009**, *125*, 3-10.

112. Pope, C. G. Adsorption of Methanol and Related Molecules on Zeolite H-ZSM-5 and Silicalite. *J. Chem. Soc., Faraday Trans.* **1993**, *89*, 1139-1141.

113. Chen, W.; Tsai, T.; Jong, S.; Zhao, Q.; Tsai, C.; Wang, I.; Lee, H.; Liu, S. Effects of Surface Modification on Coking, Deactivation and Para-selectivity of H-ZSM-5 Zeolites During Ethylbenzene Disproportionation. *J. Mol. Catal. A: Chem.* **2002**, *181*, 41-55.

114. Xiao, J. R.; Wei, J. Diffusion Mechanism of Hydrocarbons in Zeolites—II. Analysis of experimental observations. *Chem. Eng. Sci.* **1992**, *47*, 1143-1159.

115. Roquemalherbe, R.; Wendelbo, R.; Mifsud, A.; Corma, A. Diffusion of Aromatic-Hydrocarbons in H-ZSM-5, H-Beta, and H-MCM-22 Zeolites. *J. Phys. Chem.* **1995**, *99*, 14064-14071.

116. Xiao, J. R.; Wei, J. Diffusion Mechanism of Hydrocarbons in Zeolites—I. Theory. *Chem. Eng. Sci.* **1992**, *47*, 1123-1141.

117. Brogaard, R. Y.; Weckhuysen, B. M.; Nørskov, J. K. Guest–host interactions of arenes in H-ZSM-5 and their impact on methanol-to-hydrocarbons deactivation processes. *J. Catal.* **2013**, *300*, 235-241.

118. Mukti, R. R.; Jentys, A.; Lercher, J. A. Orientation of alkyl-substituted aromatic molecules during sorption in the pores of WZSM-5 zeolites. *Journal of Physical Chemistry C* **2007**, *111*, 3973-3980.

119. Takaishi, T.; Tsutsumi, K.; Chubachi, K.; Matsumoto, A. Adsorption induced phase transition of ZSM-5 by p-xylene. *J. Chem. Soc., Faraday Trans.* **1998**, *94*, 601-608.

120. Lee, C.; Chiang, A. Adsorption of aromatic compounds in large MFI zeolite crystals. *J. Chem. Soc. -Faraday Trans.* **1996**, *92*, 3445-3451.

121. Mentzen, B. F. Characterization of Guest Molecules Sorbed in Zeolites of Known Structure. Part 4 - Localization of Para-Disubstituted Benzene Molecules at Low Sorbate-Fillings in a ZSM-5 Material (Si/Al = 159). *Mater. Res. Bull.* **1992**, *27*, 953-960.

122. Nair, S.; Tsapatsis, M. The location of o- and m-xylene in silicalite by powder X-ray diffraction. *J. Phys. Chem. B* **2000**, *104*, 8982-8988.

123. Li, Y.; Jun, H. Kinetics study of the isomerization of xylene on ZSM-5 zeolites: The effect of the modification with MgO and CaO. *Appl. Catal. A-Gen.* **1996**, *142*, 123-137.

124. Buchanan, J. S.; Santiesteban, J. G.; Haag, W. O. Mechanistic considerations in acid-catalyzed cracking of olefins. *J. Catal.* **1996**, *158*, 279-287.

125. Alberty, R. A.; Gehrig, C. A. Standard Chemical Thermodynamic Properties of Alkane Isomer Groups. *J. Phys. Chem. Ref. Data* **1984**, *13*, 1173-1197.

126. Vandenberg, J.; Wolthuizen, J.; Clague, A.; Hays, G.; Huis, R.; Vanhoff, J. Low-Temperature Oligomerization of Small Olefins on Zeolite H-Zsm-5 - an Investigation with High-Resolution Solid-State C-13-Nmr. *J. Catal.* **1983**, *80*, 130-138.

Chapter 8: Appendix — Biography

I was born and raised in Savage, MN. I have one older brother, a mother in Bloomington, MN and a father in Hastings, MN. I went to Burnsville Senior High School in Burnsville, MN where I graduated in 2003 from a class of over 700. At that time, I learned to play the bass-guitar and performed with a variety of different bands (bluegrass, popular, and metal genres). While I no longer have a band, music has now become a life-long hobby.

I received my Bachelor's degree in Chemistry in 2007 from Carleton College in Northfield, MN where I graduated Cum Laude from a class of less than 400. I did research the summer before my senior year under professor Steven Drew on synthesizing and characterizing enantioselective optical sensors of volatile organic compounds. I was also presented with the honor of the James Finholt Prize for Inorganic Chemistry by the chemistry department.

After 6 wonderful years at the University of Minnesota, I am looking forward to starting my postdoc at the University of Virginia, Chemical Engineering Department under Professor Robert J. Davis studying base catalysts via IR spectroscopy. I am excited to finally live with my wife of four years in Richmond, VA with our cat Grizzabella, and hope that we can continue to align our careers in science/engineering and clinical psychology.